COMPOSITIONAL AND DIAGENETIC CONTROLS OF HARDNESS IN SILICEOUS MUDSTONES OF THE MONTEREY FORMATION, BELRIDGE OIL FIELD, CA: IMPLICATIONS FOR FRACTURE DEVELOPMENT

A THESIS

Presented to the Department of Geological Sciences

California State University, Long Beach

In Partial Fulfillment

of the Requirements for the Degree

Master of Science in Geology

Committee Members:

Richard J. Behl, Ph.D. (Chair)
Jon R. Schwalbach, Ph.D.
Thomas K. Kelty, Ph.D.

College Designee:

Richard J. Behl, Ph.D.

By Ryan M. Weller

B.S., 2006, University of Pittsburgh

May 2018

ABSTRACT

COMPOSITIONAL AND DIAGENETIC CONTROLS OF HARDNESS IN SILICEOUS MUDSTONES OF THE MONTEREY FORMATION, BELRIDGE OIL FIELD, CA: IMPLICATIONS FOR FRACTURE DEVELOPMENT

By

Ryan M. Weller

May 2018

Rock hardness, as a proxy for geomechanical properties of brittleness and unconfined compressive strength, is useful as a high-resolution tool for fracture prediction. This study examines the compositional and diagenetic influences on rebound hardness of upper Monterey Formation mudstones in the San Joaquin Basin of California. The hardness of highly siliceous mudstones evolves through multiple stages of silica diagenesis (opal-A to opal-CT to quartz). Silica diagenesis occurs in two steps that dramatically change porosity from about 60% to 40% to 20% at about 2,000 feet and 5,500 feet of burial depth, respectively. Each step creates a more crystalline and connected silica framework that is increasingly prone to brittle failure. Micro-rebound hardness (HLD) and X-ray fluorescence scanning data show that proportion of diagenetic silica relative to clay-rich detritus is the primary influence on rock hardness within any single diagenetic phase. In general, rocks with higher silica contents are harder. Silica diagenesis increases mean hardness by 69% from opal-A to opal-CT but only 10% from opal-CT to quartz. In rocks buried to 12,500 feet, hardness increases by 24% occurs with no additional silica-phase change but through compaction and cementation during illitization and catagenesis. Opal-A mudstones failed to show a clear trend of hardness to most physical properties. In opal-CT and 6000-foot quartz phase mudstones hardness trends converge at greater than 70%

diagenetic silica. Failure by brittle jointing is likely to prevail at >775 HLD in 12,000-foot quartz phase mudstones. The Monterey Formation is consistently harder and potentially more heterogeneous than the Marcellus, Niobrara, Eagle Ford, Horn River, and Woodford shale formations. This study clearly demonstrates an evolution of mechanical stratigraphy due to silica diagenesis; a process that may be under-regarded in the timing of natural fractures of other shales with siliceous components.

ACKNOWLEDGEMENTS

This work would not have been possible without the mentorship and positivity of my advisor and Monterey And Related Sediments (MARS) Project founder Richard J. Behl. I am incredibly grateful for your patience towards me and fellow students. Your intense willingness to help others and share knowledge in the geosciences is inspiring and contagious. I have learned so much from you and I deeply appreciate your friendship.

Thank you to the MARS Project affiliates who have directly supplied samples, data, equipment, and financial support to this study. The MARS project has been a very enlightening platform for discussion and guidance during numerous meetings, conferences, and field trips. I greatly appreciate your support and encouragement.

Thank you to Jon Schwalbach and Tom Kelty for their review, revisions, and comments to this work.

A tremendous thank you to my MARS family and CSULB colleagues who have supported me with helping hands, ideas, banter, food, and friendship. It has been more than a pleasure to work beside you and to be inspired by your own interests in science and beyond.

Most tenderly, thank you to Kelci Degnian, who has crossed oceans for me and who has become as committed to this project as I have been. Countless nights I missed a dinner deadline by several hours and I have only been greeted with affection and warm food. Thank you so much for supporting me on this journey through Southern California and onwards to Pittsburgh, PA.

TABLE OF CONTENTS

ABSTRACT ii

ACKNOWLEDGEMENTS iv

LIST OF TABLES vi

LIST OF FIGURES vii

1. INTRODUCTION 1
2. BACKGROUND 3
3. METHODS 16
4. RESULTS 23
5. DISCUSSION 34
6. CONCLUSIONS 71
7. FUTURE WORK 74

APPENDICES 76

A. XRF K-SHELL FLUORESCENCE YIELDS 77

B. INDUCTIVELY COUPLED PLASMA-MASS SPECTROMETRY DATA 79

C. LEEB HARDNESS DATA 81

D. ILLITE/SMECTITE ANALYSIS 83

REFERENCES 86

LIST OF TABLES

1. Typical Range of Physical Properties of Monterey Formation Siliceous Mudstones in California..... 8

2. Summary of Cores from Each Sample Group in This Study.....18

3. Typical Wireline Responses and Ranges of Each Silica Phase or Burial Group.....25

4. Summary of Hardness Data 29

5. Hardness Log Trends to Accompany Fig. 18 33

6. Aggregated Shale Data Associated with Fig. 19.....42

7. Comparison of Hardness in Samples with Similar Silica:Detritus Ratios.....48

8. Mean Hardness for Three Compositional Groups.....55

LIST OF FIGURES

1. Three phase silica diagenesis with regard to temperature and compositional controls..... 5

2. Schematic diagram of the silica diagenesis in the Sisquoc Formation and Monterey Formation across the Santa Barbara coastline. 6

3. Porosity reduction in siliceous mudstones of the Monterey Formation through physical and chemical compaction 7

4. Simplification of the identification and categorization of siliceous mudstones with trends related to composition and diagenesis 8

5. Belridge oil field in the southwest of the San Joaquin Basin, Kern County, California. ..10

6. Stratigraphy of the Belridge oil field including members of the Monterey Formation 11

7. Schematic of the Belridge oil field and cored intervals in this study.....12

8. Correlation of gamma ray (GR), resistivity (DRED, MRES), bulk density (RHOB), neutron porosity (NPHI), and sonic (DT) wireline logs where available in the four wells studied.....17

9. Visible light core image of two cores in millimeter-scale demonstrating the typical bedding and heterogeneity of cores in this study.....18

10. Regression of non-calcareous samples for the conversion of fluorescence yield-corrected and normalized XRF counts vs percent oxide from ICP-MS analysis for (a) silicon to SiO_2 and (b) aluminum to Al_2O_3 20

11. Schematic of the internal design and function of the Proceq Piccolo rebound hammer...22

12. Generalized schematic of a Monterey Formation type log showing typical changes in the standard triple-combo wireline tools important to identifying silica phase and physical properties of siliceous mudstone reservoirs.....24

13. Normalized weight percent of biogenic and diagenetic silica and detritus for each sample group presented in Tukey box and whisker plots.....27

14. Core plug porosity in each sample group with dashed log trend correlating composition and porosity 28

15. Data for >2000 average points in five burial groups relative to hardness (HLD) and silica and detritus derived from high-resolution XRF scanning. 29

16. Scatter plot similar to Fig. 14 of HLD and percent silica for opal-CT samples of the same well at 2,200' and 3,600' burial depths. 30

17. Percent silica and hardness (HLD) over an opal-CT core sample demonstrate the mechanical heterogeneity of thinly interbedded rocks of different compositions.31

18. Data from Fig. 14 grouped as mean HLD in classes of 10% compositional ranges for trend comparisons....32

19. Range and median (horizontal lines) of Leeb hardness for seven North American shale plays subdivided by lithofacies....36

20. Mean hardness per depth for each of the 8 formations and their lithotypes....37

21. Hardness variation in each diagenetic or burial group represented by percent biogenic silica groups....45

22. A 6'k-quartz (IGOR 856C-7) core in UV and plane light....46

23. Hardness vs. (a) elemental aluminum and (b) elemental potassium XRF data with elemental X-ray yield conversion and normalization to total counts 49

24. Core photo from 882D-8 (12k'quartz) in UV (above) and plain light (below)....50

25. Association of normalized elemental calcium with major components of (a) Si and (b) Al in Monterey Formation siliceous mudstones 51

26. Hardness plots with calcium (a) included in this study and (b) not included in the bulk results of siliceous mudstones....52

27. Weight percentage TOC data aligned with hardness testing plotted for the McDonald Shale interval....53

28. Quartile box-and-whisker plot of silica classes in 10% steps demonstrates the hardness increases of high-silica vs. low-silica rocks with burial....56

29. Summary of three steps of increasing median hardness associated with silica diagenesis and possible mechanisms of hardening during deep burial of quartz-phase rocks 57

30. Across all silica phases and burial depths core plug porosity has a negative correlation with hardness, but within each burial group from opal-A through 6k'-quartz phase rocks there is a positive relationship between porosity and hardness....59

31. Core photos of 1/3 section (above) and 2/3 section (below) in a 12k'-quartz interval with variation of hardness, composition, and fracture occurrence....64

32. Standard wireline suite demonstrating the resolution and scale of physical and mechanical heterogeneity in well logs 67

33. Calibrated UCS in psi from Lee et al. (2014) with overlying Monterey Formation data from literature and associated studies 70

CHAPTER 1

INTRODUCTION

Understanding rock strength is critical to correctly predicting fracture distribution in unconventional reservoirs (Pitman et al., 2001; Gale et al., 2007), predicting the sealing capacity of caprocks (Ingram and Urai, 1999), and controlling wellbore stability in drilling (Holt et al., 2011). Composition is a fundamental parameter that is well correlated to a wide range of rock strengths and mechanical behaviors in mudstones (Gross, 1995; Britt and Schoeffler, 2009; Crawford et al., 2010; Passey et al., 2010). Particular to siliceous mudstones such as the Monterey Formation, Woodford Formation, and Horn River Group, authigenic quartz has been indicated as a strong and brittle component key to creating dense and communicable fractures, while abundant clay minerals correlate with weak and ductile rocks, inhibiting fracture formation (Ross and Bustin, 2008; Blood et al. 2013; Dong et al., 2017). Several studies have qualitatively and quantitatively demonstrated differences in the structural behavior the Monterey Formation at multiple scales associated with silica phase and compositional variance (Snyder et al., 1983; Narr and Suppe, 1991; Gross, 1995; Wirtz, 2017). Most of these studies have focused on fracture style or fracture intensity in outcrop or core samples of the Santa Maria and Santa Barbra Basins. This study is the first quantification of rock hardness associated with a statistically significant compositional analysis across three silica phases from unweathered subsurface samples of the San Joaquin Basin.

The Upper Miocene upper Monterey Formation is chiefly a fine-grained and highly siliceous mudstone succession with tremendous compositional and diagenetic heterogeneity within multiple basins of central and southern California (Behl, 1999). It is an economically significant and highly complex reservoir at three distinct burial and diagenetic stages

(Schwalbach et al., 2009). It typically has a matrix porosity of 4 to 10 times that of other shale plays, yet still relies on fracture permeability and oftentimes fracture porosity for production. The Monterey Formation's play potential as a true source-rock reservoir within the oil window is poorly understood with very few prospects tested by drilling.

This study examines the geomechanical properties of the upper Monterey Formation in the San Joaquin Valley of California by measuring rebound hardness. Compositionally equivalent samples from multiple reservoir rocks at depths between 800' to 12,500' TVD are compared to quantify and distinguish the controls of rock strength in siliceous mudstones. The results apply to reservoirs estimated to hold hundreds of millions to billions of barrels of oil in California (Allan and Lalicata, 2011; Kuuskrra et al., 2013; Larue et al., 2018). Additionally, the wide variety of compositions of Monterey Formation siliceous mudstones makes them excellent analogs for the understanding and interpretation of other unconventional shale plays in which authigenic silica may be a major influence on geomechanical behavior.

CHAPTER 2

BACKGROUND

Monterey Formation

The Monterey Formation is a middle- to upper-Miocene succession of predominantly fine-grained siliceous mudstone with distinct facies that independently serve as source, seal, and reservoir rocks for many conventionally-trapped and prolific petroleum resources of Central and Southern California (Behl, 1999). The Monterey Formation is incredibly heterogeneous in composition, diagenesis, and depth with a maximum thickness of 10,000' at Chico Martinez Creek (Mosher, 2013). Much of the heterogeneity in the Monterey Formation is due to variations in biogenic productivity, terrigenous runoff, and net sedimentation rates during global climatic shifts (Kennett, 1977; Ingle, 1981). Compared to similar biogenic deposits in the deep-sea, burial was relatively rapid due to the proximity to an active margin (Pisciotto and Garrison, 1981; Graham and Williams, 1985). The Monterey Formation and its stratigraphic equivalents were deposited in several restricted basins, in part similar to the present California Continental Borderland (Blake, 1981).

The focus of this study is of the siliceous mudstones of the Monterey Formation, which are dominated by biogenic silica and clay-rich detritus (Bramlette, 1946; Pisciotto and Garrison, 1981). Biogenic silica is chiefly sourced from marine diatoms, associated with coastal upwelling and hemipelagic settling (Ingle, 1981). Fine-grained detritus is sourced from terrigenous runoff and includes clay minerals (principally mixed-layer illite-smectite), feldspars, and quartz (Isaacs, 1980; Compton, 1991a). Different members of the Monterey Formation are characterized as a generally siliceous, phosphatic, or calcareous facies although most have a siliceous influence. (Pisciotto and Garrison, 1981). The upper Monterey Formation is primarily a siliceous shale and

lacks abundant calcareous, dolomitic, or phosphatic rocks, in contrast to lower units of the Monterey (Bramlette, 1946; Pisciotto and Garrison, 1981). Varieties of highly siliceous mudstone that differ by detrital content or silica phase are given specific names such as diatomaceous mudstone, diatomite, porcelanite or chert in the California and Pacific Rim literature (Bramlette, 1946; Pisciotto and Garrison, 1981; Isaacs, 1981a). The middle Monterey Formation is characterized as phosphatic, calcareous, and organic-rich facies that is quite clay-rich in places but has an increasing predominance of siliceous rocks near the top of the section (Pisciotto and Garrison, 1981; Mosher, 2013). Bedding ranges from discretely stratified laminations and thin beds to massive or bioturbated strata due to a combination of fluctuating oceanographic upwelling, basin geometry, sediment supply, and seafloor oxygenation (Pisciotto and Garrison, 1981; Ingle, 1981; Schwartz, 1988).

Not only are silica and fine detritus the two primary components of siliceous mudstones, but they have stark and contrasting effects on the physical and mechanical properties of rocks. Opaline and diagenetic silica create a framework of interlocking biogenic to crystalline components with higher porosity and rock strength as well as increasing the propensity for burial diagenesis and brittle open-mode failure. Conversely, detritus creates a weaker framework of lower porosity and lower strength that in some cases inhibits diagenesis and typically promotes shear failure (Isaacs, 1981a, 1981b; Gross, 1995). Thus, describing Monterey Formation mudstones in terms of a silica to detritus ratio offers a quick and rough characterization of its physical and mechanical properties. Carbonate, organic matter, and authigenic phosphate are minor components in the distinctly siliceous intervals of the upper Monterey Formation and thus excluded from a bimodal descriptor of silica and detritus.

Biogenic silica is highly unstable and undergoes a two-step diagenetic transformation driven by time and temperature with kinetics modified by sediment composition. With burial to ~40-50°C, biogenic opal-A silica (amorphous hydrous silica, in this case diatomaceous) undergoes an *in situ* dissolution and precipitation into metastable opal-CT (microscopic spheres of cristobalite and tridymite). A similar reaction occurs again at ~65-80°C when Opal-CT undergoes an *in situ* dissolution and then precipitation as diagenetic quartz (Fig. 1; Pisciotto, 1981; Keller and Isaacs, 1985). The range of alteration temperature are primarily related to the presence of smectite clays, which retard the opal-A to opal-CT transformation but accelerate the opal-CT to quartz-phase transformation (Murata and Larson, 1975; Isaacs, 1981b). When intervals with heterogeneous compositional stratification enter the transition zone, they become diagenetically stratified with highly contrasting physical properties (Fig. 2; Isaacs, 1981b; Lockman, 2012).

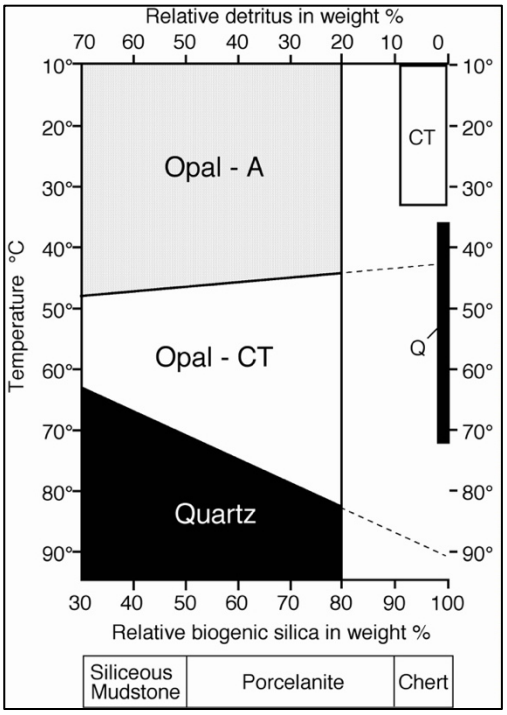

FIGURE 1. Three phase silica diagenesis with regard to temperature and compositional controls. Note that cherts (right side of chart) can form at much lower temperatures than opal-CT porcelanite and siliceous mudstone. From Behl and Garrison (1994).

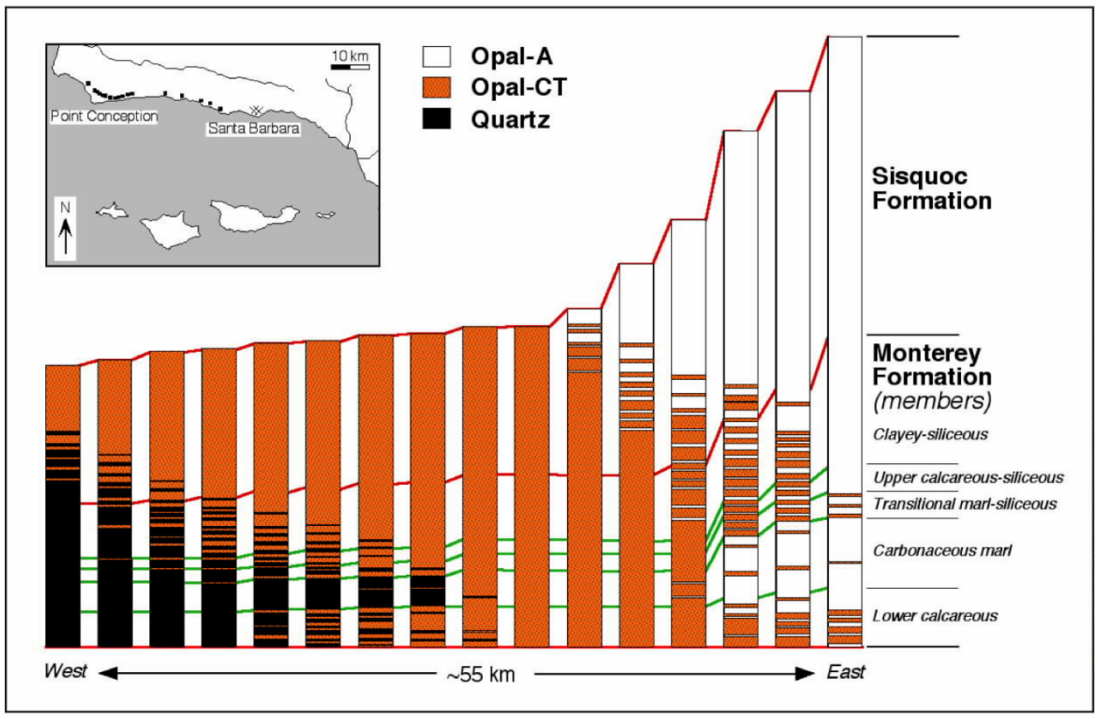

FIGURE 2. Schematic diagram of the silica diagenesis in the Sisquoc Formation and Monterey Formation across the Santa Barbara coastline. Interbedded silica phases in transition zones are due to the interbedded compositional differences effect on the kinetics of diagenesis. Note the dramatic volume reduction from physical and chemical compaction that occurs, especially with opal-A (white) to opal-CT (orange) burial diagenesis. Modified from Isaacs (1981b).

Silica diagenesis reduces porosity and thus volume in stepwise shifts of physical and chemical compaction, resulting in dramatic alteration to mechanical rock properties (Fig. 3; Isaacs, 1981b; Compton 1991b). Porosity loss changes permeability and physical strength by altering pore geometry, effective pore connectivity, and grain-to-grain contacts creating a denser rock volume (Isaacs, 1980; Schwabach et al., 2009; Kassa, 2016). Rocks of greater diagenetic silica content have more matrix dispersed diagenetic silica – either cryptocrystalline opal-CT or microcrystalline quartz – and a strong crystalline framework with higher strength and higher brittleness (Isaacs, 1981a; Snyder et al., 1983; Gross, 1995; Fig. 4). Highly siliceous opal-CT and quartz-phase lithotypes resist burial compaction while detritus-rich lithotypes experience greater compaction via grain rotation, crushing, and deformation (Isaacs, 1981b). Monterey Formation

rocks are classified by both their bulk composition and diagenetic phase with associated properties relevant to their porosity and fracture potential. (Fig. 4; Table 1.).

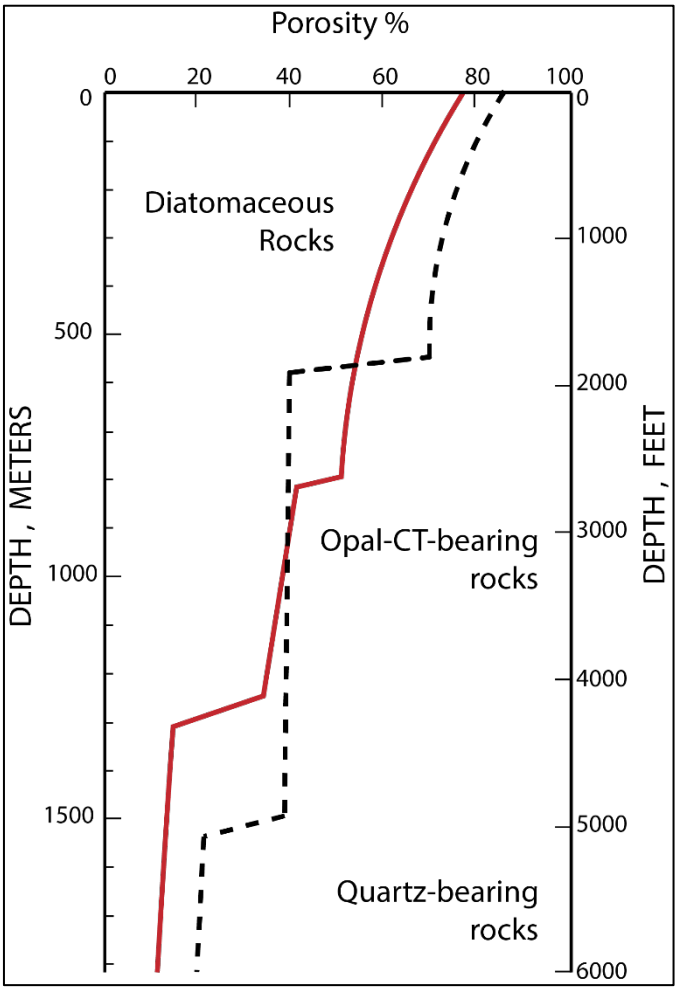

FIGURE 3. Porosity reduction in siliceous mudstones of the Monterey Formation through physical and chemical compaction. The solid red line represents detritus-rich rocks, altering from opal-A to opal-CT at greater depths and compacting more in each phase, the dashed line represents low-detritus rocks with greater porosity and greater resistance to compaction (modified from Isaacs, 1981b).

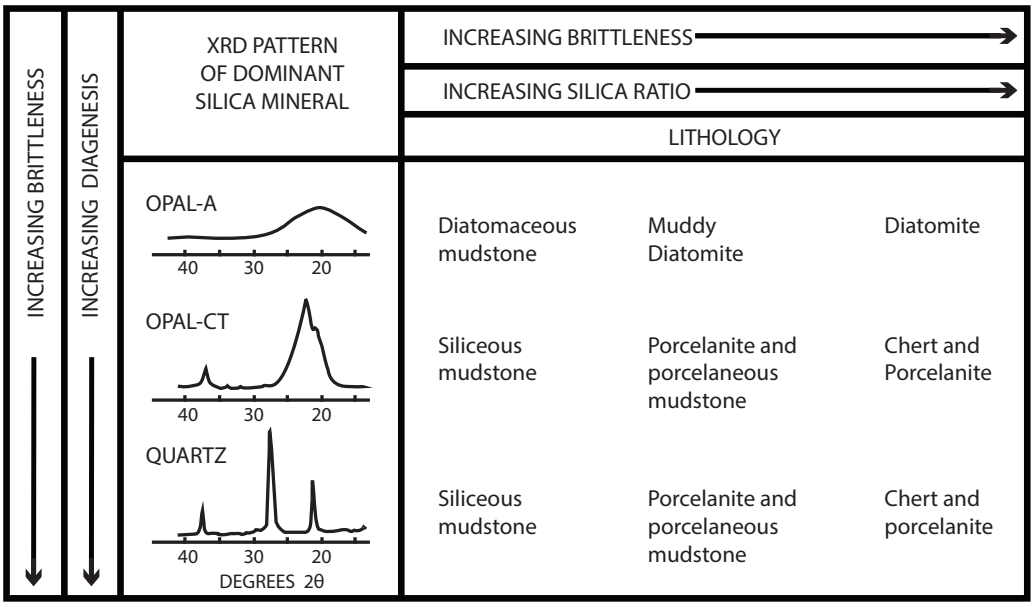

FIGURE 4. Simplification of the identification and categorization of siliceous mudstones with trends related to composition and diagenesis (modified from Pisciotto and Garrison, 1981 and Snyder et al., 1983).

TABLE 1. Typical Range of Physical Properties of Monterey Formation Siliceous Mudstones in California (from Allan and Lalicata, 2011; Schwalbach et al., 2009)

Silica Phase	Approx. Depth (ft)	Grain Density (g/cc)	Porosity (%)	Perm (air, md)	Oil Saturation (%)
Opal-A	0 – 2,000’	1.7-1.9	40 - 70	0.1 - 1.0	40 - 65
Opal-CT	2,000 - 5,500’	2.15-2.35	25 - 40	0.01 – 0.1’s	0 - 30
Quartz	5,500 – >14,000’	2.50-2.65	5 - 30	0.1 – 1.0’s	30 - 60

Location

The Belridge oil field is located in the southwestern San Joaquin Basin approximately 45 miles NW of Bakersfield, 55 miles SE of Coalinga, and 5 miles east of Chico Martinez Creek in Kern County, California (Fig. 5). Monterey Formation members examined in this study of the Belridge oil field include the Reef Ridge (locally the Belridge Diatomite) and the McClure Shale

(locally divided as the Antelopes Shale and McDonald Shale) (Fig. 6; Graham and Williams, 1985). The underlying Devilwater Silt and Gould Shale are also included in the McClure Member of the Monterey Formation but are not included in this study. The Belridge oil field is an elongated *en echelon* anticlinal structure in the western San Joaquin Basin (Graham and Williams, 1985; Mount and Suppe, 1987). In general, the northern Belridge oil field is more clay-rich than the southern Belridge oil field due to its proximity to terrigenous input during the time of deposition (Schwartz, 1988; Allan et al., 2010).

Highly siliceous mudstones of the Monterey Formation in the Belridge oil field have thin to thick beds of variable silica:detritus ratios and are buried at different depths (400' – 14,000') along the flanks of the anticline where physical and diagenetic contrasts develop within laterally continuous strata (Fig. 7). The opal-A-phase Belridge Diatomite is predominately located at less than 2,000' TVD along the crest of the anticline, with opal-CT phase Belridge Diatomite (aka "brown shale") or the Antelope Shale encountered below those depths to a maximum of 5,800' (Schwartz, 1988; Bowersox, 1990). Along the flanks of the anticline, the Antelope-McDonald stratigraphic horizon plunges from approx. 6,100' to greater than 12,500'. Some uplift likely occurred after maximum burial and diagenesis at the site of the 856C-7 'IGOR' well (blue) when considering the shallower top of the opal-CT to quartz phase transition than the 882D-8 'Thorndyke' well (red) (Fig. 7). This relationship of an uplifted diagenetic transition zone was first predicted and discussed in Mizutani (1977).

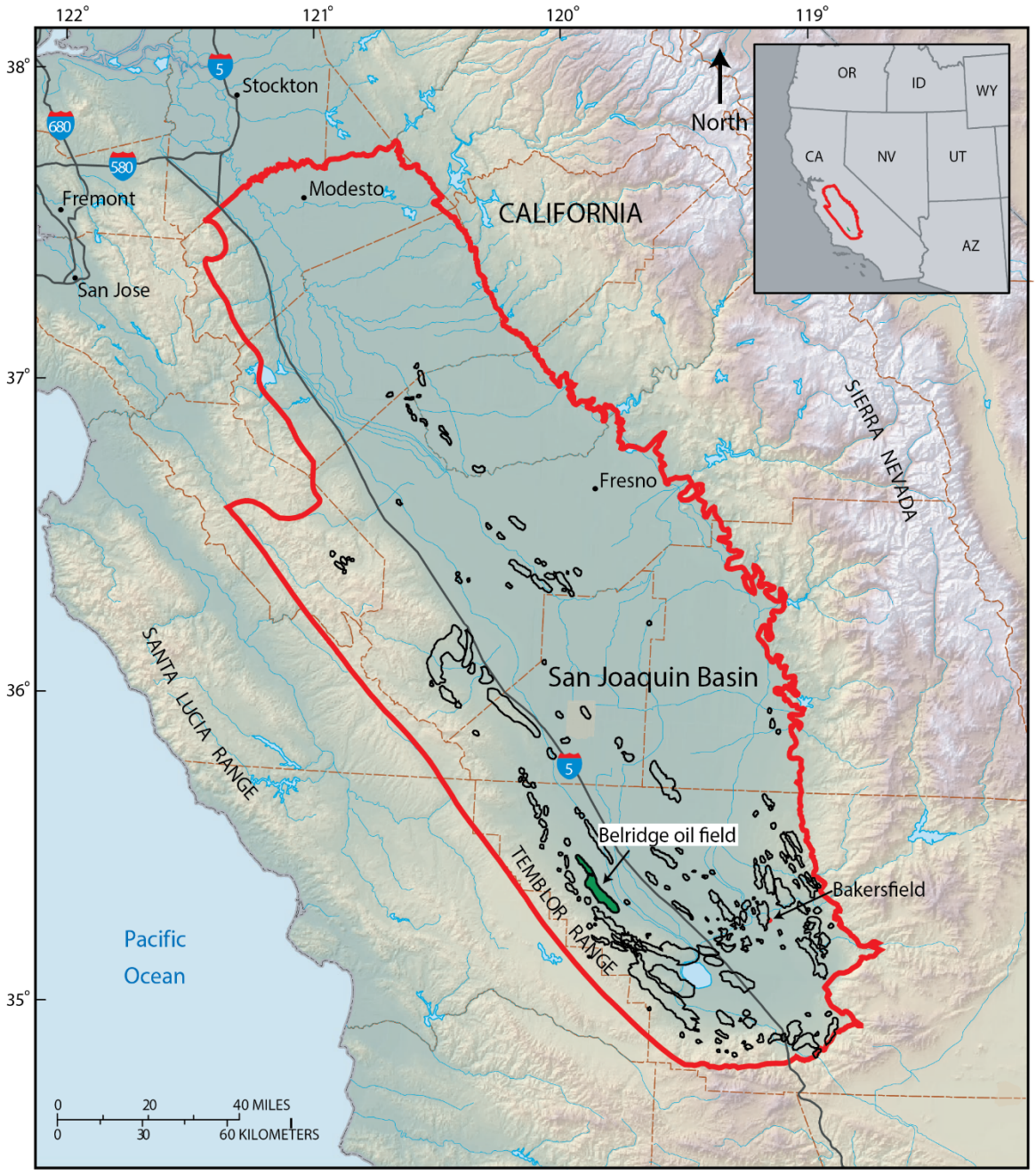

FIGURE 5. Belridge oil field (green) in the southwest of the San Joaquin Basin (red outline), Kern County, California. Other San Joaquin oil fields are outlined in black. Modified from USGS PP 1713, Hosford Scheirer (2007).

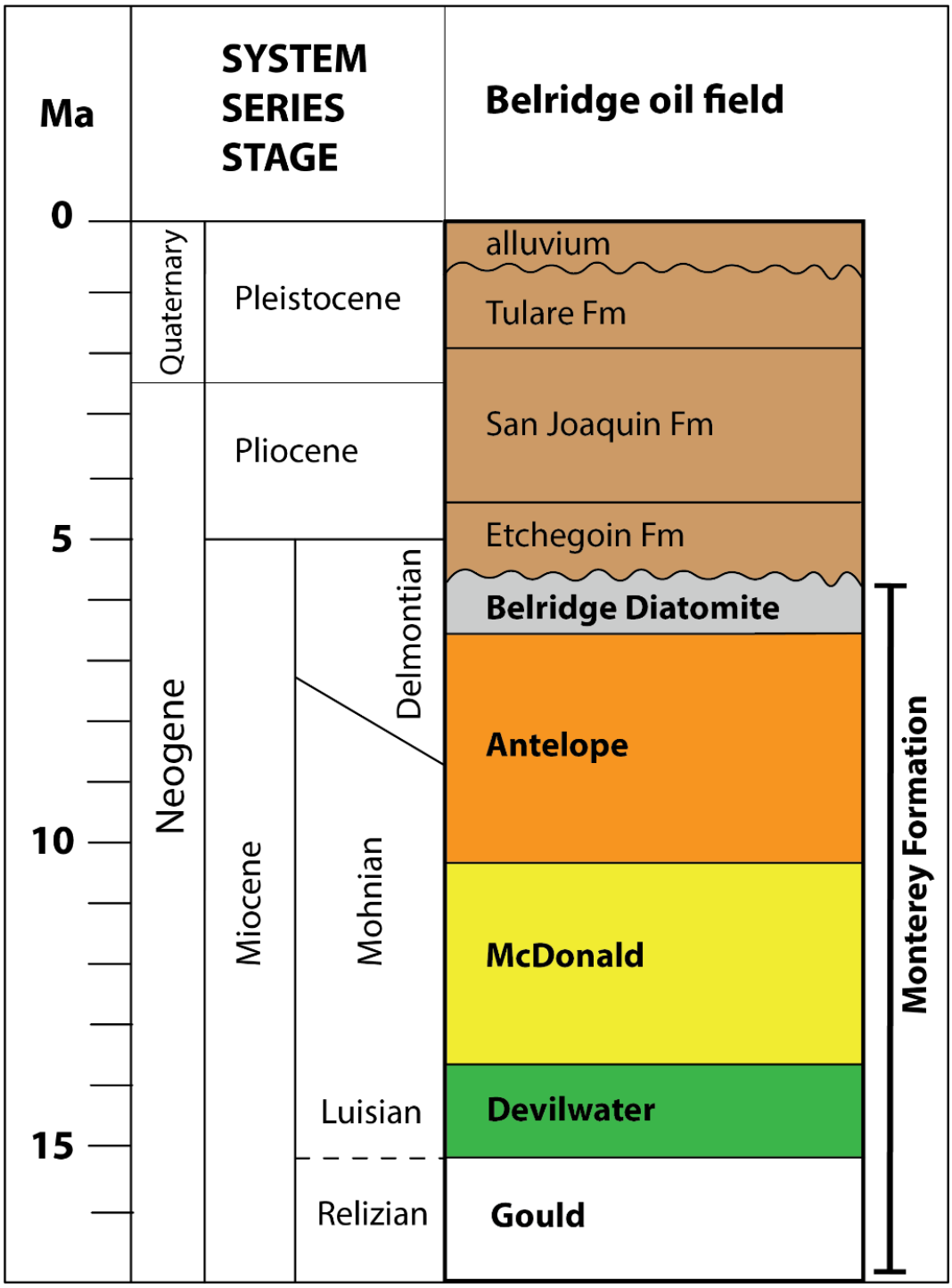

FIGURE 6. Stratigraphy of the Belridge oil field including members of the Monterey Formation. After Hosford Scheirer (2007) and Schwartz (1988).

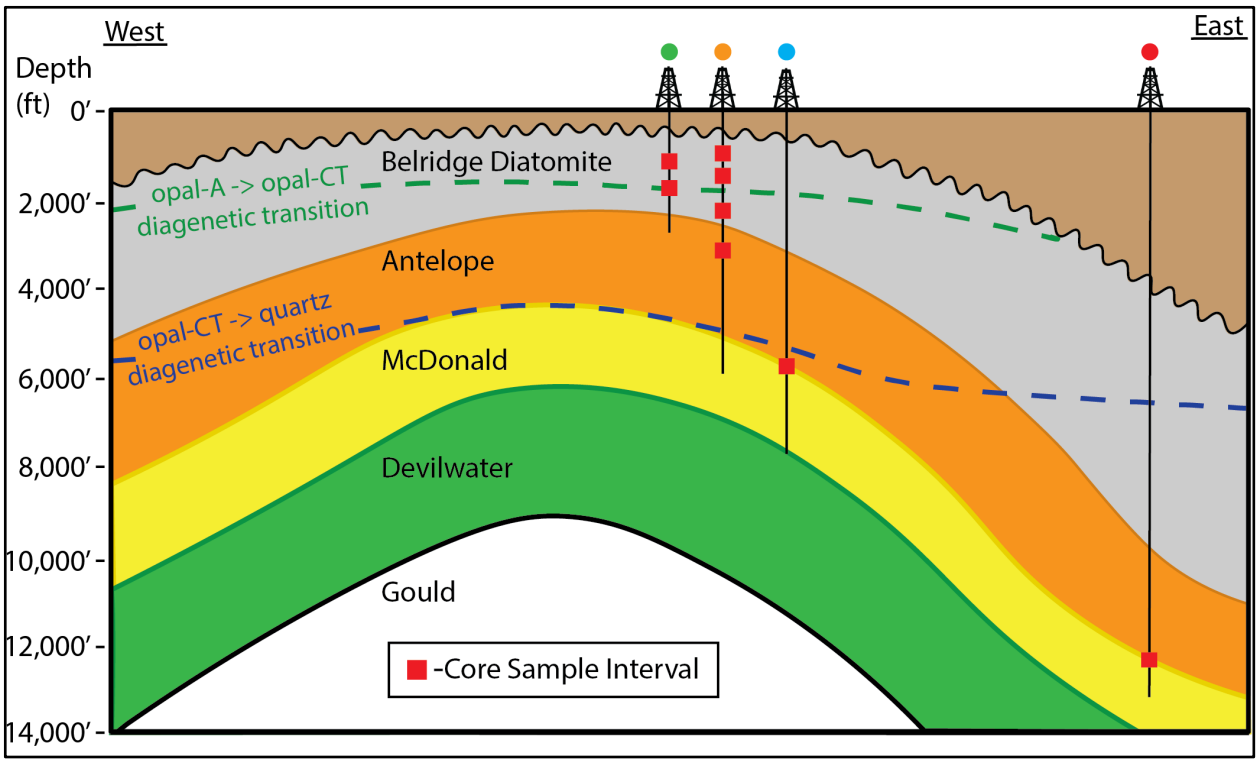

FIGURE 7. Schematic of the Belridge oil field and cored intervals in this study. Note the differences in diagenetic horizons (dashed) that cut lithostratigraphic members.

Previous authors have expansively detailed the stratigraphy, characteristics, and petroleum development of Monterey Formation reservoirs in the Belridge oil field (Graham and Williams, 1985; Schwartz, 1988; Bowersox, 1990; Miller and McPherson, 1992; Allan and Lalicata, 2011). Monterey Formation reservoirs in the Belridge oil field have produced over 300 million barrels of oil with a long history of primary and secondary recovery techniques used to produce 25-39° American Petroleum Institute (API) standard oil from low-permeability rocks including various fracture techniques (Allan and Lalicata, 2011). The abundant and publically accessible subsurface data along with recent drill cores is ideal for the integration of prior studies and industrial application of this study.

Previous Monterey Formation Studies

It is widely documented that the Monterey Formation has a diverse expression of physical properties and mechanical behaviors related to primary composition (silica and detritus) and silica diagenesis (Bramlette, 1946; Isaacs, 1981b; Snyder et al., 1983; Gross, 1995; Wirtz, 2017). In general, rocks of any silica phase with greater percentages of clay-rich detritus are easier to scratch, less cohesive, and prone to faulting rather than jointing, while greater amounts of diagenetic silica have the opposite influence on nearly every physical or mechanical property (Isaacs, 1981a; Snyder et al., 1983). Chert is different than the bulk of other siliceous rocks and has an exceptionally high hardness, low porosity, and distinct vitreous texture (Isaacs, 1981a; Snyder et al., 1983; Behl and Garrison, 1994).

Fracture studies from outcrop and core established a strong relationship between lithology and deformational style. Along the Santa Barbara and Santa Maria coastline, Gross (1995) documented open-mode brittle fracturing in beds with <9% weak minerals (defined as opal-A, kaolinite, muscovite, montmorillonite, and apatite) while shear failure or faulting prevailed in beds with >22% weak minerals. Both failure modes occur in between. In the Santa Maria and Pismo basins of coastal central California, fracture spacing is wider in more clay-rich rocks (Narr and Suppe, 1991; Strickland, 2013). Outcrop observations document that weak or detritus-rich rocks in any diagenetic stage can be mechanical barriers that impede the propagation of through-going fractures (Gross, 1995; Strickland, 2013; Gale et al., 2014).

Authigenic or diagenetic quartz is regularly identified as one the most influential minerals in increasing hardness, rock strength, Young's Modulus, and brittle geomechanical behavior by creating a lithology of a better connected and lower-porosity crystalline matrix (Chang et al., 2006; Jarvie et al., 2007; Rickman et al., 2008; Dong et al., 2017; Becerra-Rondon, 2017).

Intervals of the Monterey Formation are rich in diagenetic quartz and below 5000-6000 feet quartz-phase porcelanite and chert are important fractured reservoirs (Snyder et al., 1983; Schwalbach et al., 2009). Allogenic or detrital quartz has not been shown to enhance strength or hardness properties of other siliceous mudstones and can be distinguished from diagenetic quartz via the geochemical analysis of local detritus (Dong et al., 2017; Isaacs, 1980). The different impact of opal-CT and quartz-phase diagenetic silica on mechanical properties has not been quantified (Isaacs, 1981a). Additionally, no published studies have reported on the alteration of quartz-phase mudstones at depth of greater than 10,000'.

Prior to diagenesis, opal-A rocks are generally characterized as weak lithotypes that have a low fracture gradient (Strubhar et al., 1984) and common problems include subsidence, shearing, and well failure (Chase and Deitrich, 1989; Allan and Lalicata, 2011). Field observations indicate a compositional difference in rock strength between diatomaceous mudstone and high-purity diatomite (>80% opal-A); the later is notably stiffer and prone to brittle jointing under tensile stress (Behl and Garrison, 1994).

Previous Hardness Studies

Rebound hardness (HLD), a ratio of a probe's impact velocity divided by the rebound velocity as defined by Leeb (1979), has been demonstrated to be a fast, non-destructive, and effective tool for estimating unconfined compressive strength (UCS) at less than a 1 cm^2 resolution (Verwaal and Mulder, 1993; Aoki and Matsukura, 2008; Lee et al., 2014). Rebound hardness is not the same as Mohs (1825) mineralogical hardness, although there is a weak positive exponential relationship (Broz et al., 2006). Several studies have demonstrated a strong correlation of rebound hardness to sonic velocity and/or fracture style due to lithological

variation in core and outcrop (Ritz et al., 2014; Rolfs, 2015; Murray, 2015; Offurum, 2016; Becerra-Rondon, 2017; Dong et al., 2017).

CHAPTER 3

METHODS

Core, core data, and wireline logs were studied from four wells in the Belridge oil field area. Compositionally and diagenetically diverse intervals were targeted at stratigraphically similar horizons to test an extensive range of siliceous Monterey Formation rocks from the crest, shoulder, and plunging flanks of the Belridge Anticline (Fig. 8). I used well logs (gamma ray, density, neutron-porosity, and sonic velocity), core photos, and core data evaluating composition, porosity, and oil saturation, as well as observations of bedding and texture to select a range of core samples that represent the range of lithofacies for analysis. Core samples are from both silica-rich and clay-rich beds from similar stratigraphic intervals in multiple wells. Thinly bedded, laminated, massive, and gradational bedding fabrics (Fig. 9) are represented.

A total of twenty-eight core sections – each of the 2/3 slab and approximately three feet in length – were used for this study (Table 2). Five sample groups (opal-A, mixed-A+CT, opal-CT, 6k'-quartz, and 12k'-quartz) were defined by silica phase and/or burial depth. Core intervals with volcanic ash, carbonate, abundant fractures, or extreme fissility were initially included in measurements, but later excluded to focus on variations in the properties of siliceous mudstones while minimizing complicating variables. Although rejecting highly fractured intervals may have excluded data from some of the most brittle rock types, the wide range and large number of accepted measurements likely incorporated these end-member lithotypes, nonetheless.

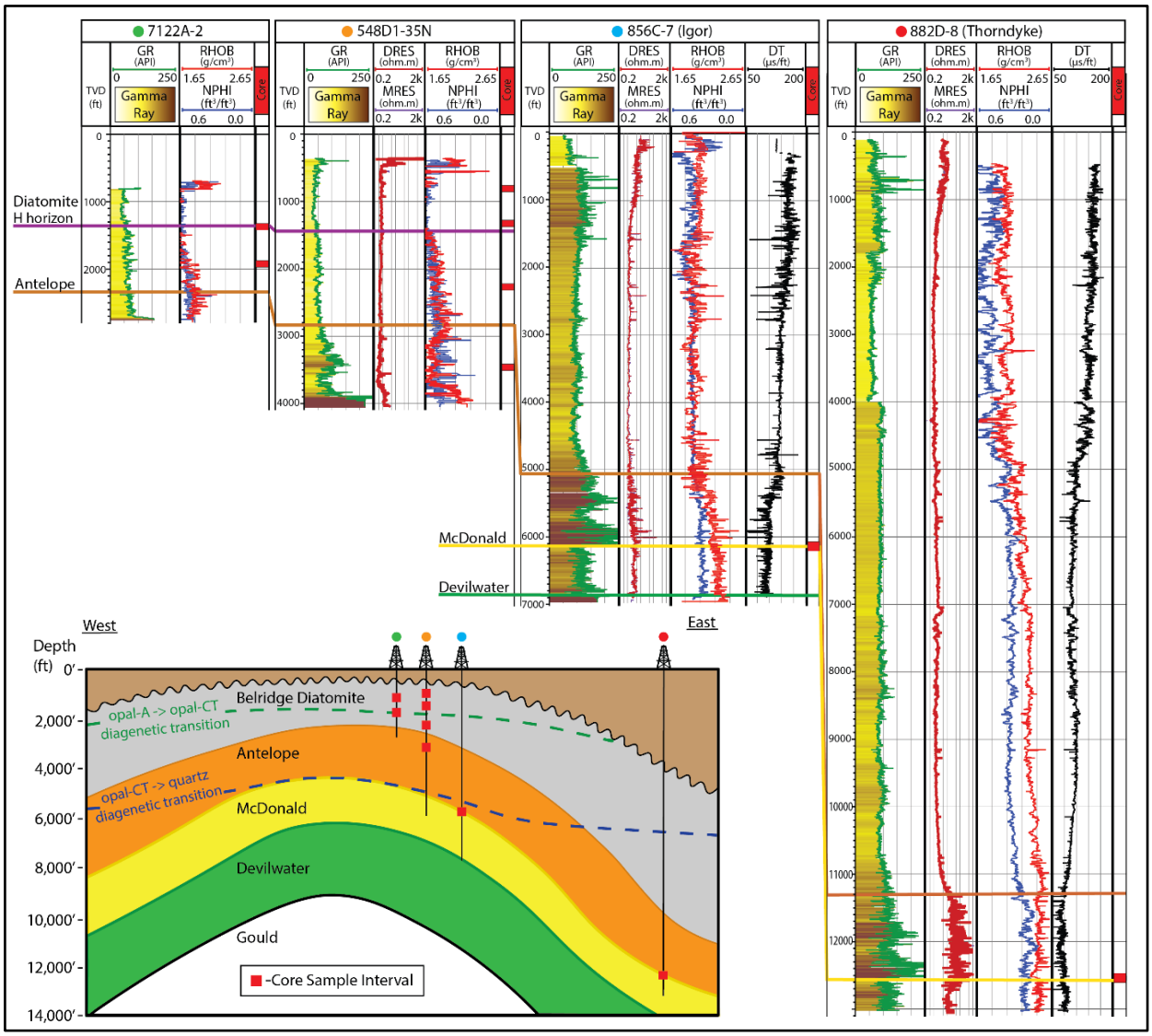

FIGURE 8. Correlation of gamma ray (GR), resistivity (DRED, MRES), bulk density (RHOB), neutron porosity (NPHI), and sonic (DT) wireline logs where available in the four wells studied. Cored intervals are in red blocks. Simplified cross-section from Fig. 7 for additional reference.

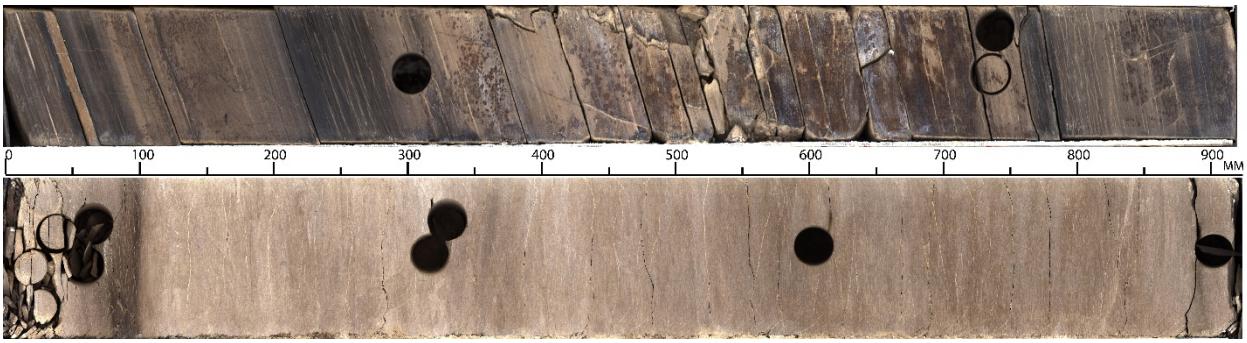

FIGURE 9. Visible light core image of two cores in millimeter-scale demonstrating the typical bedding and heterogeneity of cores in this study.

TABLE 2. Summary of Cores from Each Sample Group in This Study

Sample Group Name	Depths (TVD)	Member	Silica Phase	HLD Points Accepted	Field Location	Year Cored	Porosity (%)
Opal-A	800' – 1,370'	Belridge Diatomite	opal-A	454	North and South Belridge	2000	59 – 67
Mixed-A+CT	1,900' – 1,930'	Belridge Diatomite & Antelope Shale	13% opal-A 87% opal-CT	118	South Belridge	2000	46 – 55
Opal-CT	2,200' – 3475'	Belridge Diatomite & Antelope Shale	opal-CT	313	North Belridge	2000	33 – 56
6k'-quartz	6,100' – 6,150'	lower Antelope & upper McDonald	quartz	189	SE North Belridge	2013	12 – 27
12k'-quartz	12,500' – 12,577'	lower Antelope & upper McDonald	quartz	415	East of Belridge (Buttonwillow)	2012	2 – 7

I removed surficial degradation and mineral precipitates by nylon brush and metal scraper to prepare the cores for photography, X-ray Fluorescence (XRF) scanning, and hardness testing. An Avaatech XRF core scanner was used at 10kV energy and 10 second counts on a 10 mm x 10 mm section at 10 mm step intervals over each core resulting in a semi-quantitative elemental analysis of Al, Si, P, S, Cl, K, Ca, Ti, Cr, Mn, Fe, and Rh. Elemental data at 2,310 locations were recorded. I divided raw XRF counts by the fluorescent-yield of each element (Kahoul et al., 2011; Appendix A) to correct for the greater fluorescence emitted by heavier elements. Each

yield-normalized elemental count was then divided by the total yield-normalized counts of all XRF-measured elements to derive a final normalized representation of XRF counts. I used several elemental ratios, including Si/Al, Ca/Fe, Si/Ti, etc., as compositional proxies (cf. Rothwell and Croudace, 2015) to guide additional testing and allow us to identify the greatest range and heterogeneity of the cores available.

XRF counts from high-calcium samples exhibited either a noisy or inherently antithetic relationship to Al counts. To maintain a focus on siliceous mudstones and a valid description of silica-detritus ratios, samples with greater than 20 normalized percent Ca were removed. Additionally, high-calcium samples were mostly within the 6k'-quartz section and therefore could not be compared to other sample sets of different silica phases or depths.

I selected twenty-five specimens across a varied range of compositions to analyze by X-ray diffraction (XRD), inductively coupled plasma-mass spectrometry (ICP-MS) (Appendix B). XRD was used to verify silica phase. ICP-MS results were used to correlate XRF data counts to a percentage of elemental oxides by regression analysis of XRF yield-normalized counts versus ICP-MS major elemental oxide percentages with loss on ignition (LOI) subtracted.

Yield-normalized XRF counts had a positive linear correlation with ICP-MS elemental oxide compositions of SiO_2 and Al_2O_3 (Fig. 10). Most data fell within one standard deviation of the mean trend line. A normalized composition of percent silica (biogenic or diagenetic) and detritus (aluminosilicates and detrital quartz) were then converted from percent oxides of SiO_2 and Al_2O_3 using Isaacs's (1980) equations developed for the Monterey Formation in the Santa Barbra coastal area.

$$\text{Biogenic + Diagenetic Silica \%} = SiO_2 - (3.5 \times Al_2O_3) \qquad \text{Eqn. 1}$$

$$\text{Detritus \%} = 5.6 \times Al_2O_3 \qquad \text{Eqn. 2}$$

The equations generated from Isaacs (1980) are good estimates of relative components, however, it is likely that Isaacs's (1980) equations slightly underestimate silica and slightly overestimate detritus in the San Joaquin Basin. This because detritus of the San Joaquin Basin is expected to have greater amounts of quartz and albite feldspars, both with lesser aluminum to silica ratios than mixed-layer illite-smectite of the Santa Barbra Basin.

a

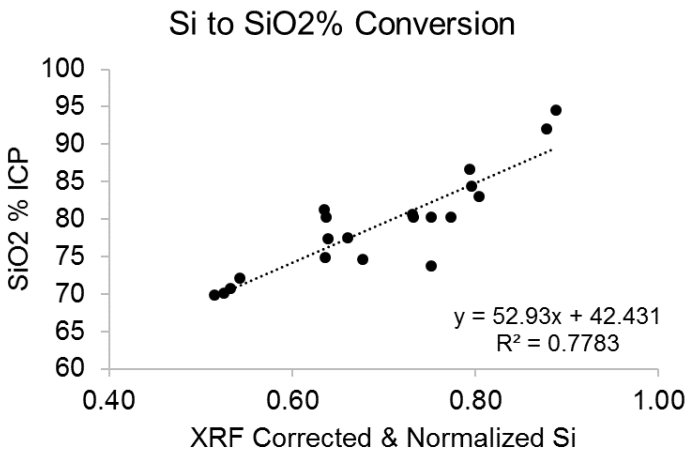

b

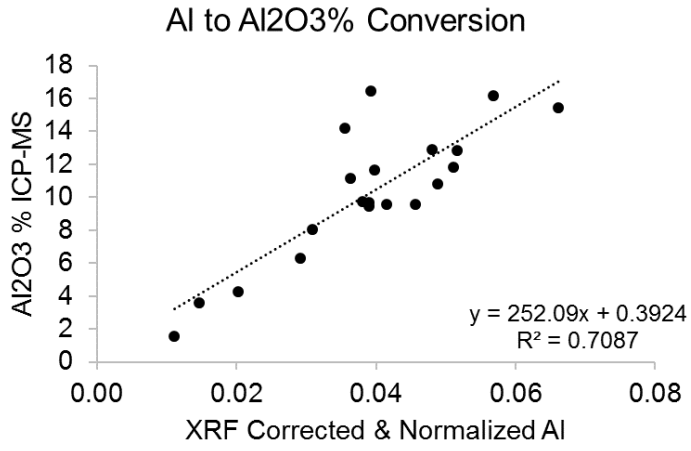

FIGURE 10. Regression of non-calcareous samples for the conversion of fluorescence yield-corrected and normalized XRF counts vs percent oxide from ICP-MS analysis for (a) silicon to SiO_2 and (b) aluminum to Al_2O_3.

Hardness

A Proceq Equotip Piccolo 2 tester with a type-D impact tip was used to measure Leeb-hardness type-D (HLD) values. The Piccolo tester releases a 3mm diameter spring-loaded tungsten-carbide tipped impact probe onto the surface the core then measures, calculates, and records an HLD value (Fig. 11; Kompatscher, 2004). The Single Impact Method was carefully followed to reduce variability and make measurements consistent with other recent hardness studies (Lee et al., 2014; Ritz et al., 2014). Lee et al. (2014) and Ritz et al. (2014) have developed widely used techniques for hardness testing and discussed important considerations that can influence quantitative results. For example, halving sample thickness from about 5.1 to 2.5 cm may increase Leeb rebound hardness (HLD) variance and lower readings by approximately 50 HLD (Lee et al., 2014). Other variables such as core age, fluid saturation, and maximum vs current burial depth may also lead to inconsistencies. Care has been taken to reduce inconsistencies and for the most part, these effects are relatively minor and do not significantly impact the comparison of hardness between samples and formations. Common differences of 50 HLD are not usually statistically significant.

Hardness testing was taken at the same location and spatial resolution as XRF data by using a scale from line scan images recorded on the Avatech XRF scanner. In the case of dipping strata, I attempted to maintain HLD measurements within a single continuous bed or laminae set. Slabbed core samples within a PVC or metal sleeve were rested on a tray and firmly secured to a workbench (Fig. 11b).

Five to eight of the highest measurements taken across the central portion of the 2/3 section slabbed core were averaged to a single value. While over 12,000 measurements were taken, suspiciously low values, typically due to surface defects, were removed. A final 9,928

HLD measurements were averaged into 1,546 points and labeled by their associated silica phase or burial group for analsysis (APPENDIX C).

a

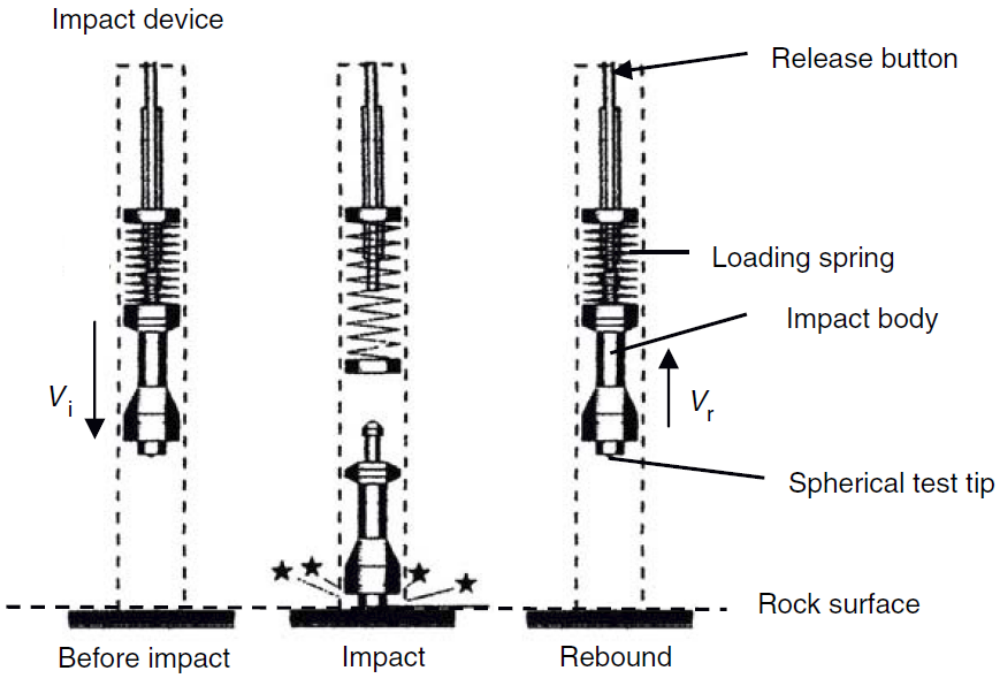

b

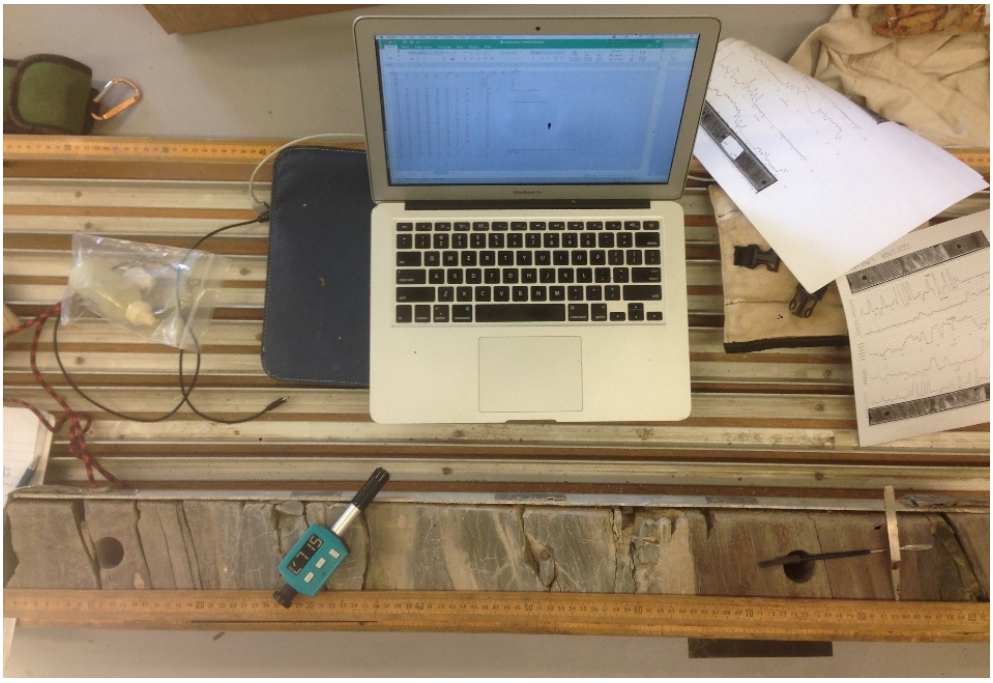

FIGURE 11. (a) Schematic of the internal design and function of the Proceq Piccolo rebound hammer (from Aoki and Matsukura, 2008). (b) Workstation of core testing set up and device for scale.

CHAPTER 4
RESULTS
Well Logs

Highly siliceous Monterey Formation rocks exhibit low gamma-ray API, high porosity, and low-density wireline log responses. Density and porosity logs commonly capture a variability of physical properties of siliceous mudstones due to (1) heterogeneous or cyclic bedding of contrasting compositions at <1 to 10's of feet and (2) the bulk shifts in silica phase or other diagenetic reactions with burial at intervals of 1000's of feet. Two steps in silica diagenesis are identified and correlated by a relatively abrupt increase in density and decrease in porosity (Table 3). Porosity from density (DPHI) is calculated from wireline logs via:

$$\Phi = \frac{\rho_{\mathrm{ma}} - \rho_{\mathrm{b}}}{\rho_{\mathrm{ma}} - \rho_{\mathrm{f}}} \qquad \text{Eqn. 3}$$

Equation 3: Alberty, 1992, Matrix density (ρ_{ma}) from core plug grain density within this study. Average grain density of opal-A and opal-CT rocks = 2.42 g/cm^3, average grain density of quartz-phase rocks = 2.52 g/cm^3. This differs from average grain density of pure silica mineralogy. Formation bulk density (ρ_b) taken from RHOB log value. Fluid density (ρ_f) = 1.

In the study area, opal-A intervals typically exhibit the highest porosity (average 63% DPHI) (verified by an average core plug porosity of 62.5%) and lowest bulk density (RHOB)(Fig. 12). In the 7122A-2 and 548D1-35N wells, the opal-A to opal-CT transition zone is identified by an initial rapid shift from 55% porosity to less than 49% porosity over a 185' to 200' thick interval, followed by a 315' to 400' section with a slower rate of porosity reduction to < 46%. A small gamma-ray (GR) increase of 10-15 API is observed over the opal-A to opal-CT transition zone due to the condensed volume of rock (Fig. 12).

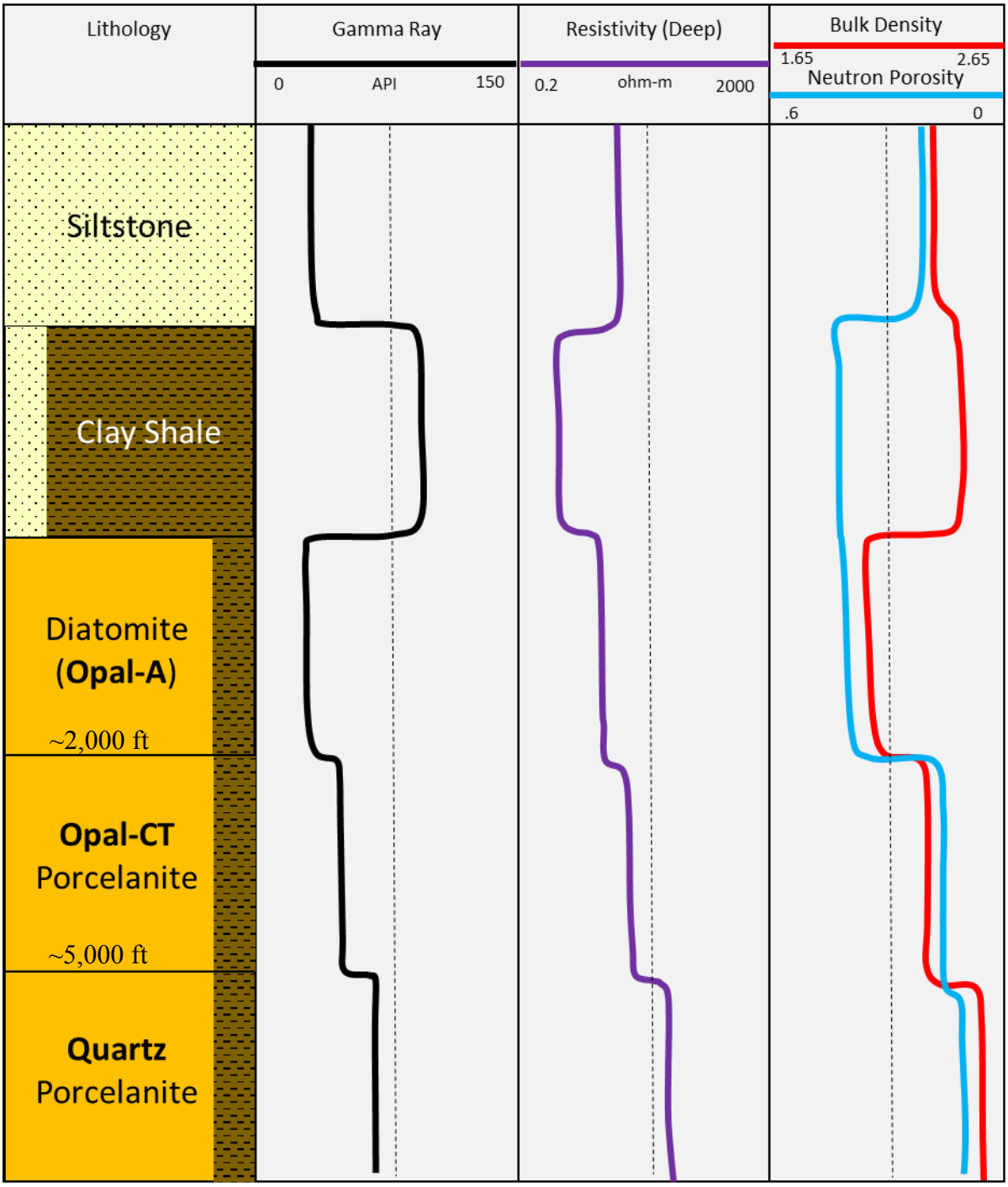

FIGURE 12. Generalized schematic of a Monterey Formation type log showing typical changes in the standard triple-combo wireline tools important to identifying silica phase and physical properties of siliceous mudstone reservoirs. (Leo Gianneta, personal communication, January 2018).

The bulk opal-CT interval has a consistent and stable log character with minor lithological variance within the Antelope Shale. In the Belridge oil field, the full 2000' to 2900'-thick opal-CT interval has limited penetration because the economic reservoir is typically limited to the opal-A interval. In the 882D-8 'Thorndyke' and the 856C-7 'Igor' wells, the base of the opal-CT zone and the top of the opal-CT to quartz phase transition are at 4525' and 5300' respectively. The offset of transition zones depths likely indicates some uplift in the Igor well, while the Thorndyke well is at or near the maximum burial depth (Fig. 8). The opal-CT to quartz phase transition zone in both wells is approximately 420' thick with an 18% to 20% reduction in porosity and a 30 μs/ft increase in sonic velocity.

Quartz-phase rocks (at 6000' - 9500' TVD) have a 10% to 15% DPHI and 2.3 g/cm^3 bulk density. An anomalous step in reduced porosity, increased density, and increased sonic velocity occurs between 9,640' and 10,950'. While this shift appears to be a typical response to physical and chemical compaction via silica diagenesis, the silica mineralogy is quartz phase above and below. The 12k'-quartz phase intervals of the Antelope Shale and McDonald Shale have the lowest porosity (<8% DPHI) and the fastest sonic velocities (70-80 μs/ft) of all of the wells.

TABLE 3. Typical Wireline Responses and Ranges of Each Silica Phase or Burial Group

Silica Phase	DPHI (%)	RHOB (g/cm^3)	Phase Base (ft TVD)	Transition Zone Thickness (ft)
opal-A	57 – 70	1.53	~1,600'	200' – 400'
opal-CT	35 – 43	1.90	~5,600'	420'
6k'-quartz	10 – 15	2.33	~9,640' *	1,310'
12k'-quartz	2 – 7	2.48	-	

Transition zone marks the top of the silica phase change. *Base of 6k'-quartz is top of anomalous step in quartz porosity loss.

Composition

XRD analysis confirms the silica phase of each burial group including the mixed opal-A+CT samples with approximately 13% opal-A and 87% opal-CT at ~1925' TVD. If the progression of silica diagenesis was derived from the degree of wireline porosity shift, the mixed opal-A+CT samples would be estimated to have 30% opal-A and 70% opal-CT; a slightly less developed transition than XRD estimates. XRD analysis confirms that the high-calcium samples excluded from the final results are 45-63% calcite and up to 5% dolomite. Opal-A and opal-CT samples contain a mean of 2.5 weight % detrital quartz. Detrital and diagenetic quartz are not differentiated in deeper samples. By unmagnified visual inspection, any sample with > 20% sand was excluded and interpreted as detrital quartz. Total clay typically ranges between 15-33 weight percent. Clay species were not differentiated by this study, but data provided to Aera Energy by a commercial laboratory indicate an average of 39% mixed-layer illite-mica, 34% illite-smectite, and 27% kaolinite at depths less than 7,000'.

Monterey Formation rocks in the Belridge oil field are compositionally heterogeneous and capture a wide range of siliceous composition as indicated by XRF counts normalized to biogenic and diagenetic silica weight percentages versus gross detrital weight percentages (Fig. 13). Opal-A and mixed-A+CT sample groups have a lower mean silica percentage of about 35% and range from 15-50% biogenic and diagenetic silica, whereas opal-CT and both quartz-phase sample groups have higher mean silica percentages of about 49% and range from 35-70% diagenetic silica (Fig. 13). Following Isaacs (1981a) classification, rocks with less than 50% silica are classified as opal-A diatomaceous mudstone or opal-CT and quartz-phase siliceous mudstone. Samples with greater than 50% silica in opal-CT and quartz-phase are classified as

porcelanite. Very pure silica chert samples (>95% diagenetic silica) were not captured in this study.

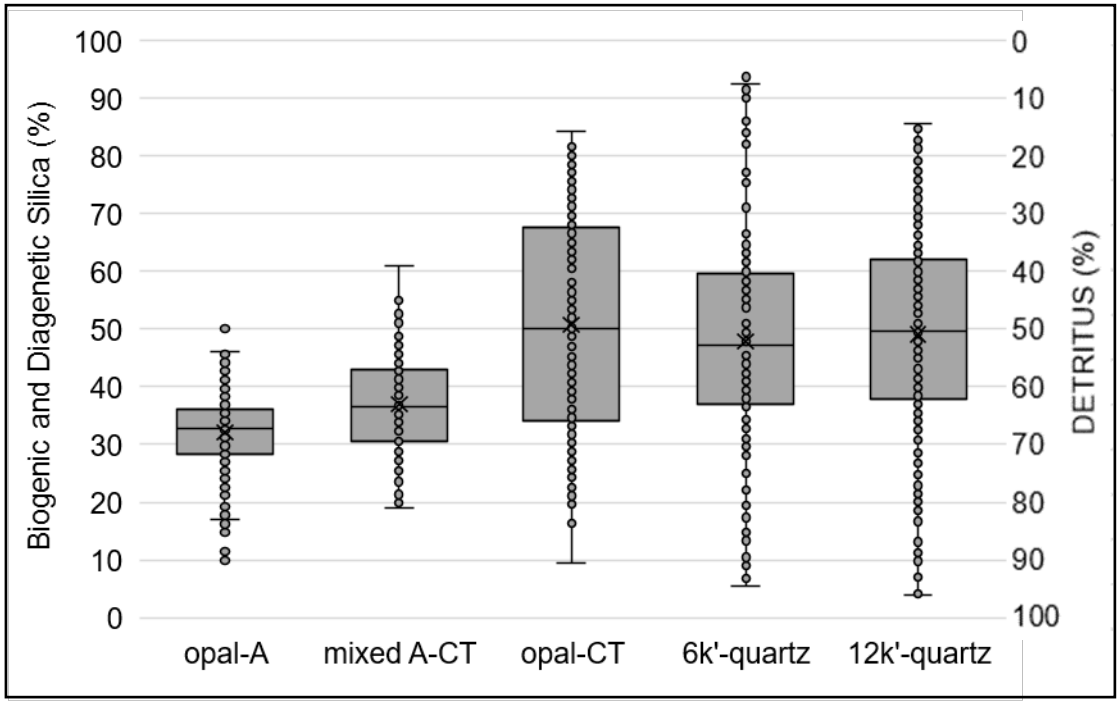

FIGURE 13. Normalized weight percent of biogenic and diagenetic silica and detritus for each sample group presented in Tukey box and whisker plots. Limits to each of the maximum whiskers plotted are 1.5 x Inner Quartile Range.

Matrix Porosity

A relatively distinct and narrow range of both core plug and wireline calculated porosity is associated with each diagenetic stage or burial group. Opal-A samples have the highest porosity and 12k'-quartz samples have the lowest porosity (Fig. 14). Porosity loss from silica diagenesis is seen in the step from opal-A to opal-CT and then opal-CT to 6k'-quartz. Within each group except the 12k'-quartz group, porosity variation follows a positive linear trend relative to percent biogenic and diagenetic silica. High silica-detritus ratio opal-CT samples have the highest porosity while lower silica samples have up to 22 percent points lower porosity (Fig.

14). The porosity of the 12k' quartz group is exceptionally low with little variation across the entire range of silica-detritus ratios.

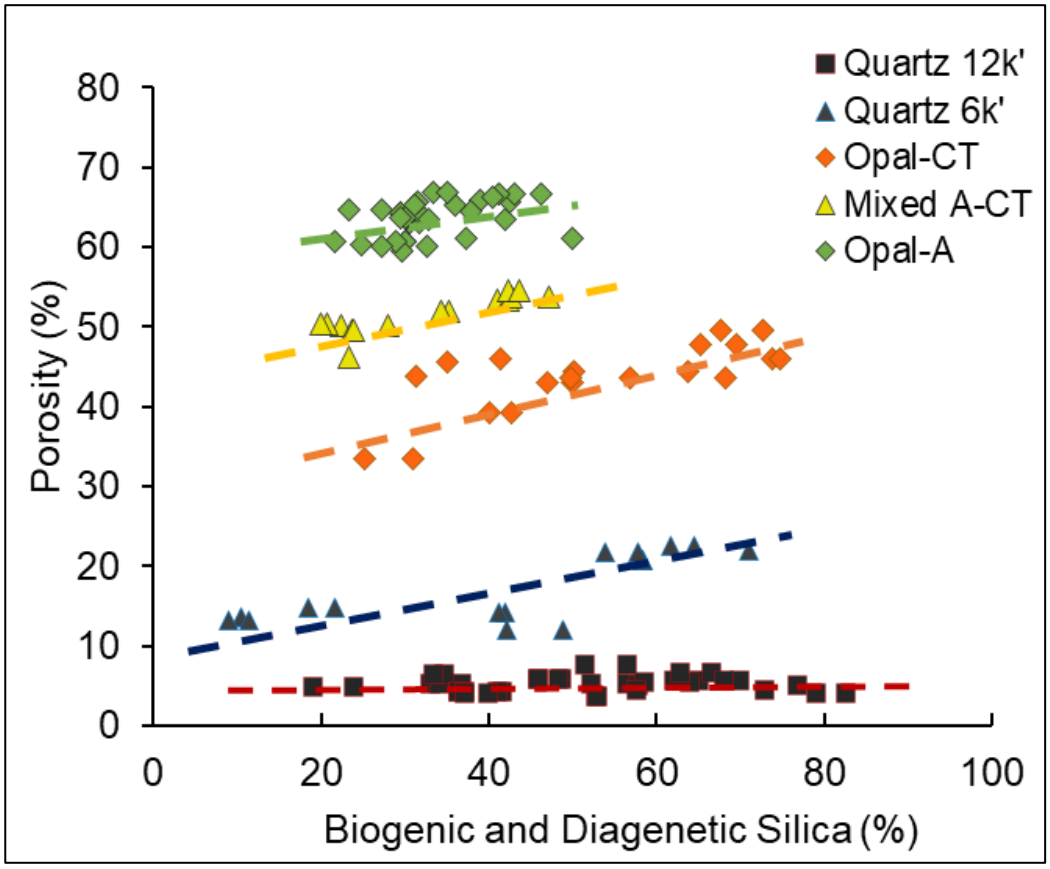

FIGURE 14. Core plug porosity in each sample group with dashed log trend correlating composition and porosity. Note the flattened trend and <8% porosity across all percentages of silica in 12k'-Quartz rocks.

Hardness

Monterey Formation siliceous mudstones increase in hardness with each increasing step of diagenesis. Each phase also has a distinct range of hardness relative to composition (Fig. 15). Variations between hardness and silica-detritus ratios have a positive association and strong linear trend in every sample set except for the limited compositional range dataset for opal-A (Fig. 15).

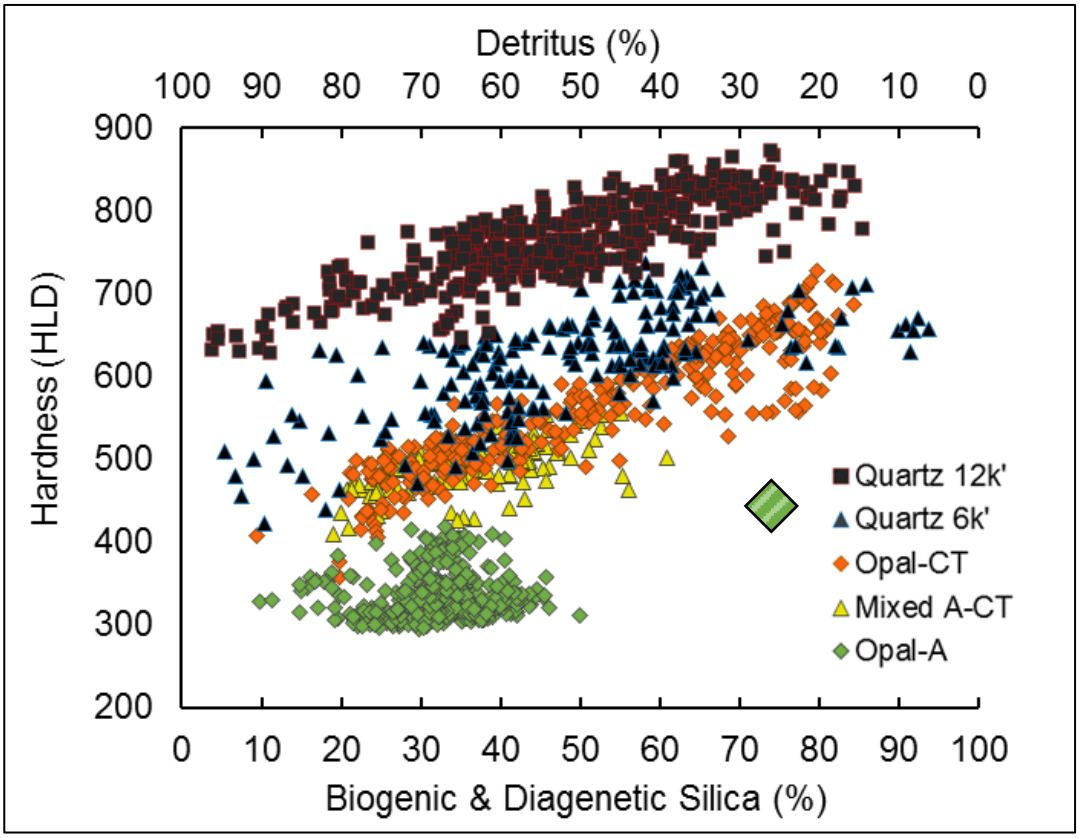

FIGURE 15. Data for >2000 average points in five burial groups relative to hardness (HLD) and silica and detritus derived from high-resolution XRF scanning. The hardness of each burial group progressively increases and follows a compositional trend associated with its group. Opal-A samples with greater than 50% silica were not encountered in the cores analyzed. The large hatched-green diamond represents a conservative estimate of > 70% silica opal-A HLD measurements taken from outcrop samples.

TABLE 4. Summary of Hardness Data

Silica Phase	Mean Sample Depth	Mean % Silica Biogenic or Diagenetic	Mean HLD of 50-60% silica	Min HLD	Max HLD	HLD Range
opal-A	1,207’	33.9	334	296	410	124
mixed A+CT	1,924’	39.8	505	410	600	191
opal-CT	3,176’	49.9	534	357	728	371
6k’-quartz	6,124’	54.7	603	423	737	314
12k’-quartz	12,526’	50.0	755	628	872	244

Data are associated with Fig. 15, excluding opal-A hand sample data.

Opal-A samples have very little to no trend with composition and have the lowest and narrowest range of HLD values. Since no high-silica samples were available from the opal-A cores, three outcrop samples with >70% biogenic silica composition were measured for approximate comparison. Samples have rebound hardness values ranging from 400 to 480 HLD, suggesting a higher HLD in clean and dry diatomite (Fig. 15 hatched diamond). Mixed opal-A+CT samples increase on a scale and trend similar to opal-CT.

Opal-CT samples have the largest range of hardness values (370 HLD) and greatest rate of change relative to silica and detritus (Fig. 15). Opal-CT samples from two burial depths (2,200' and 3,600') in the same well have equal offset along the same compositional trend despite 1,300' of additional burial (Fig. 16).

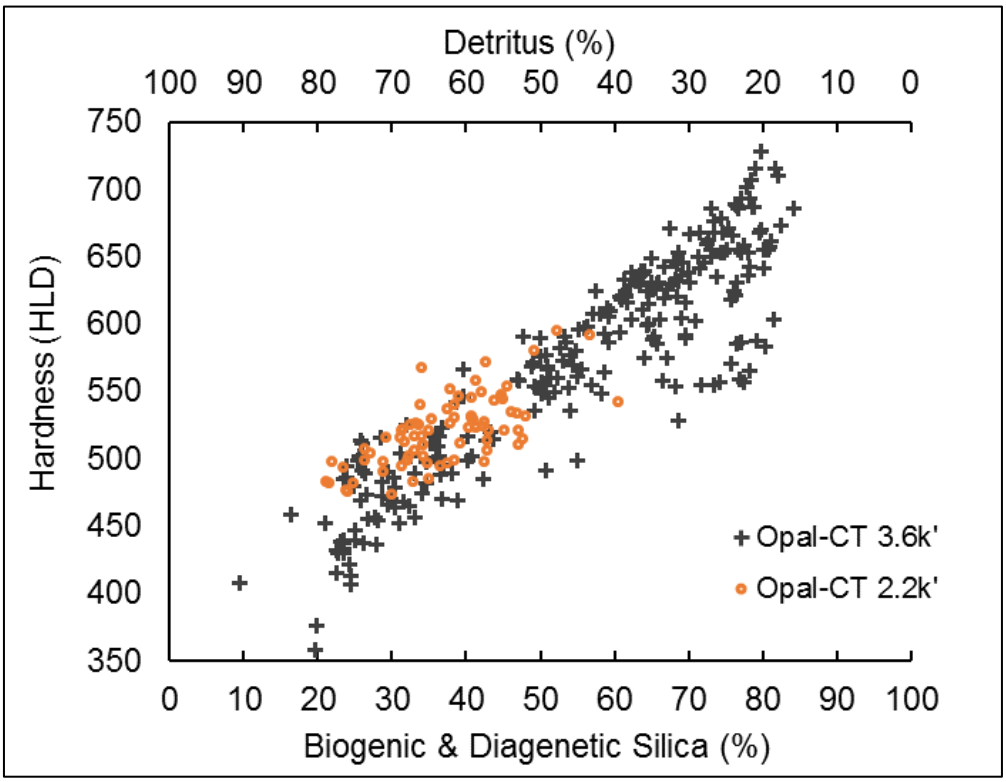

FIGURE 16. Scatter plot similar to Fig. 14 of HLD and percent silica for opal-CT samples of the same well at 2,200' and 3,600' burial depths.

Hardness in 6k'-quartz samples is considerably scattered, possibly due to highly heterogeneous bedding (Fig. 15 & 17) and minor calcium interference in XRF measurements. On average, HLD is 20% greater in 12k'-quartz samples than 6k'-quartz phase samples. Overall, hardness is the highest in 12k'-quartz samples for any compositional range (maximum 872 HLD).

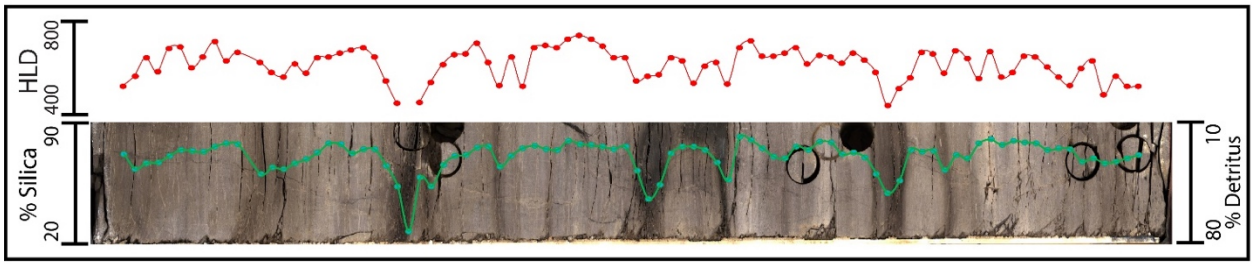

FIGURE 17. Percent silica and hardness (HLD) over an opal-CT core sample demonstrate the mechanical heterogeneity of thinly interbedded rocks of different compositions. Well is 548D1-35 from 3466.5'-3469.5' (opal-CT).

The diagenetic transition from opal-A to opal-CT has the greatest increase in mean hardness (+220 HLD). Opal-CT to quartz phase has a lesser increase in hardness (+60 HLD). Between 6k'-quartz and 12k'-quartz samples there was additional burial, porosity loss (Fig. 14), and hardening (+148 HLD) without a change in silica phase.

Beds of volcanic ash and high-calcium samples are excluded from siliceous mudstone categories but are encountered frequently enough to note. Ash beds, typically 1-3 cm thick, are planar to irregular (possibly redeposited), friable, and weak with a mean of 280 HLD. High-Ca samples at 6k' have a mean of 656 HLD and 21% porosity. At 12k', high-Ca beds have a mean 748 HLD and 2% porosity.

The compositional influence on each burial group does not affect mechanical behavior at the same rate (Fig. 18). The rate of change in hardness relative to the change in composition was

greatest in opal-CT, lowest in opal-A, and less consistent in 6k'-quartz phase and mixed-A+CT samples. The hardness of opal-CT and 6k'-quartz phase samples are equal at > 70% silica. The 6k'- and 12k'-quartz phase samples over 60 to 70% silica approach an asymptotic relationship with HLD (Fig. 15 and 18), suggesting a maximum hardness at over 70% silica.

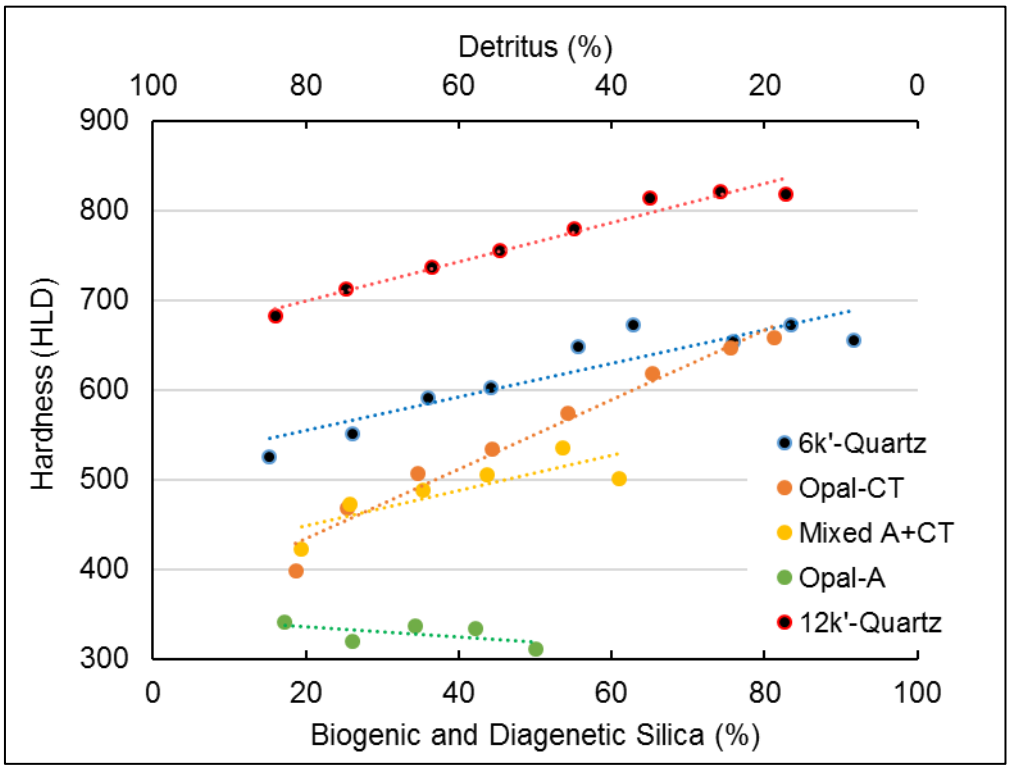

FIGURE 18. Data from Fig. 14 grouped as mean HLD in classes of 10% compositional ranges for trend comparisons. See Table 5 for log trends and Appendix C for classes and data values.

TABLE 5. Hardness Log Trends to Accompany Fig. 18.

Sample Group	Log Trend of mean HLD points	Correlation of determination (R^2)
opal-A	HLD=-0.55 x (% Si) + 346.91	0.33
mixed opal-A+CT	HLD= 1.99 x (% Si) + 408.24	0.71
opal-CT	HLD= 3.88 x (% Si) + 356.33	0.97
6k'-quartz	HLD= 1.86 x (% Si) + 517.38	0.83
12k'-quartz	HLD= 2.18 x (% Si) + 655.86	0.97

Opal-CT has the tightest correlation and greatest HLD rate of change with composition.

CHAPTER 5

DISCUSSION

This high-spatial-resolution investigation of the hardness of siliceous mudstones in the Monterey Formation allows quantification and consideration of reservoir heterogeneity at a scale commonly seen in core and outcrop, but difficult to characterize with wireline or core plug data. I compare these results to data from other shale formations, discuss the fundamental controls of rebound hardness, and relate hardness to fractures viewed in core and outcrop.

A key assumption is that hardness is well correlated to other geomechanical characterizations such as sonic velocity, brittleness, and unconfined compressive strength (Murray, 2015; Yang et al., 2015; Aoki and Matsukara, 2008; Lee et al., 2014; Lee, 2015). Low hardness rocks are most likely to deform ductility, to inhibit fracture propagation, and/or to lead to proppant embedment (Sonnenfeld et al., 2015). These implications are most significant where low and high hardness rocks are interbedded, influencing the style and timing of fractures in a mechanically stratified succession.

Comparisons to Other Mudstone Hardness Studies

The hardness of siliceous mudstones of the upper Monterey Formation shares many similarities and trends with other North American unconventional shales plays (Fig. 19 & Table 6). Foremost, it is consistently found that that composition is a 1st order control of rock hardness. Argillaceous components have a strong negative correlation with hardness and biogenic or authigenic mineralogy of stiff minerals (dolomite, calcite, opal-CT, quartz, and pyrite) typically increases hardness (Ritz et al., 2014; Rolfs, 2015; Murray, 2015; Offurum, 2016; Becerra-Rondon, 2017; Dong et al., 2017). Lithotypes offer additional compositional context where quantitative mineralogical data are not available for comparison, (Fig. 19). In every case, each

lithotype maintains a range of values influenced by clay content. For example, the hardest values from the thinly laminated pyritic & siliceous lithotypes of the Horn River Formation are predominately composed of pyrite and authigenic quartz, while the lowest HLD values are predominately clay-rich with only minor disseminated components of pyrite and authigenic quartz. In the Monterey Formation, this compositional trend is sustained throughout successive stages of burial and diagenesis.

Direct comparisons to other formations are difficult because burial histories are dissimilar between basins and even locations for the same formation. Some samples have experienced deep burial and significant uplift as indicated by thermal maturity and diagenetic state, but the maximum burial depth is not considered (or known) for each formation referenced here (Fig. 20). We note that each study tested intervals that represent their respective source-rock reservoir properties at whatever depth they occur and simply focused on variations in mineralogy, organic matter, and fabric or texture. There was typically little consideration to the effect that burial history has on hardness. This study of the Monterey Formation captures siliceous mudstones in an early burial state, not possible with the other formations and it demonstrates how hardness evolves through progressive burial and diagenesis.

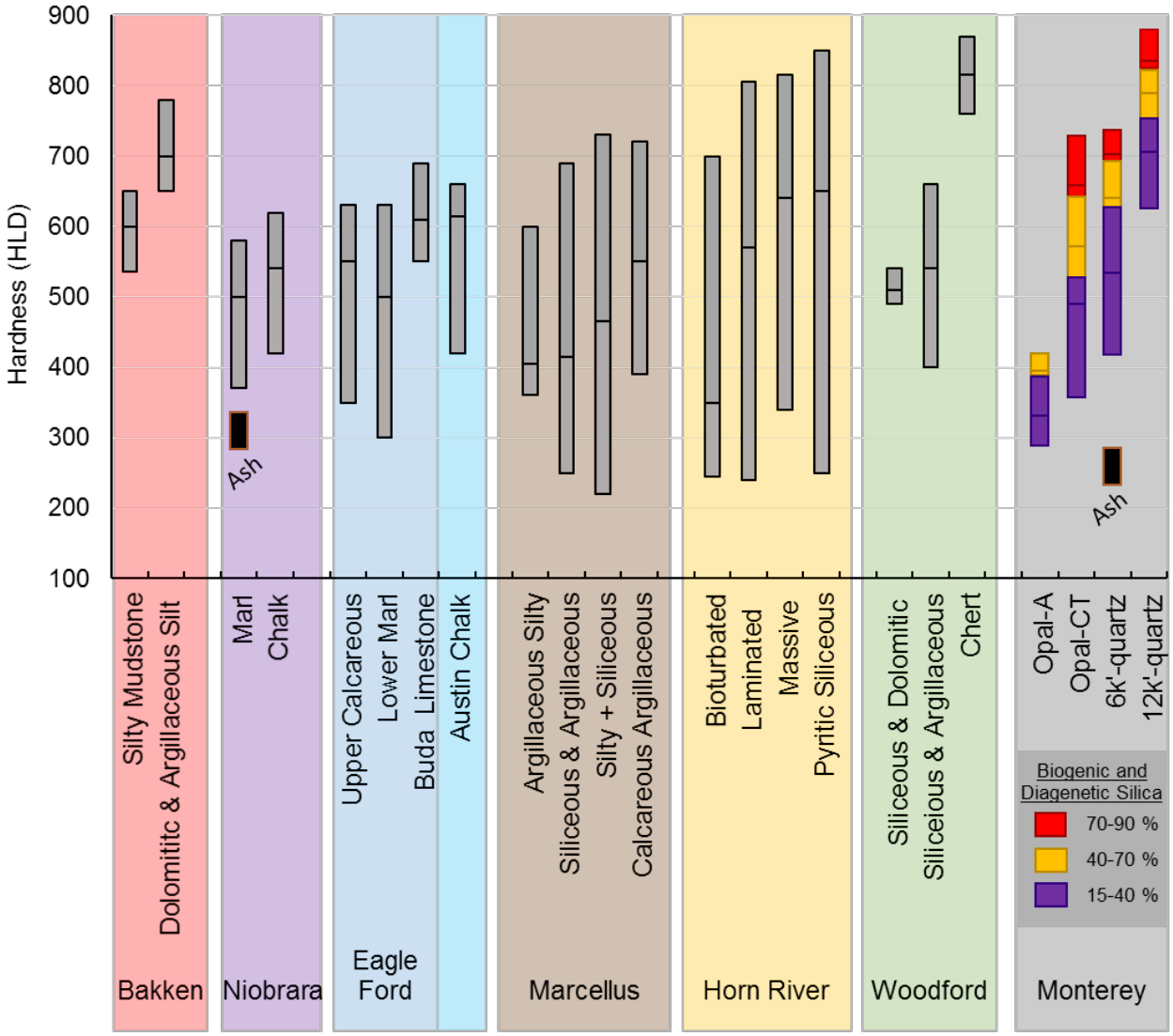

FIGURE 19. Range and median (horizontal lines) of Leeb hardness for seven North American shale plays subdivided by lithofacies. Monterey Formation samples are displayed by burial group and colored categories based on silica %. Within each lithotype, there is a strong negative correlation with clay mineralogy, similar to the Monterey Formation. Thus, the most argillaceous or detritus-rich sediments of each lithotype would match the lowest hardness values. Also, ash beds with extremely low HLD values from the Monterey and Niobrara are independently plotted. (Compiled from Ritz et al., 2014; Rolfs, 2015; Murray, 2015; Offurum, 2016; Becerra-Rondon, 2017; Dong et al., 2017).

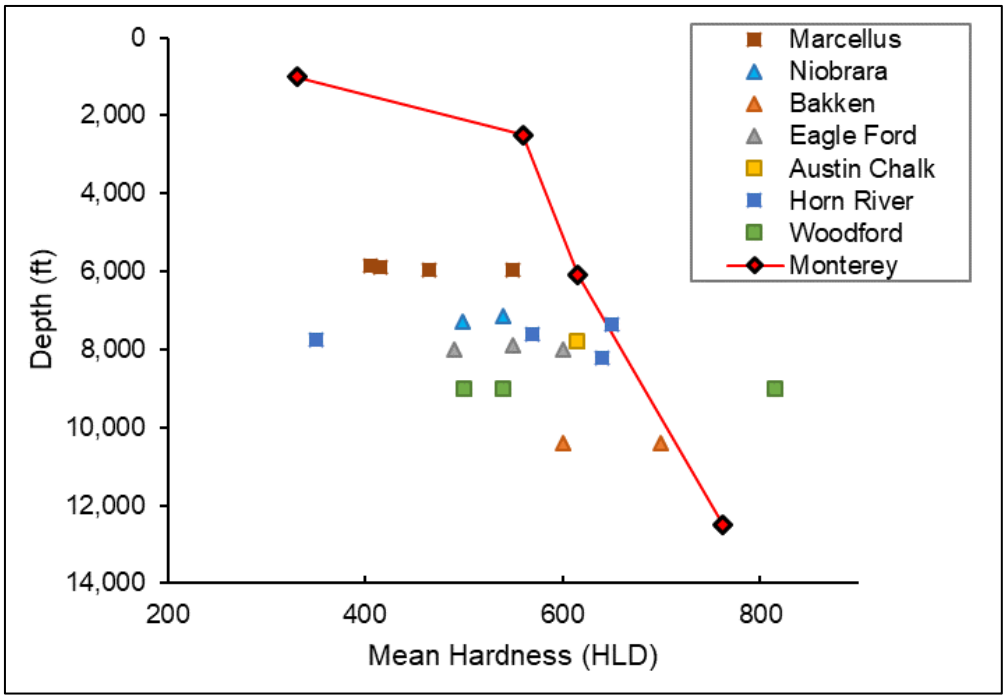

FIGURE 20. Mean hardness per depth for each of the 8 formations and their lithotypes (Table 5). Trend (red) links the highly siliceous mudstones of the Monterey Formation.

Opal-A

Opal-A diatomaceous rocks in the Monterey Formation have lower mean hardness values than opal CT or quartz lithotypes. Diatomaceous mudstones of the upper Monterey Formation have a porosity of 55-70%, a maximum burial depth of ~2,000 ft, and an age of 5.5 – 6.5 Ma. Mudstones from other formations compared here have a porosity of <10%, are buried to >8,000 ft, and are 10's to 100's of millions of years older. In these other mudstones, all original opal-A mineralogy would have been transformed to quartz-phase silica. Yet, Monterey Formation opal-A rocks share equal hardness to some detritus-rich mudstones of the Marcellus and Horn River Formation. Their significance in comparison is that both low-hardness lithotypes are fracture inhibiting units. Opal-A rocks are known to be fracture barriers when juxtaposed against much harder opal-CT rocks (Gross, 1995; Lockman, 2012). The low hardness lithotypes of the Horn

River and Marcellus likely have the same influence in creating a boldly contrasting mechanical stratigraphy within those successions.

Opal-CT

Opal-CT rocks are as hard as or harder than many mudstone rocks from other formations although they occur at shallower maximum burial depths. Opal-CT rocks have a range of hardness (about 370 HLD) and a potential mechanical heterogeneity similar to many other shales. Opal-CT samples of >70% silica have a hardness of about 650-725 HLD, which is equal to or greater than the most silica-rich or carbonate-rich intervals of the Marcellus Formation, Niobrara Formation, Eagle Ford, or Austin Chalk, all of which are known - and relied upon - to strain with brittle fractures at greater depths. Notably, lower hardness opal-CT rocks of 370-515 HLD are similar to the marls of the Niobrara and Eagle Ford, or clay-rich intervals of the Marcellus and Woodford shales. Each of these lower hardness shales have been shown to exhibit shear failure, fracture inhibition, and low fracture intensity (Murray, 2015; Ritz et al., 2014; Offurum, 2016; Becerra-Rondon, 2017) similar to the behavior of clay-rich opal-CT siliceous mudstones established by Monterey Formation outcrop studies (Gross, 1995; Strickland, 2013). The analogous geomechanical behavior of opal-CT rocks and other shales with similar HLD values supports the assumption that HLD measurements can be translated to mechanical properties and extended beyond a local set of data.

Metastable opal-CT mineralogy is rarely found in rocks older than Cretaceous or buried more than a few thousand feet. Thus, the most relevant comparisons are to other well-studied unconventional shale reservoirs are from quartz-phase mudstones at similar burial depths (6k'-quartz and 12k'-quartz Monterey Formation rocks).

6'k-Quartz

Quartz-phase rocks of the upper Monterey Formation are as hard as, or typically harder than, most other more deeply buried shales. Highly siliceous intervals of the 6k'-quartz section are harder than any of the highly calcareous lithotypes of the Niobrara, Eagle Ford, or Austin Chalk (Ritz, 2014; Murray, 2015). For example, Niobrara chalks with a high mineralogical purity (70 – 90% calcite mineralogy) and >8,000' total burial, have a lower HLD than Monterey 6k'-quartz rocks with just greater than 50% silica and about 6,150' of burial (Fig. 15, 19, & 20; Murray, 2015). This suggests that authigenic or diagenetic quartz has a greater rebound hardness than calcite. Similarly, Hue et al. (2015) found that quartz mineralogy produces more brittle rocks than calcite. Hardness and rock mechanics is not a sole function of mineralogical purity or an absence of detritus in the way that some mineralogical brittleness indexes propose (Jarvie et al., 2007; Wang and Gale, 2009).

In the Monterey Formation, diagenetic or authigenic quartz is very effective at hardening. Just 15% diagenetic quartz in 6k'-quartz samples creates a higher minimum and median hardness lithology than detrital-rich and more deeply buried intervals of the Marcellus, Horn River, and Eagle Ford shales (Fig. 19). The Woodford Shale samples studied by Becerra-Rondon (2017) are a very interesting comparison to 6k'-quartz rocks as they have a very similar silica:detritus ratio and are also thermally immature. Much of the Woodford Shale has a similar HLD range to 6k'-quartz rocks and possibly only of a lower maximum hardness by lesser volumetric percentages of authigenic silica due to higher weight percentages of TOC (Fig. 19; Becerra-Rondon, 2017). Shales with greater HLD than high-silica 6k'-quartz rocks are associated with a non-calcite authigenic cement (quartz, dolomite, and/or pyrite), and/or are have greater burial and thermal maturity (the gas-rich Marcellus and Horn River shales) (Fig. 19). The contrasts in burial depth,

porosity, and thermal maturation that make 12k'-quartz phase samples a better comparison to other source-rock reservoir shales.

12'-Quartz

12k'-quartz-phase rocks of the upper Monterey Formation are some of the most consistently hard successions of fine-grained mudstones known to exist. They have similar burial depths and physical properties to fracture-dependent source-rock reservoirs elsewhere in North America. The least hard and most detritus-rich 12k'-quartz samples from the Monterey Formation are frequently as hard or harder than the bulk of Niobrara, Eagle Ford, Austin Chalk, Bakken, and Woodford Shale lithotypes (Fig. 19). 12k'-quartz rocks with >40% silica are also harder than most of the measured siliceous intervals of the Marcellus Formation and equal to or greater than most of the Horn River Formation. Overall, 12k'-quartz rocks with greater than 70% silica are immensely hard, with a mean 820 HLD that is only comparable to Woodford Shale chert. In fact, many deep and hard Monterey shales have often been identified as "argillaceous cherts" in subsurface mudlogs (Richard Behl, personal communication, September 2017).

Chert

Cherts are discussed separately as they are exceptionally hard rocks identified in many formations and stratigraphic depths. They have potential to be formed in relatively shallow diagenetic reactions by pore-filling cementation or carbonate replacement (Behl and Garrison, 1994), which may not undergo much additional compaction or hardening.

Cherts of the Woodford Shale are measured as uniquely hard lithotypes with a mean 815 HLD. Woodford Shale cherts are black to dark-grey with conchoidal fractures sets similar to those encountered in the Monterey Formation (Becerra-Rondon, 2017; Behl and Garrison, 1994). Cherts of both formations are a high-purity microcrystalline siliceous rock with < 3% porosity

and < 5% TOC. Both cherts are known to have a high intensity of vertically fractured brittle strain in outcrop as opposed to a lesser strain intensity in lower hardness siliceous shales (Gross, 1995; Becerra-Rondon, 2017). Although chert samples (>95% diagenetic silica) were not encountered in the cored intervals of this study, deformational style in outcrop and subsurface core indicate that Monterey Formation cherts have an extremely hard and brittle character (Belfield, 1983; Dunham and Blake, 1987; Behl and Garrison, 1994). Cherts are typically associated with many of the most highly productive and permeable zones of the Monterey Formation and in core and outcrop, many macro- and microfractures are commonly open and coated with petroleum or sealed with clear silica cement (Schwalbach et al., 2009).

Cherts of opal-CT and quartz phase should have no difference in rebound hardness just as highly-siliceous opal-CT and 6k'-quartz phase porcelanites have no significant difference in rebound hardness associated with their mineralogy. We expect cherts of the Monterey to have an equal hardness to Woodford Shale cherts (Fig. 19).

Ash Beds

Ash beds exhibit the lowest hardness (230 HLD to 340 HLD) for any single lithotype providing significant contrast to adjacent beds of most other rocks (Fig. 19). Discrete ash beds in the 6k'- and 12k'-quartz core sample sections frequently occur at roughly 5- to 10-foot intervals. Hardness testing is difficult due to their low competencies and thinness – typically 1-4 cm. HLD values in the Monterey Formation are very similar to the volcanic ash altered to bentonite in the Niobrara (about 320 HLD), which inhibit fracture efficiency by promoting fracture step-over and promote proppant embedment (Sonnenfeld, 2015).

TABLE 6. Aggregated Shale Data Associated with Fig. 19

Formation Common Member	Lithology or Facies	Depth (Approx. Feet)	Hydrocarbon Type	Porosity (%)	HLD mean	HLD min	HLD max	Source
Bakken Middle	Dolomitic to argillaceous siltstone	10,415	Oil	5-10**	700	650	780	Rolfs (2015)
Bakken Middle	Silty shale	10,400	Oil	n/a	600	535	650	Rolfs (2015)
Austin Chalk	Chalk	7,800	Oil	8-25**	615	500	660	Ritz et al. (2014)
Eagle Ford Upper	Calcareous mudstone	7,900	Liquid-rich	2-11**	550	380	630	Ritz et al. (2014)
Eagle Ford Lower	Limestone	8,000	Liquid-rich	2-11**	600	520	640	Ritz et al. (2014)
Eagle Ford Lower	Marl	8,000	Liquid-rich	2-11**	490	380	550	Ritz et al. (2014)
Horn River	Pyritic mudstone	7,350	Gas	5.4	650	250	850	Dong et al. (2017)
Horn River	Massive mudstone	8,200	Gas	5.3	640	340	815	Dong et al. (2017)
Horn River	Laminated siliceous mudstone	7,611	Gas	4.6	570	240	805	Dong et al. (2017)
Horn River	Bioturbated mudstone	7,740	Gas	4.4	350	245	700	Dong et al. (2017)
Woodford Shale	Siliceous Shales, fissile laminated	9,000 *	immature	4-10**	540	400	660	Becerra-Rondon (2017)
Woodford Shale	Chert, hard and massive	9,000 *	immature	0-1**	815	760	870	Becerra-Rondon (2017)

TABLE 6. Continued

Formation Common Member	Lithology or Facies	Depth (Approx. Feet)	Hydrocarbon Type	Porosity (%)	HLD mean	HLD min	HLD max	Source
Woodford Shale	Siliceous-dolomitic shale	9,000*	immature	n/a	500	490	530	Becerra-Rondon (2017)
Niobrara Smokey Hills	Chalk	7,150	Liquid-rich	7-10	540	420	620	Murray (2015)
Niobrara Smokey Hills	Marl	7,300	Liquid-rich	n/a	500	370	580	Murray (2015)
Marcellus Ondaga & Lower	Calcareous argillaceous mudstone	5,970	Gas	4.0	550	390	720	Offurum (2016)
Marcellus Lower	Silty mudstone	5,950	Gas	7.9	465	220	730	Offurum (2016)
Marcellus Lower Base	Pyritic siliceous argillaceous mudstone	5,900	Gas	7.4	415	250	690	Offurum (2016)
Marcellus Cherry Valley	Packstone grainstone	5,860	Gas	3.0	700	660	710	Offurum (2016)
Marcellus Upper Marcellus	Argillaceous silty mudstone	5,840	Gas	6.0	405	360	600	Offurum (2016)

Data from published Leeb hardness studies on other North American unconventional shales. Min, max, and mean HLD values are presented with approximate depths from a typically larger range of sampling. Members are suggested by their common association for context, while hardness is mostly associated with lithology or facies type. *Woodford samples are from outcrop with an estimated max burial depth from reported %Ro values. **Porosity estimated from general literature.

Controls of Hardness

The siliceous mudstones of the Monterey Formation have a tremendous variance in hardness at any stage of burial. Our data show that rebound hardness is related to composition, diagenesis, and burial history. A solid understanding of the fundamental controls of hardness would allow effective utilization of the measured values to predict strain style and fracture intensity.

Composition

Composition is the primary control of hardness within any burial group of siliceous mudstones of the Monterey Formation. These findings are consistent with other studies on hardness (Ritz et al., 2014; Dong et al., 2017; Becerra-Rondon, 2017). Additionally, our results parallel the compositional relationship to natural fractures styles (Gross, 1995; Lorenz et al., 2002; Gale et al., 2014), unconfined compressive strength (Zoback, 2010), and Young's Modulus (Kumar et al., 2012) documented from mudstone studies of many other formations. While silica diagenesis or burial depth might be expected to be a principal control on hardness, transformations between silica phases generally only affect hardness by single-steps of 150-220 HLD (Fig. 21). Although the full range of hardness variance by diagenesis of a single composition mudstone may be greater than 400 HLD, the scope of a completion interval would typically only span one or a max of two diagenetic phases. Compositional variance of biogenic and diagenetic silica vs. clay-rich detritus within any one silica phase or burial depth can affect hardness by a range of 275-350 HLD (Fig. 21).

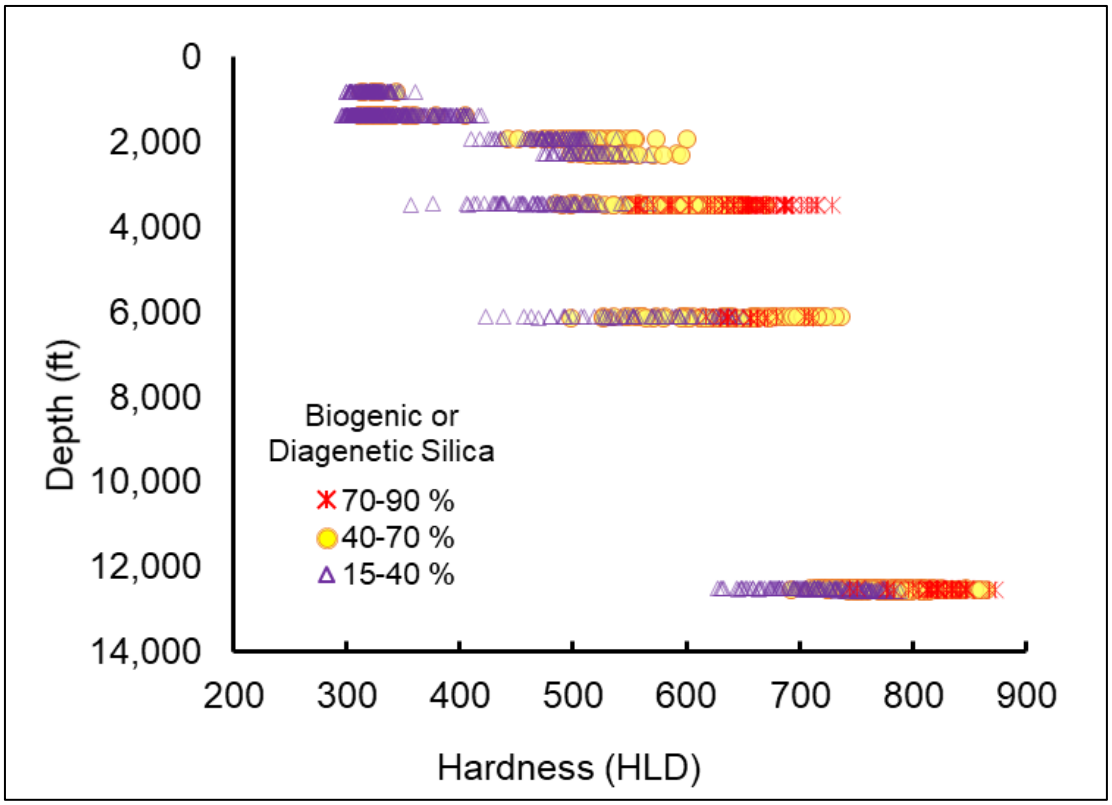

FIGURE 21. Hardness variation in each diagenetic or burial group represented by percent biogenic silica groups. The range of hardness variation in each group varies more by compositional differences than single differences in diagenetic stages or burial depth.

Diagenetic Silica

Diagenetic silica is considered a strong mineral (Gross, 1995) and the hardest rocks from each burial group have higher percentages of diagenetic silica. There is a strong positive correlation between diagenetic silica and hardness in opal-CT (R^2=0.83) and 12k'-quartz (R^2=0.67) (Fig. 15). Increasing the weight percent (and consequently volume percent) of diagenetic silica increases the amount of loading onto these stiff minerals while decreasing the amount of weak or ductile grain interaction in clay-rich detritus. Even at a low weight percentage (about 10-15%), diagenetic silica exists as a stiff and hard crystalline matrix component, having the ability to effectively bind and bridge non-silica components.

Yet, hardening by silica reaches an effective maximum at 70% silica for quartz-phase rocks and does not increase further with greater silica content (Fig. 15). This suggests that at >70% diagenetic silica, there is an interconnected silica framework with enough strong and stiff connections to mitigate the influence of ductile detritus components. Opal-CT rocks do not have a similar maximum HLD, possibly due to the higher porosity or different crystal geometry (Kassa, 2016) in opal-CT rocks that maintain the influenced of weak clay components at load-bearing junctions. The overlap in silica-rich opal-CT and 6-k'-quartz phase hardnesses implies that quartz-phase is not mineralogically harder than opal-CT silica (Fig. 18).

The weak positive correlation (R^2=0.46) of diagenetic silica and hardness for mixed-A+CT and 6k'quartz intervals may be obscuring the actual compositional relationship by measurement mis-ties. XRF core scanning indiscriminately measured overlapping compositions of thin and steeply dipping beds while HLD testing was focused on measuring within a single bed across the core (Fig. 22). Thus, in many instances, the XRF measurement of two beds or multiple laminae were attributed to a hardness of a single bed.

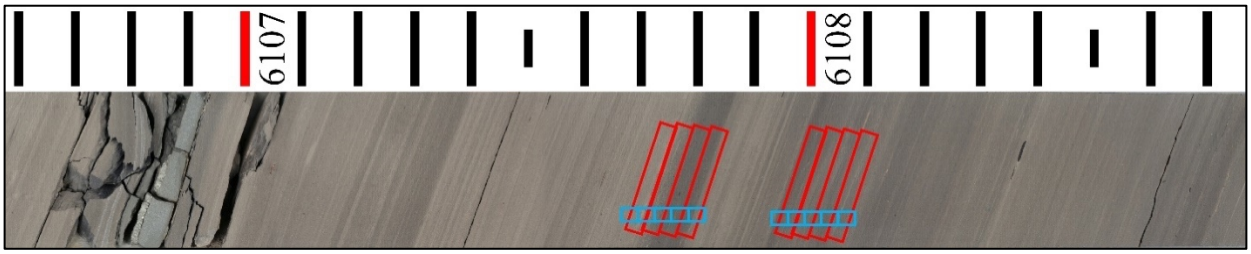

FIGURE 22. A 6'k-quartz (IGOR 856C-7) core in UV and plane light. Multiple thin laminations are dipping 18-20° from the vertically cored interval. XRF measurement in 1cm x 1cm (blue boxes) tested mixed compositions while hardness testing (red boxes) likely suffered a bias of testing a single bed more consistently.

Biogenic Silica

Opal-A, or biogenic silica, is of low hardness with no significant correlation to compositional percentages (Fig. 15). Defining opal-A as a soft, weak, or low strength lithotype is supported by observations of mode II (shear) fracturing in rocks of >47% biogenic silica (Gross, 1995). Rocks with any opal-A diatomaceous composition only joint in outcrop when mixed with >68% strong minerals (opal-CT and calcite) (Gross, 1995). Opal-A rocks tested in this study have lower HLD values than any of the most detritus rich opal-CT or quartz-phase samples and only most similar to ash-bed rebound hardness.

Although no samples of greater than 50% opal-A mineralogy were encountered and tested in core, outcrop-acquired hand samples with greater than 70% opal-A mineralogy were about 100 HLD higher and known to strain with brittle jointing in outcrop (Fig. 15; Behl and Garrison, 1994). However, it is recognized that the tested hand samples were very dry and never oil saturated. Saturation has a negative correlation with hardness (Josh et al., 2012) and may be very influential to opal-A rocks in particular due to extraordinarily high porosity (>50%) and thus volumetric saturation. It is uncertain at what compositional fraction opal-A becomes harder with greater purity.

Mixed opal-A+CT HLD results suggest that opal-A has a slightly higher rebound hardness than detrital components. Of rocks with equal weight percentages of opal-CT mineralogy, mixed opal-A+CT rocks at 1,920’ are a mean 5.4 greater HLD than samples with only opal-CT and detritus at 2,600’ (Table 7). However, because grain density of opal-A is less than opal-CT, there is a lower volumetric percent of opal-CT in mixed opal-A+CT rocks than completely altered opal-CT rocks. The slightly higher hardness in mixed opal-A+CT rocks may relate to the marginally greater HLD of opal-A compared with detritus or a strengthened mixed-

silica framework as suggested by Ishii et al. (2011). The projected HLD of a 100% detrital mudstone at opal-CT depths is similar to most opal-A rocks (Fig. 15, Table 7) and likely only harder due to an additional 1,350' of burial compaction.

TABLE 7. Comparison of Hardness in Samples with Similar Silica:Detritus Ratios

Silica Phase Interval	Mean Depth (ft)	Total Biogenic or Diagenetic Silica (weight %)	Opal-A (weight %)	Opal-CT (weight %)	Detritus (weight %)	Mean Hardness (HLD)
Opal-A	1,250'	0	0	0	100	330*
Opal-A	1,250'	45	45	0	55	331
Mixed-A+CT	1,920'	50	9	41	50	530
Opal-CT	2,600'	41	0	41	59	525
Opal-CT	2,600'	0	0	0	100	356*

Rows 3 and 4 have equal weight percentages of opal-CT, 9% variation of opal-A and detrital percentages, and no significant difference in HLD. *Projected HLD from Fig. 18 trends, suggest that pure-detritus rocks have similar HLD to 45% opal-A rocks.

Detritus

Clay-rich detritus creates weak rocks with lower hardness. There is a strong negative correlation between detritus and hardness that is opposite to the positive correlation between silica and hardness (Fig. 15). Using the normalized XRF elements of Al and K as proxies for clay, we substantiate that clay mineralogy is the foremost control of low hardness in diagenetically altered mudstones (Fig. 23).

There is little differentiation between the hardness of opal-A and clay-rich samples. This lack of trend implies that clay and opal-A constituents have an equal or similar rebound hardness as previously discussed. It is not understood why some opal-A samples are above the base trend of about 340 HLD. The small difference in hardness may be associated with a number of variances in rock fabric or texture, i.e., diatom packaging, fragmentation, sorting, or species, or a localized history of strain hardening and/or variable fluid saturation.

a

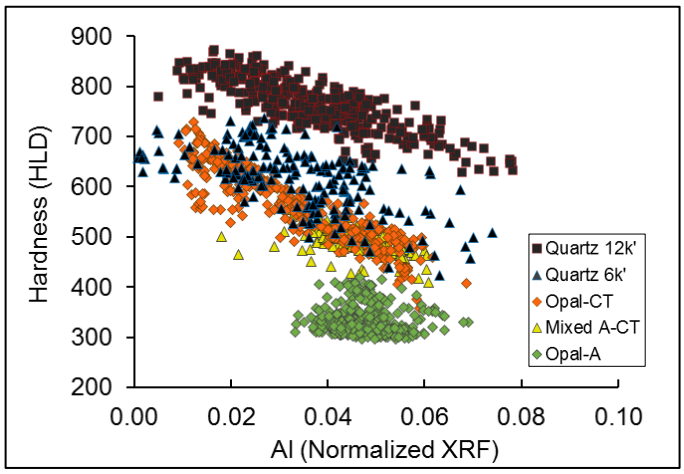

b

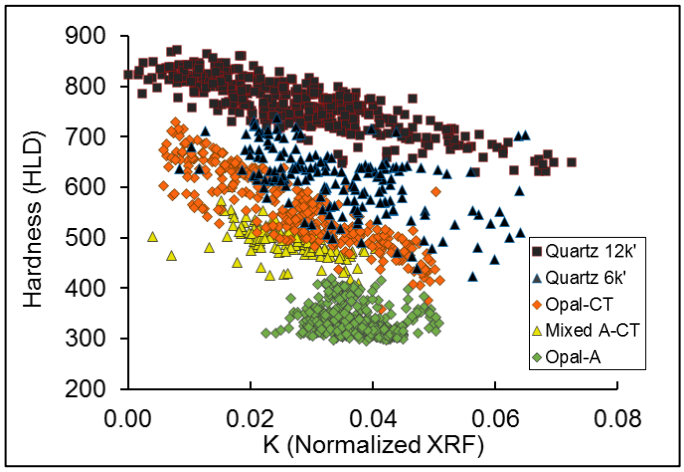

FIGURE 23. Hardness vs. (a) elemental aluminum and (b) elemental potassium XRF data with elemental X-ray yield conversion and normalization to total counts. Each element is a strong proxy for clay content in the Monterey Formation (Isaacs, 1980; Schwalbach et al., 2009). The negative correlations are inverse to the positive correlations with diagenetic silica as in Fig. 15.

Clay type can have very distinct and discrete effects on hardness. Bentonite is known to form from the alteration of volcanic ash beds in the Monterey Formation (Compton, 1991a). Identified by the UV fluorescence in core, montmorillonite-rich bentonites have extremely low hardness, often 550 to 300 HLD lower than surrounding siliceous mudstones (Fig. 19). Other studies have shown that bentonite layers can effectively increase mechanical heterogeneity and decrease the efficiency of fracture connectivity by inhibiting fracture propagation, permitting

proppant embedment, or promoting slip at bedding planes (Strickland, 2013; Sonnenfeld, 2015; Offurum, 2016) (Fig. 24). In terms of mechanical stratigraphy of the Monterey Formation, many bed-scale fractures terminate at bentonites that serve as mechanical layer boundaries.

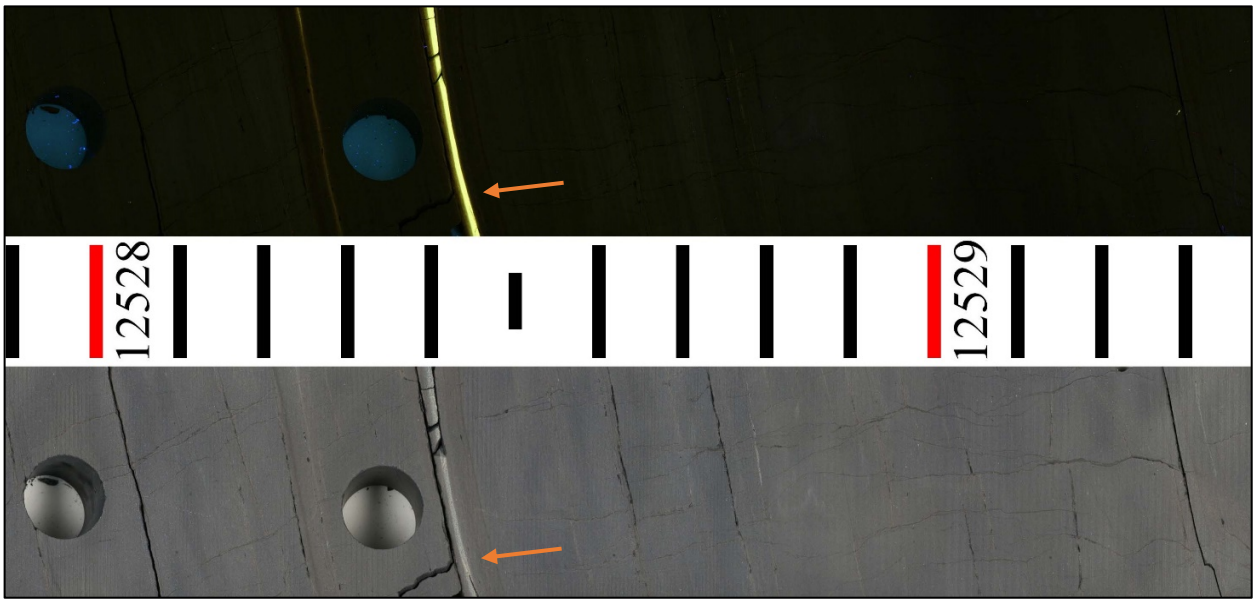

FIGURE 24. Core photo from 882D-8 (12k'quartz) in UV (above) and plain light (below). A 0.3-inch bentonite bed is at 12,528.4' (orange arrow). The bed is recessed and cracked from drying. This low hardness bed is a significant mechanical barrier to an open joint above. Swarms of 0.5 to 6 in-long sealed joints are abundant above and below the ash bed while no through-going fractures penetrate it.

Carbonate

Hardness associations with carbonate are more complex. Calcium is interpreted to be mostly affiliated with carbonate rather than Ca-plagioclase detritus due to the generally negative correlations between Ca and aluminosilicate components Si and Al (Fig. 25). An association of calcium and HLD is inconclusive (Fig. 26), suggesting that, at these compositions, carbonate is not a framework hardening mineralogy in the Monterey Formation and hardness is best defined in terms of the major mineralogical components of silica and detritus. In opal-CT samples, elevated hardness occurs in very low calcium counts (< 0.012 Ca), which are attributed to a predominance of greater than 50% diagenetic silica and low percentages of clay.

a

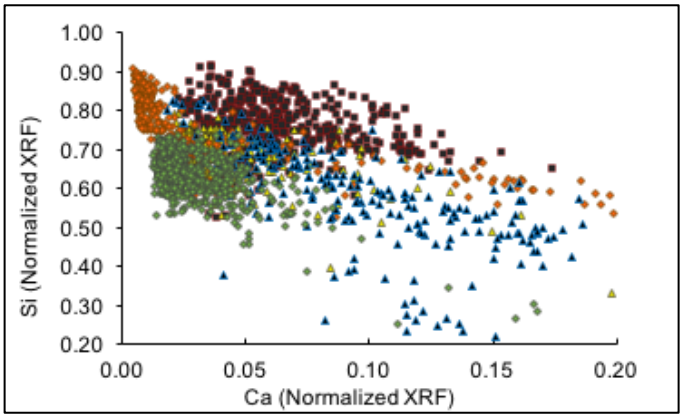

b

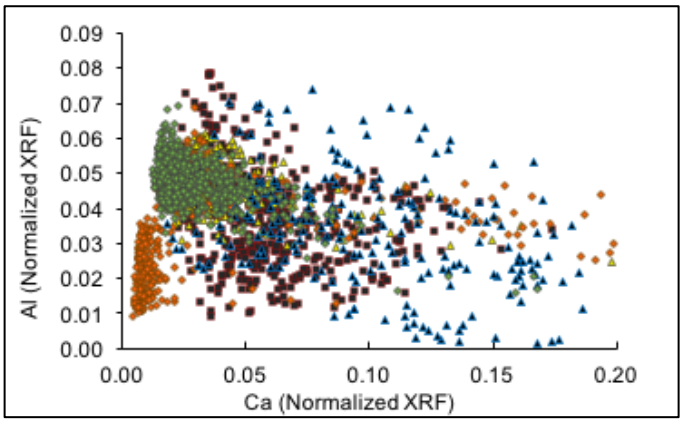

FIGURE 25. Association of normalized elemental calcium with major components of (a) Si and (b) Al in Monterey Formation siliceous mudstones.

Carbonate beds (often dolomitic) have a hardness of 700-800 HLD with no hardness trend associated with increasing Ca concentration (Fig. 26b). These beds with greater than 0.7 normalized elemental Ca in XRF results have been generally excluded from the analysis of siliceous mudstones and identified in XRD as calcite and dolomite mineralogy. Fractured carbonate beds are common in the 6k'-quartz interval and competent beds tested have an HLD equivalent to siliceous mudstones of greater than 50% diagenetic silica. However, with increased burial to 12k', carbonate beds do not increase in hardness (Fig. 26b). Burial-induced hardness appears to effect siliceous mudstones greater than carbonate mudstones and the evolution of mechanical stratigraphy in a carbonate bedded succession may be extremely complex.

a

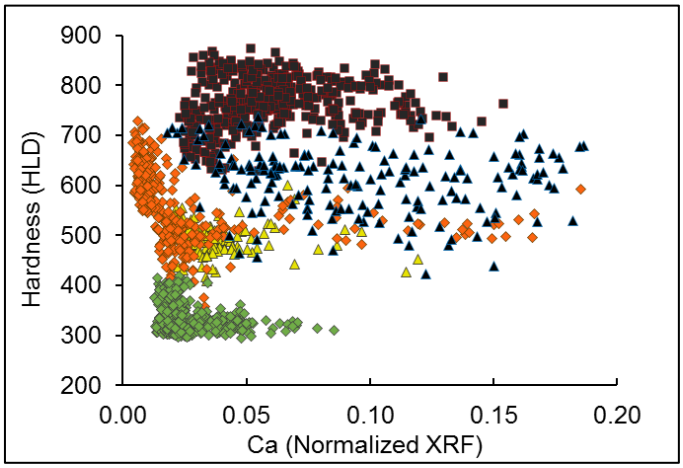

b

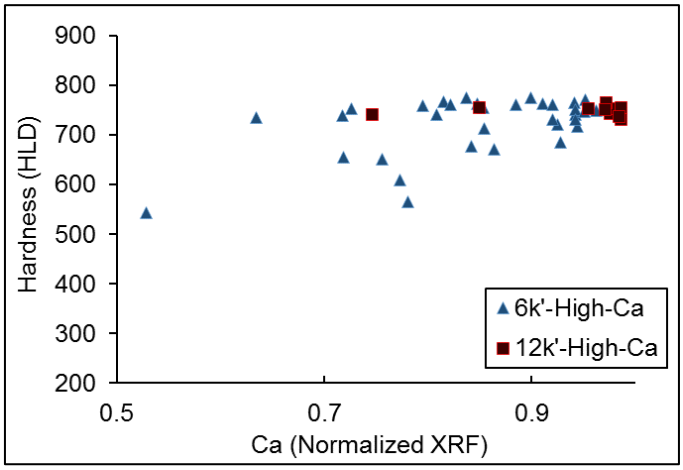

FIGURE 26. Hardness plots with calcium (a) included in this study and (b) not included in the bulk results of siliceous mudstones. Ca of >0.7 normalized concentration are identified as carbonate beds, typically dolomite, with no increase in hardness from 6,000' to 12,500' of burial.

Total Organic Carbon

There is a weak negative correlation between percent total organic carbon (TOC) and hardness for the 6k'-quartz and 12k'-quartz intervals (Fig. 27a). Organic matter (OM) is a high-volume, low-density, and generally weak component of many mudstones that is believed to reduce the overall strength of rocks (Kumar, 2015). At 4-10% of the weight of a rock mass, OM is estimated to make up 8-20% of the rock volume. However, Kennedy et al. (2002), Isaacs and Rullkötter (2001), and this limited dataset demonstrate that clay-rich detritus also has a correlative relationship with TOC and the effect on hardness is not clearly separated (Fig. 27b).

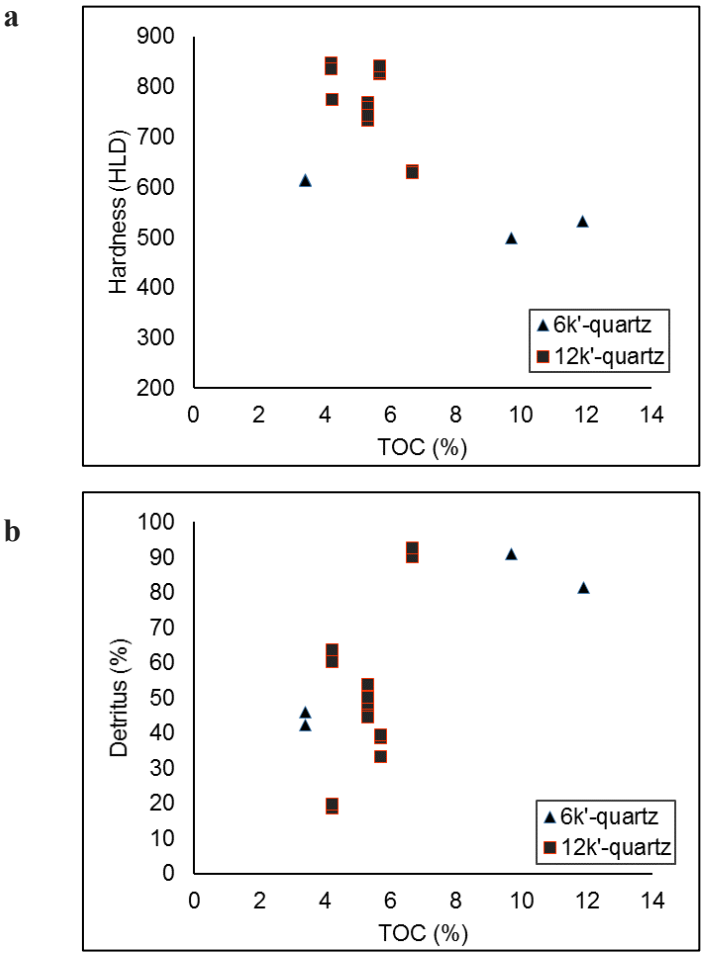

FIGURE 27. Weight percentage TOC data aligned with hardness testing plotted for the McDonald Shale interval. (a) Demonstrates higher HLD in 12k'-quartz samples and a weak negative correlation of hardness and TOC. (b) A weak positive correlation of clay-rich detritus and TOC is agreeable with Isaacs (2001) and Kennedy et al. (2002) observations.

Silica Diagenesis

The physical and chemical transformation of silica by burial diagenesis dramatically hardens rocks in two steps although each step of silica diagenesis has a unique hardening effect (Fig. 28 & 29). On average, hardening of siliceous mudstones by silica diagenesis is greater from opal-A to opal-CT (average 228 HLD or +68%) than from opal-CT to quartz-phase (average 56 HLD or +10%). It is the siliceous components are hardened the greatest in the opal-A to opal-CT transformation. In opal-CT to quartz-phase transformation hardness increases from the

rearrangement, compaction, and strain hardening of detritus components while siliceous components do not significantly harden (Fig. 28).

Mixed opal-A+CT samples demonstrate a relative strengthening by the ratio of opal-CT to opal-A mineralogy. Rocks with 87% of their biogenic silica converted to opal-CT have 85% of the hardness of a fully transitioned opal-CT rock (Fig. 28). This is dissimilar to the opal-A to opal-CT transition of the siliceous Wakkanai Formation in Hokkaido Japan reported by Ishii et al. (2011), where the unconfined compressive strength of a mixed-opal-A+CT transition zone is approximately double (+15 MPa) that of purely opal-CT rocks. Ishii et al. (2011) attributed the partial cementation of opal-CT onto a framework of opal-A diatoms to the creation of a stiffer and stronger transition zone. As previously discussed, mixed opal-A+CT rocks in this dataset may have a marginally greater hardness than pure opal-CT rocks, but not on a similar or statistically significant scale as reported in the Japanese study. The differences might be attributed to a different type of detritus, rock fabric, or burial history. Mixed opal-A+CT rocks display a trend and range of hardness very similar to the compositional trend of opal-CT rocks. Contrary to the bold hardness contrast between opal-A and opal-CT rocks, the opal-CT to quartz-phase transition is much less distinct and more difficult to distinguish by observing physical properties from outcrop or core samples (Isaacs, 1981a).

A key goal of this study was to identify and characterize the differences in geomechanical properties between opal-CT and quartz-phase mudstones. We find that highly siliceous opal-CT and quartz phase porcelanites of greater than 70% diagenetic silica have a very similar mean hardness of about 675 HLD (Fig. 28). However, data show that quartz-phase mudstones with less silica - or greater detritus – are 9 to 32% harder than opal-CT mudstones. For example, in mudstones with 40-50% total diagenetic silica, quartz-phase rocks are a mean 70 HLD harder

than opal-CT rocks (Fig. 28). In mudstones with 20%-30% diagenetic silica (70-80% detritus), quartz-phase rocks are 82 HLD harder than opal-CT rocks of the same silica/detrital ratio. Higher hardness in quartz-phase mudstones with greater amounts of detritus is likely due to the greater physical compaction in clay minerals with burial allowing for a better connected crystalline silica framework from advanced silica diagenesis (Jarvie et al., 2007). The nearly equal hardness of opal-CT and quartz-phase porcelanite is exceptional considering that their respective porosities of 47% and 21% are quite different. However, the physical compaction, deep alteration, and porosity reduction to single digits at 12,500'of burial does significantly increase quartz-phase hardness. Thus, it seems that opal-CT and quartz-phase silica mineralogy may not have much of a difference in hardness, but there is a major compositional influence on how effective diagenetic silica is connected or how effective detritus is in inhibiting a connected framework of silica. Future petrographic investigations may offer greater insight.

zzTABLE 8. Mean Hardness for Three Compositional Groups

	20-30% Silica 'Low-Silica'		**40-50% Silica 'Mod-Silica'**		**70-80% Silica 'High-Silica'**	
Silica Phase	**Mean**	**Δ HLD**	**Mean**	**Δ HLD**	**Mean**	**Δ HLD**
opal-A	320	-	334	-	425*	-
opal-CT	469	149	534	200	626	211
6k'-quartz	551	82	603	69	654	28
12k'-quartz	712	161	755	152	820	166

Change (Δ) in HLD is from previous silica phase or burial group to the current row. *No 'High-Silica' opal-A data was obtained, thus a conservative estimate of 425 HLD was based on outcrop sample testing.

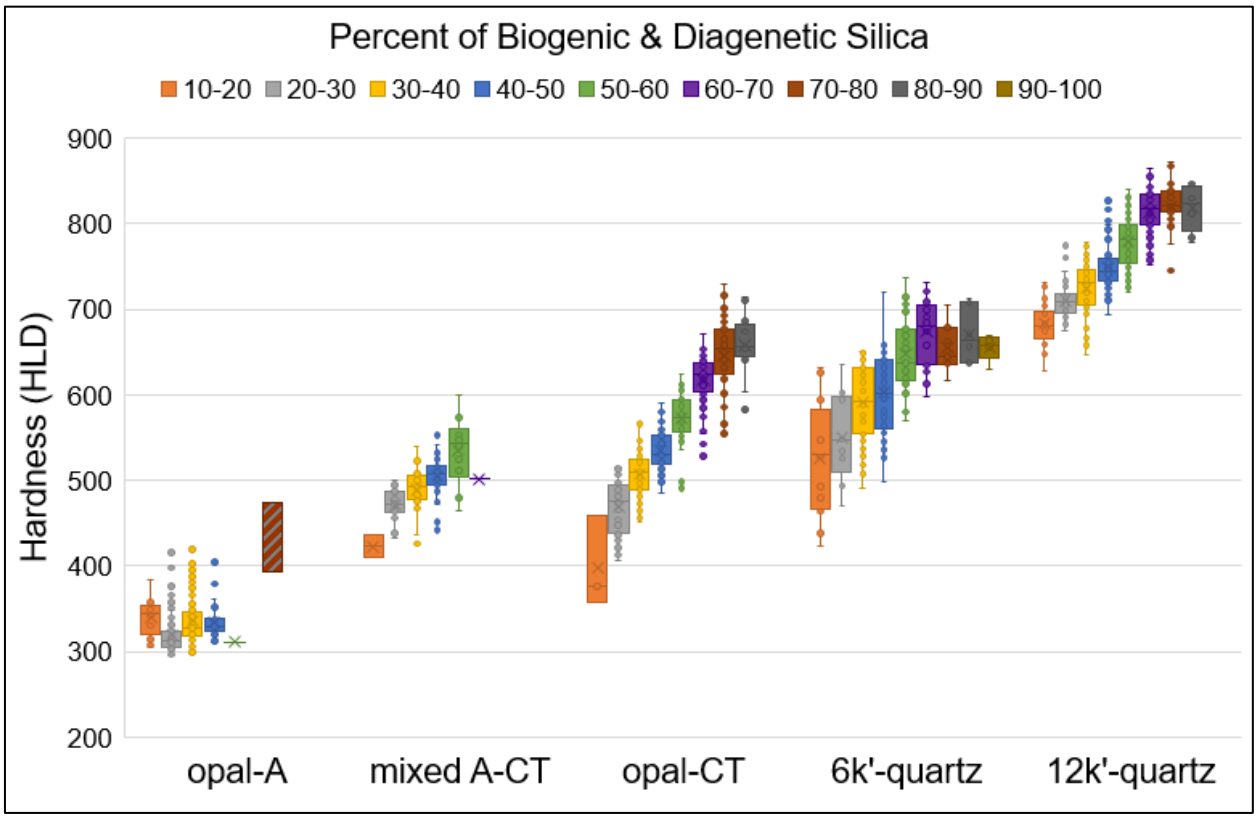

FIGURE 28. Quartile box-and-whisker plot of silica classes in 10% steps demonstrates the hardness increases of high-silica vs. low-silica rocks with burial. High-silica opal-CT and 6k' quartz phase rocks have very similar hardness properties. Mixed A-CT samples have a 13:87 A/CT ratio. *Hashed bar in opal-A group represents a conservative HLD estimate of >70% biogenic silica (opal-A) based on outcrop measurements.

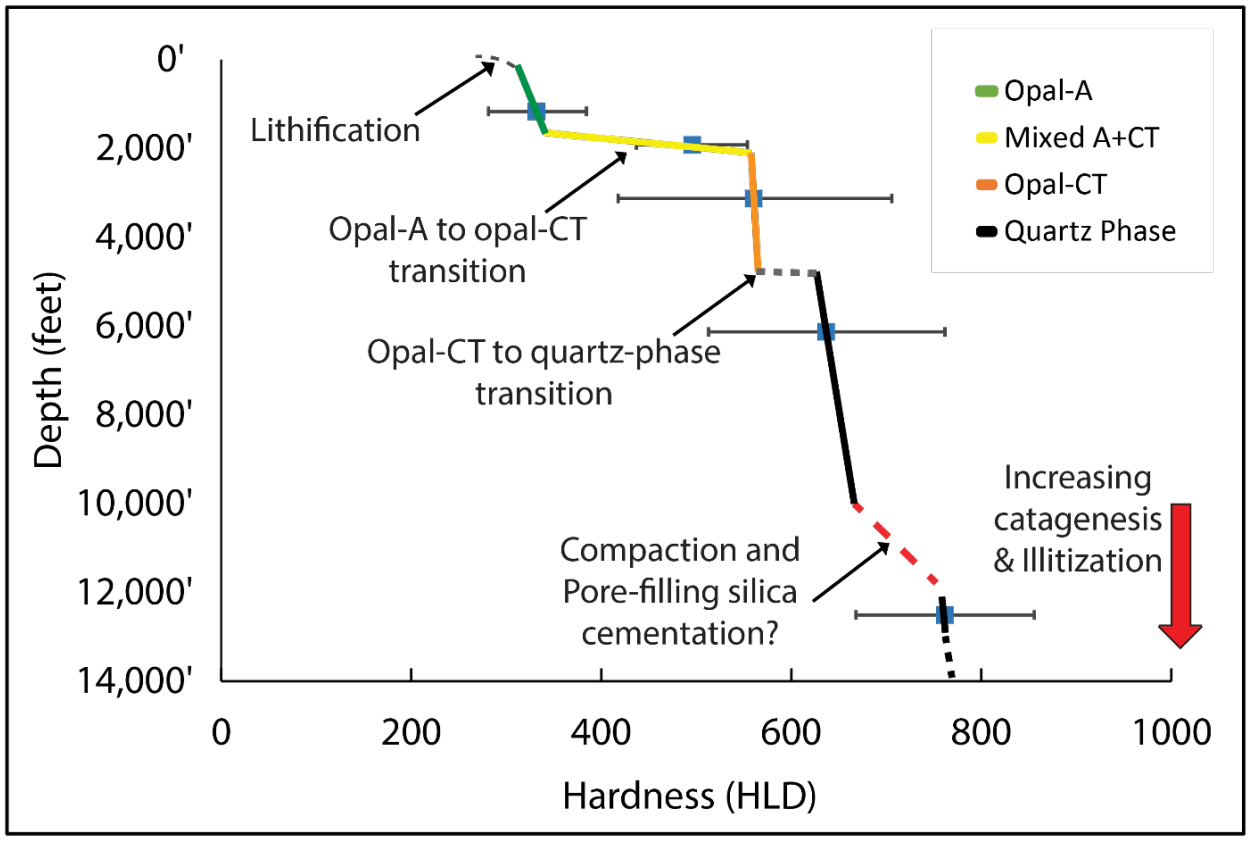

FIGURE 29. Summary of three steps of increasing median hardness associated with silica diagenesis and possible mechanisms of hardening during deep burial of quartz-phase rocks. Bars at each burial group point represents two standard deviations from median hardness. 12k-quartz alteration of catagenesis and illitization discussed in Deep Burial section below.

Porosity

It is largely accepted that porosity and sedimentary rock strength have a continuous negative correlation (Chang et al., 2006). This relationship is largely derived from sandstone and limestone (Vernik et al., 1993; Farquhar et al., 1994; Palchik, 1999), mudstones with less than <15% porosity (Lashkaripour, 2002), mudstones with moldic porosity (Zahm and Elderlin, 2010), or unconsolidated Tertiary or younger shales (Horsrud, 2001; Chang et al., 2006). These studies correlate higher rock strength with lower porosity and greater surface area of grain-to-grain contacts that increases during cementation and burial compaction.

In siliceous mudstones at less than 7,000' of burial, detritus occludes porosity and reduces strength (Fig. 15, Fig. 14; Isaacs, 1981b). In the absence of detritus, siliceous mudstones have greater rock strength by a highly porous and well-connected crystalline framework of diagenetic silica (Snyder et al., 1983). Crystalline silica grains are not free to reorient and compact as in highly porous sandstones and silica-rich and detritus-poor rocks maintain porosity through burial and only decrease in porosity and increase in hardness at diagenetic steps.

In the siliceous mudstones of the Monterey Formation, porosity is not fundamentally correlative to rebound hardness or rock strength (Fig. 30). In other sedimentary rocks, lower porosity usually correlates to increased rock strength. However, within most burial groups of siliceous mudstones lower porosity correlates to lower HLD. This is relative to the negative correlation of porosity and detrital content (Fig. 14) - detritus occupies pore space in a siliceous matrix- as well as the reduction of HLD by detritus (Fig. 15). An overall increase in HLD occurs over 100s to 1,000s of feet of burial related to variable physical and chemical compaction during diagenetic silica-phase change, pore-filling silica cementation, and thermo-chemical alteration of clays and organic matter discussed below. Porosity of highly siliceous mudstones is quite complex and unlike that of typical mudstones that experience a gradual consistent burial compaction (Isaacs, 1981b; Compton, 1981b), and therefore is not a reliable indicator of hardness or rock strength.

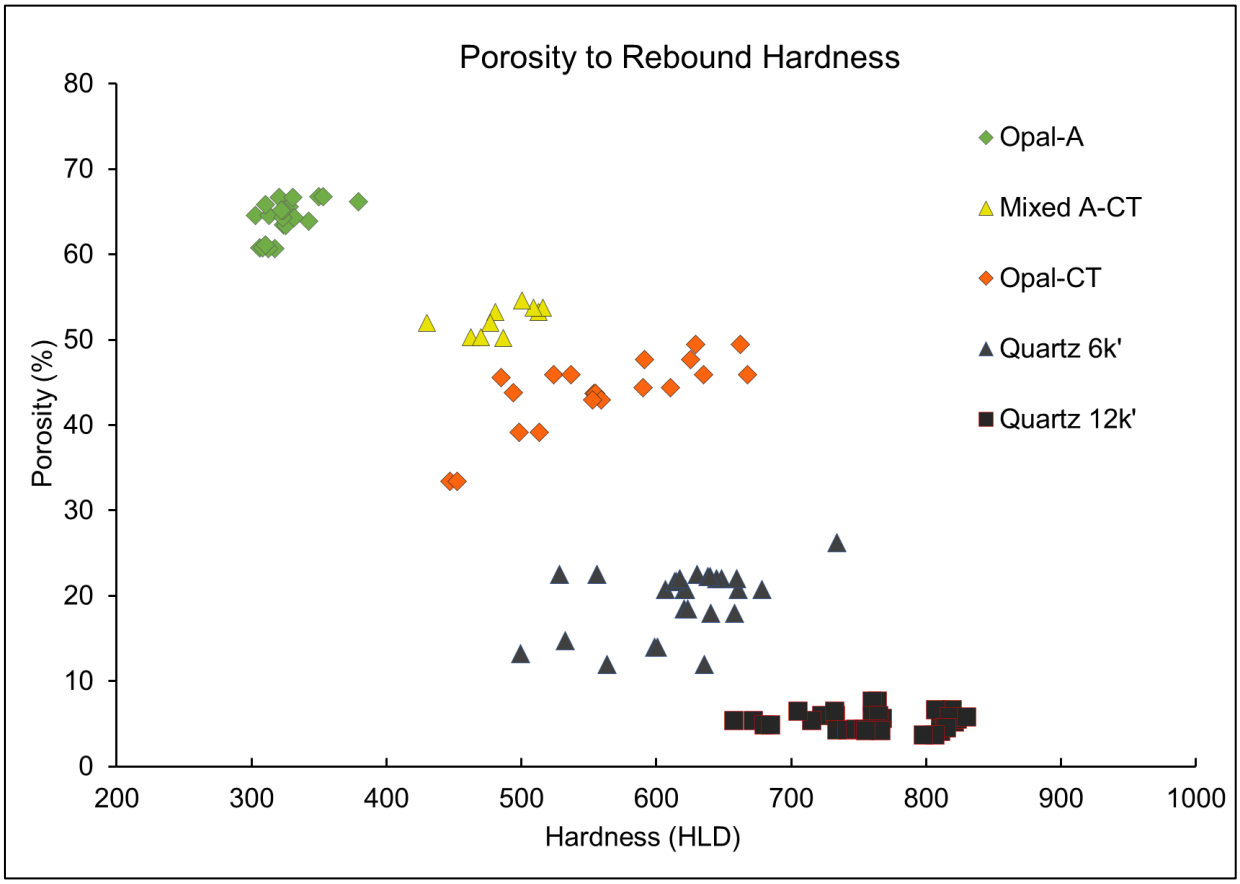

FIGURE 30. Across all silica phases and burial depths core plug porosity has a negative correlation with hardness, but within each burial group from opal-A through 6k'-quartz phase rocks there is a positive relationship between porosity and hardness. Although mean HLD increases with phase change, each step is less than the variability within any one silica phase group. Note the flattened trend in 12k'-Quartz rocks (similar to Fig. 14) where a low and narrow range of porosity is non-correlative to the wide variability in hardness.

Deep Burial

12k'-quartz rocks are the deepest, hardest, and lowest porosity rocks in this study. These are among the first Monterey samples obtained from these depths so their physical and mechanical properties have not been previously documented. These 12k'-quartz rocks are buried an additional 6,500' compared to the stratigraphically equivalent 6k' samples. Both sample sets are quartz-phase silica. As previously mentioned, porosity was reduced with burial from a mean of 20% to 3-8% (Fig. 30) and there is an average increase in hardness by 150 HLD or 24% that affects nearly all compositions equally (Table 8). 12k'-quartz samples - like most other burial

groups - have a rebound hardness well correlated to compositional variance (Fig. 15), but no discernable relation to porosity. The more than doubling of overburden stress and heating applied to 12k'-quartz phase rocks suggest three possible physical and chemical alterations that increased hardness: illitization/quartz cementation, catagenesis, and compaction.

Clay Diagenesis

Previous studies have noted that clay diagenesis may modify the geomechanical properties of shales, resulting in a faster sonic velocity (Dræge et al., 2006; Thyberg and Jahren, 2011; Murray, 2015). Although clay species were not differentiated in this study, we expect normal clay burial diagenesis and a consequent effect on the hardness of Monterey Fmz rocks.

Illitization of smectite involves the redistribution of potassium and release of silica (normally precipitated as quartz) in the simplified equation:

$$\text{smectite} + \text{potassium} = \text{illite} + \text{quartz} + H_2O \qquad \text{(Boles \& Franks, 1979)}$$

Compton (1991a) noted that both the ordering of mixed-layered illite/smectite (I/S) and the illitization of smectite begins gradually at the opal-CT to quartz-phase transition (~5,500' TVD) with a more rapid transformation from 75% I/S at 6,500' to 35% or less I/S at 7,500' - 8,200' in the Santa Maria Basin. Assuming enough potassium exists in the system and a similar 45°C geothermal gradient for siliceous mudstones of the San Joaquin Valley (Reis, 1990), we expect illitization to occur between the 6k'- and 12k'-quartz intervals, accounting for some of the porosity loss and hardening.

Illitization hardens rocks in several ways including (1) the transfer of load from weaker clays to stronger or at least better arranged and more compact components by volumetric reduction of mixed-layer I/S and thermally reduced shearing resistance at particle contacts (Duffy, 2011) and (2) porosity loss and cementation by the precipitation of quartz (Kamp, 2011).

Because hardness was increased across rocks of variable porosity and composition, both the reordering clays, the compaction of clays, and the addition of silica are likely important mechanisms in deep burial hardening.

Thermal Maturity

Thermal maturation data (calculated vitrine reflectance or $\%R_o$) supplied by Aera Energy for this study indicate that 6k'-quartz samples are thermally immature (mean 0.39% R_o) while 12k'-quartz samples are within the early window of oil generation (mean 0.67% R_o). Although thermal maturation has been reported to have negative effects on the elastic moduli and sonic velocity of kerogen (Zargari et al., 2011; Allan, et al., 2016) maturation is also known to shrink kerogen (Curtis et al., 2012) and alter the texture and matrix distribution of kerogen within a source rock (Zargari et al., 2011; Zhao et al., 2016). Similar to illitization, the overall effect can be a transfer of stress from load-bearing organic matter to unmodified components resulting in compaction and a net increase in the elastic moduli of shales (Zhao et al., 2016). Based on the limited data of hardness at only 6k' and 12k' locations, the increase in hardening associated with kerogen maturation is unclear but expected.

Fabric

Measurements in this study were taken from laminated, thinly bedded and massive core intervals, but the relationship of hardness with rock fabric was not detailed. Significant mechanical anisotropy due to laminations or bedding is likely. Some HLD variance, especially in 6k'-quartz samples, maybe result from thin and dipping beds (Fig. 22). Differences in grain packing or sorting may explain some minor variability in hardness values, but the strong correlation between composition and HLD is the most fundamental explaination that does not require additional complexity from multiple difficult to measure variables. However, other

formations do show a relationship between fabric and HLD. For example, within a Marcellus Formation carbonate succession, marl, wackestone, packstone, boundstone, etc. can be distinguished by hardness, in spite of their similar mineralogy; the great diversity of fabric heterogeneity, porosity, and TOC clearly affect rock hardness (Offurum, 2016). Additionally, in the Marcellus Formation, rock fabrics are important to describing lithofacies within a framework of sequence stratigraphy used for predicting the spatial variations of reservoir quality (Boyce, 2010). In the Monterey Formation, the physical characteristics of a reservoir (porosity, permeability, and geomechanics) are closely related to and predominately described by diagenetic and compositional variance (Schwalbach et al., 2009).

Implications

Failure Criteria

Gross (1995) suggests a <9% weak mineral cutoff to Monterey Formation rocks capable of open-mode brittle failure (jointing). Furthermore, rocks with >22% weak mineral failed by shear brittle shear failure (faulting). Although almost no samples in this study would meet the <9% weak mineral limit (Fig. 13), many core samples do have evidence of brittle jointing (Fig. 31). Rebound hardness values are associated with deformational styles observed in outcrop and core to predict strain style in non-fractured intervals. Yet, it is very uncertain if brittle failure in opal-A rocks can be determined from rebound hardness testing because of the limited compositional range of this study set. Additionally, the rebound hardness and composition of highly fractured intervals was not captured in this study due to inherent difficulties of testing fractured core.

In 12k'-quartz cores the most highly-fractured intervals contain approximately 80% diagenetic silica (normalized to detritus) (Fig. 31). HLD in that interval is unusually variable,

likely due to fracture interference in those measurements (Fig. 31). The interval near 12,532' with >53% diagenetic silica or <47% detritus and at least 775 HLD has common swarms of vertical micro-fractures indicating a present or past brittle jointing potential (Fig. 31). A section at 12,533' has higher detrital percentages (>60%) and an average of 725 HLD, but exhibits no vertical fracturing (Fig. 31). This lower section appears either be fracture inhibiting due to increased detritus or has a different history of applied stress. Thus, >775 HLD and >53% diagenetic silica may be predictors of open-mode brittle failure for 12k'-quartz phase mudstones.

Of course, it is not expected that a single rebound hardness value is a firm and universal identifier of failure mode for rocks with different physical properties. In the quartz-phase Woodford Shale, rocks fail with brittle jointing at greater than ~700 HLD and have a mixed strain-style from 600-700 HLD (Becerra-Rondon, 2017). In the Horn River Formation natural fractures only occur in rocks with greater than 550 HLD (Yang et al., 2015).

The focus of this study was not on fracture identification and a simple and consistent correlation of fractures in Monterey Formation opal-CT and quartz-phase rocks was not observed. We note that the upper limit to hardness at approximately 650 HLD in 6k'-quartz phase Monterey Formation rocks of >70% silica is similar to the brittle criteria for other formations and may be a threshold for change in geomechanical properties.

As previously mentioned, due to the lower confining pressures and higher matrix porosities, opal-CT rocks are expected to exhibit natural brittle failure at lower values than quartz-phase rocks. However, if disregarding typical burial depth and confining pressures, both opal-CT and quartz phase porcelanite have the same HLD at 70% silica and may have similar rock strengths and strain behavior.

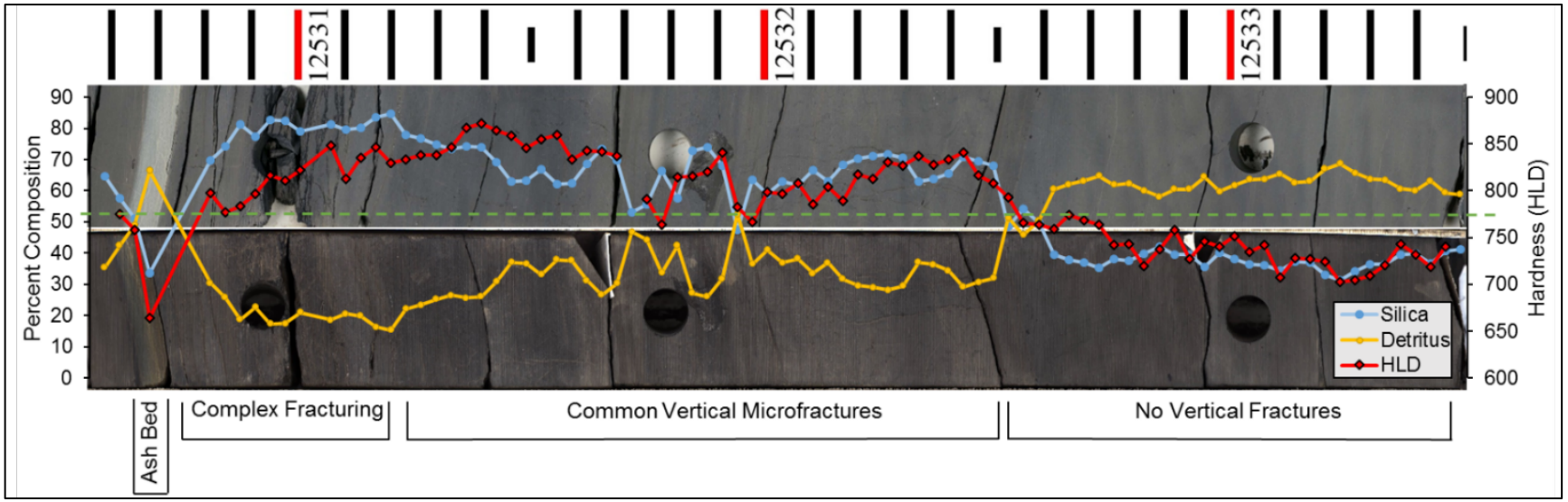

FIGURE 31. Core photos of 1/3 section (above) and 2/3 section (below) in a 12k'-quartz interval with variation of hardness, composition, and fracture occurrence. Difficult to see are swarms of vertical fractures in a section with >50% diagenetic silica and >775 HLD. Dashed green line suggests a division of strain styles or intensity at 775 HLD.

Mechanical Heterogeneity

Each burial group has a potential mechanical heterogeneity based upon its range of hardness values (Fig. 28, Table 4). Heterogeneity in strain style exists not only if the range of hardness values spans a failure mode but as a degree of fracture intensity or fracture inhibition related to the compositional variation in bedding (Narr and Suppe, 1991; Strickland, 2003). Opal-A has the lowest range of hardness (Δ125 HLD) - even when including the measured hand samples (~Δ200 HLD) - and may be generalized as having the lowest potential mechanical heterogeneity of siliceous mudstones. Opal-CT has the greatest range of hardness (Δ371) and must represent the diverse range of mechanical behaviors witnessed in outcrop including both fracture inhibition in detritus-rich mudstones and profuse brittle fracturing in opal-CT porcelanite. The range of hardness in 6k'-quartz phase mudstones is lower than opal-CT mudstones and lessens again with burial to 12k'-quartz (Table 4). This study reveals an evolution of mechanical stratigraphy with burial and secondary alterations in the Monterey Formation also witnessed in other formations (Hovorka, 1998; Pitman et al., 2001; Olson et al., 2009; Laubach et al., 2009).

By understanding the range and controls of hardness, we can model the historical, current, or theoretical mechanical heterogeneity of a succession. For example, Lockman (2012) and Isaacs (1981c) described diagenetically stratified opal-A to opal-CT transition zones without mixed-silica mineralogy beds but discretely alternating beds of opal-CT porcelanite or chert and opal-A muddy diatomite. Although rebound hardness was not measured in these sections, we can model the mechanical contrast as the minimum opal-A HLD and the maximum opal-CT or chert HLD equaling a range of at least Δ425 – greater than any single phase and associated with the multiple styles and intensity of fractures in those successions. In contrast, mechanical

heterogeneity would be reduced at a diagenetically stratified opal-CT to quartz-phase transition zone from Δ371 to ~Δ200 HLD (Fig. 28). This is due to compositional influence on diagenesis where detritus-rich beds transform to quartz-phase first and would be interbedded with more siliceous opal-CT rocks (Fig. 1 & 2).

The true heterogeneity of an upper Monterey Formation burial group is hugely influenced by the inclusion of chert, dolomite, and volcanic ash beds. While ash beds add only limited mechanical contrast to an opal-A succession, ash beds can be enormously significant mechanical barriers in opal-CT or quartz-phase successions (Fig. 19). The impact is opposite with cherts. Highly brittle cherts are over twice the hardness of most opal-A rocks, but not expected to be significantly different to most 12k'-quartz rocks (Fig. 19). Several studies of strain variation and fracture timing in the Monterey Formation document examples of map-scale to sub-centimeter scale deformation effected by the mechanical heterogeneity quantified in this study (Behl and Garrison, 1994; Gross, 1995; Wirtz, 2018).

The ability to resolve variations in rebound hardness measurements at a 1-cm scale reveals a mechanical heterogeneity that is missed or misrepresented in outcrop or standard wireline interpretations. Many outcrop and core studies clearly demonstrate this fine scale of heterogeneity, but fracture observations are largely influenced by bedding thickness, historical stress load, or historical stress direction (Gross, 1995). Several 10-inch (25cm) thick carbonate bands are identified in density, neutron, and sonic logs, but these logs fail to resolve the fine-scale heterogeneity in HLD produced by several weak beds of volcanic ash and detritus-rich mudstones (Fig. 32).

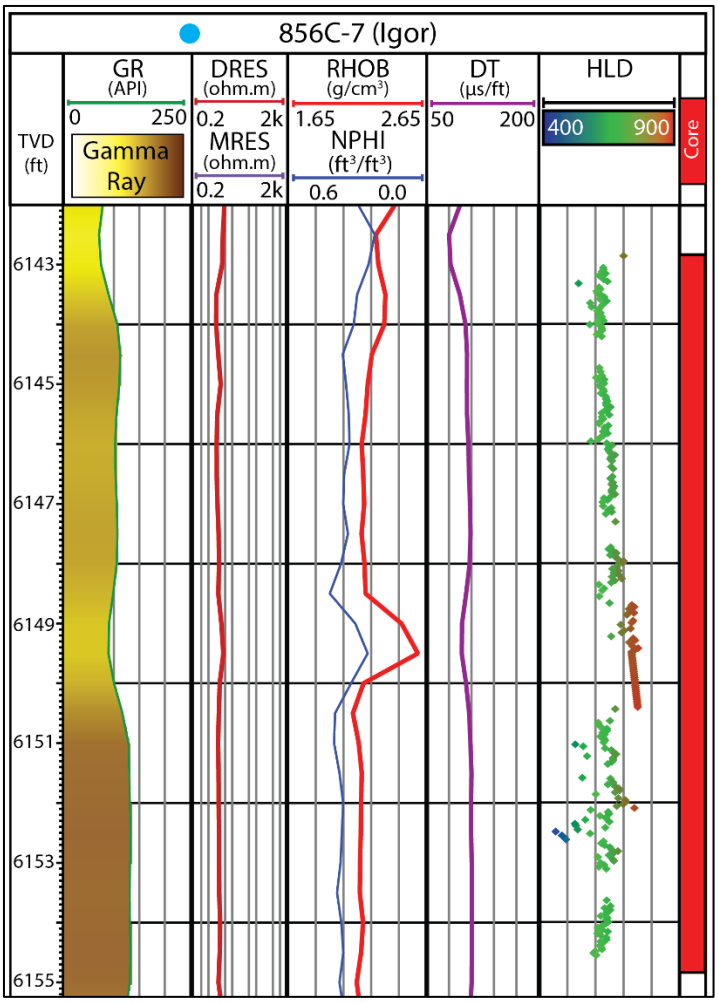

FIGURE 32. Standard wireline suite demonstrating the resolution and scale of physical and mechanical heterogeneity in well logs. Both wireline and hardness measurements capture the carbonate bed at 6,149' but other than indicating a generally higher GR, wireline logs fail to resolve the mechanical heterogeneity within the 6,151' to 6,153' section.

The understanding of evolution of hardness and mechanical stratigraphy can be applied to the interpretation of deformational timing and style in the Monterey Formation and other formations. For example, although both opal-CT and quartz-phase porcelanite are of nearly equal hardness, shallower opal-CT intervals may fracture more than 6k'-quartz phase porcelanites of equal bed thickness. This is because there is a negative correlation between confining stress and brittleness (Hucka and Das, 1974; Holt et al., 2011); similar to the negative correlation of confining pressure and compressive strength (Zoback, 2010) and opal-CT occurs at shallower

depths and lower confining pressure. The propensity for early brittle strain may be missed if one assumed that rocks only became harder and more brittle with greater burial and diagenesis. The prediction of more fractureable opal-CT rocks agrees with observations of Monterey Formation opal-CT outcrops having an equal or greater fracture intensity than Eagle Ford, Niobrara, or Barnett shale outcrops (Gale et al., 2014); as well as the understanding that low matrix permeability opal-CT rocks may be fractured and form a common migration pathway to charge overlying opal-A or sandstone reservoirs (Dholakia, 1998). Additionally, the physical, chemical, and mechanical alterations between 6k'- and 12k'-quartz is understudied. Additional investigations of silica diagenesis, clay diagenesis, fracture timing, and kerogen maturation in deep Monterey Formation rocks may elucidate the past histories of many other siliceous source-rock reservoirs.

Unconfined Compressive Strength

To aid in the comparison with other formations and to other measurements in the Monterey, hardness data were converted to unconfined compressive strength (UCS) using published empirical correlations. The technique for converting HLD to UCS was originally developed by Verwaal and Mulder (1993) and further expanded by several others to include shale lithology measurements (Aoki and Matsukura, 2008; Lee et al., 2014). Several authors suggest linear correlations between rebound hardness and UCS values based on consideration of very narrow ranges of hardness and UCS (Aoki and Matsukura, 2008; Becerra-Rondon, 2017; among others). The much larger range of physical and mechanical properties measured in this study in siliceous mudstones of varied diagenetic phase better suits the wider-fitting, non-linear correlation suggested by Lee et al. (2014) and Kahraman (2001). The calculated compressive strength values for opal-A and opal-CT samples of this study agree reasonably to opal-A, opal-

CT, and 6k'-quartz phase UCS values from a literature review of nearby wells (Fig. 33). However, the calculations of >30,000 psi for 12k'-quartz phase rocks appear hyperbolic and are much higher than UCS measurements from 12k'-quartz core samples that did not overlap the hardness testing of this study. Additional UCS testing of core plugs for quartz phase mudstones, especially those from 7,000' – 14,000', may help improve UCS calculations from HLD for each burial group.

Mapping Hardness

Data from this study shows that we can map current and historical geomechanical variability in the subsurface through a spatial integration of compositional variation along with an understanding of the alteration of physical properties in siliceous mudstones of the Monterey Formation that evolve relative to burial and silica diagenesis. Such mapping can be applied to the identification of reservoir "sweet-spots", migration pathways, or seal analysis. Mapping compositional heterogeneity into diagenetic heterogeneity can bolster the identification of fractured or fracturable intervals or suggest fairways for play concepts such as a dual permeability reservoir target like the opal-A to opal-CT transition zone or TOC- and detritus-rich beds intercalated with brittle porcelanite in a 12k'-quartz reservoir.

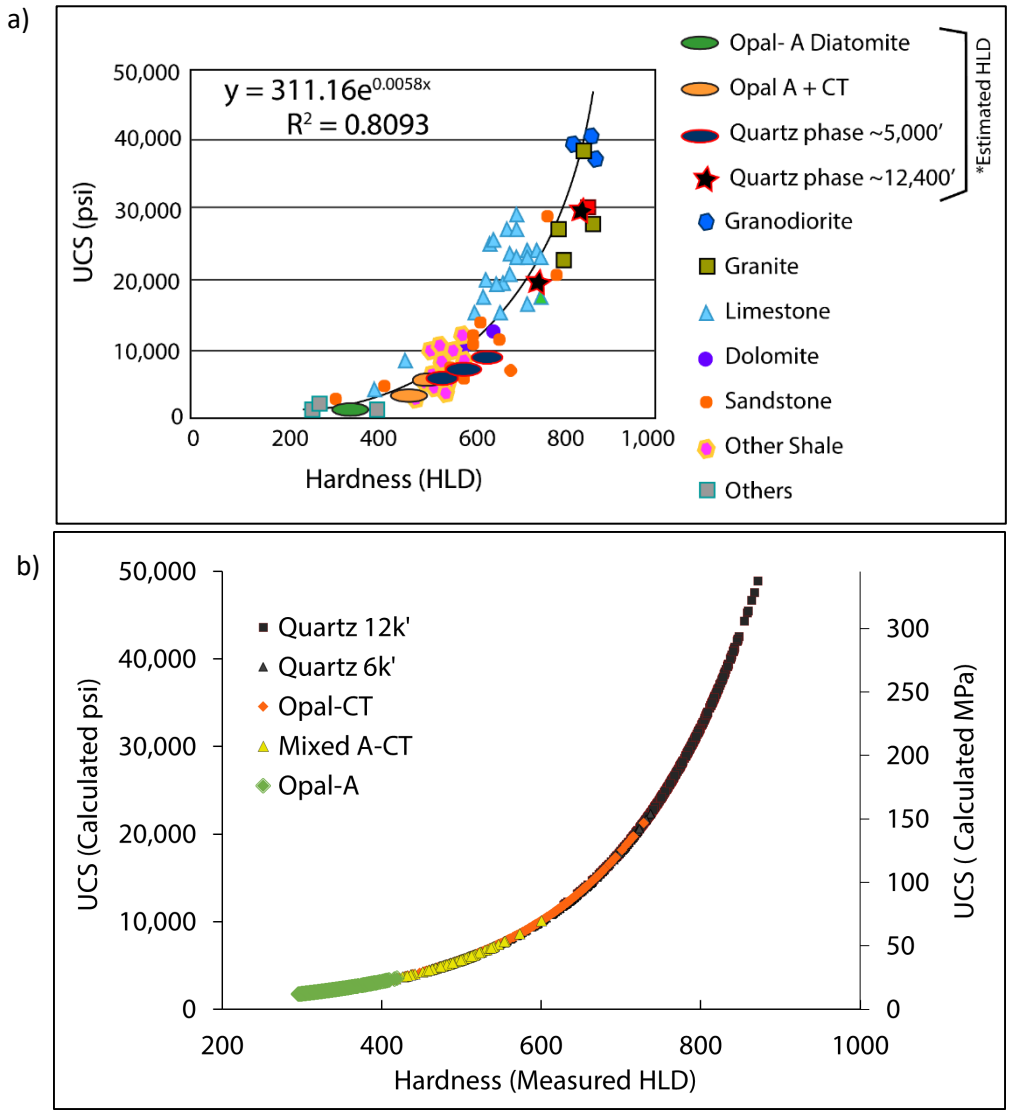

FIGURE 33. (a) Calibrated UCS in psi from Lee et al. (2014) with overlying Monterey Formation data from literature and associated studies. (b) Calculated UCS from this HLD in this data set. *Extremely-high UCS for 12k'-quartz phase rocks are likely overestimated and misrepresentative without additional laboratory testing.

CHAPTER 6

CONCLUSIONS

This study has quantified the hardness of siliceous mudstones of varied diagenetic stages and burial depths. X-ray florescence scanning (XRF) and micro-rebound hardness (HLD) measurements show how the hardness of siliceous mudstones increase and evolve through two major steps of silica diagenesis. A third increase in hardness at greater than 10,000' of burial depth is less understood but likely related to clay diagenesis, kerogen catagenesis, and physical compaction. The main findings are:

1. Composition (defined by silica:detritus ratios) is a 1st-order control of rock hardness within any burial group. Argillaceous components have a strong negative correlation with hardness values. Diagenetic silica has a strong positive correlation with hardness. Hardness variability due to compositional variability is greater within each burial group than hardness variation is between stages of silica diagenesis (Fig. 29).
2. Hardening by silica diagenesis in silica-rich rocks is greatest at the opal-A to opal-CT (+47.3% HLD) transition and much less at the opal-CT to quartz-phase transition (+4.5% HLD) (Fig. 28). At the opal-CT to quartz-phase transition, greater hardening occurs through clay compaction and greater grain connectivity in detritus-rich rocks (17.5% HLD).
3. Porosity is not a reliable indicator of hardness in siliceous mudrocks. Although hardness increases and porosity decreases with steps of silica diagenesis, within each silica phase, porosity has a negative correlation with detrital content and thus a positive correlation with hardness (Fig. 30). These findings are contrary to other studies that find a continuous negative correlation of porosity and rock strength.

4. Opal-A rocks in the Belridge oil field have the smallest and lowest range of hardness values of any burial group. Opal-A rocks have no clear trend between rebound hardness and compositional variance.
5. Opal-CT rebound hardness had the best fit correlation and greatest rate of change in hardness with compositional variation. Opal-CT hardness does not increase with burial and resists mechanical alteration by burial compaction.
6. Opal-CT porcelanite and quartz-phase porcelanite have very similar rebound hardness values. Quartz-phase rocks in this dataset with > 70 % silica do not increase in hardness with additional silica, as opal-CT rocks do. Chert hardness was not tested but is likely 15-20% harder than porcelanite and similar in HLD to cherts in the Woodford Shale.
7. Quartz-phase rocks at >12,000' of burial depth undergo a 25-30% increase in hardness from 6k'-quartz rocks without further silica phase change. I propose that clay diagenesis and early oil catagenesis accelerates burial compaction and hardening. Additionally, silica cementation released by the illite-to-smectite transformation may also play a role in porosity reduction and the increase of hardness.
8. Highly-siliceous opal-CT and quartz-phase mudstones of the Monterey Formation are often harder, or at least as hard as, many other North American shales that rely upon brittle fracturing for source-rock reservoir production. Even the most detritus-rich quartz phase rocks at 12,000' TVD are about as hard or harder than some other North American unconventional shales (Fig. 19 & 20).
9. Authigenic and/or diagenetic quartz mineralogy creates harder rocks than rocks with an equal or greater percentages of calcite mineralogy.

10. Micro-rebound hardness may predict the deformational style of opal-CT and quartz-phase rocks. Precise testing can identify localized physical and chemical heterogeneity below wireline scale and be used as a rapid method of mechanical property evaluation to aid drilling and fracture stimulation design.

CHAPTER 7

FUTURE WORK

I have quantified the evolution and impact of hardness related to compositional variance, silica diagenesis, and other burial alterations across a nearly complete range of reservoir and non-reservoir siliceous mudstones at multiple burial depths in the Belridge oil field of the San Joaquin Basin. To further expand and apply this research I recommend several additional investigations.

An expansion and infill of rebound hardness testing of rocks not captured by this study would further the understanding of hardness controls. I suggest HLD testing of high-purity diatomite and chert samples which were not encountered in the Belridge oil field cores, a range of dry or unsaturated subsurface samples, and a suite of outcrop samples to better tie hardness observations to field-based fracture studies.

A petrographic investigation is recommended to understand hardness at a finer scale of rock fabric variability including grain arrangements (i.e., diatom packaging, fragmentation, sorting, or species), laminations, the variable micro-porosity documented by Kassa (2016), organic matter distribution, and cementation.

Since it remains unclear if opal-A lithotypes have significant mechanical variation related to compositional and physical properties, I recommend controlled testing of UCS or another mechanical index to varied compositions of opal-A rocks. It is possible that rebound hardness testing is not effective in high-porosity diatomaceous rocks.

This study has just begun to consider deep burial alterations of highly siliceous mudstones and their potential as a source-rock reservoir. I suggest a petrographic analysis of rocks between 6k’ and 12k’ to further understand clay diagenesis (Appendix D), compaction,

cementation, and porosity alterations with burial and catagenesis. Further investigations of fracture and cementation timing in deeply buried quartz-phase intervals under different temperature and pressure conditions would likely add to the correlation of rebound hardness to the geomechanical behavior of Monterey Formation source rocks. It is possible that the extreme hardening of 12k'-quartz rocks may have surpassed a beneficial extent of embrittlement and created thick intervals of failure-resistant rocks.

A calibration of rebound hardness to standard wireline logs is also recommended. In this study, I have assumed the strong correlations of UCS, Young's Modulus, and Poisson's Ratio with rebound hardness witnessed in other studies. The correlations of HLD to density, porosity and sonic logs as well as drilling rate of penetration (ROP) and various elastic moduli can be locally confirmed or refined for comparison to other unconventional shale studies.

Observations in the highly-siliceous mudstones of the Monterey Formation are useful as an end-member comparison of how silica diagenesis and diagenetic quartz effects physical properties and mechanical behavior of other unconventional shales. The Woodford Shale, in particular, stands out as a compositionally similar formation for geomechanical comparisons. Future work and comparisons may continue to challenge or develop the understanding of porosity as a mechanical indicator (Chang et al., 2006); the characterization of brittleness in terms of mineralogy, physical properties, and confining pressure (Yang et al., 2013); and the relationship of rock strength and fracturability (Bai, 2016).

Lastly, the tens of thousands of XRF measurements captured in this study could be further analyzed to better define mineralogical assemblages of detritus and uncover a high-resolution of chemostratigraphic variability in middle- to upper-Miocene aged mudrocks of the western San Joaquin Basin.

APPENDICES

APPENDIX A

XRF K-SHELL FLUORESCENCE YIELDS

APPENDIX A: XRF K-Shell Fluorescence Yields

Element	XRF Elemental Efficiency Conversion
Al	0.03
Si	0.05
S	0.07
Cl	0.10
K	0.14
Ca	0.15
Ti	0.21
Cr	0.29
Mn	0.31
Fe	0.35
Rh	0.79

K-shell fluorescence yields for elements in this study compiled from mean values of Kahoul et al. (2011). Raw x-ray counts acquired by XRF scans for each element were divided by the appropriate fluorescent yield to normalize the data to relative elemental abundances in the first step of creating a quantitative calibration. Raw XRF data for 12 elements at 2,300 data points available upon request to the author.

APPENDIX B

INDUCTIVELY COUPLED PLASMA-MASS SPECTROMETRY (ICP-MS) DATA

APPENDIX B: Inductively Coupled Plasma-Mass Spectrometry (ICP-MS) Data

Depth (ft)	Silica Phase	SiO2 (%)	Al2O3 (%)	Fe2O3 (%)	MnO (%)	MgO (%)	CaO (%)	Na2O (%)	K2O (%)	TiO2 (%)	P2O5 (%)	LOI (%)	Total (%)	XRF Si (%)	XRF Al (%)
832.61	Opal-A	61.69	9.79	4.17	0.03	1.24	1.41	2.23	1.40	0.41	0.29	16.06	98.72	0.68	0.05
1,357.46	Opal-A	60.81	8.47	3.91	0.03	1.29	0.65	1.64	1.14	0.37	0.19	20.82	99.32	0.66	0.05
1,358.39	Opal-A	62.52	7.53	2.97	0.02	0.98	0.75	1.52	1.05	0.33	0.22	21.42	99.31	0.73	0.04
1,368.53	Opal-A	57.62	8.69	3.48	0.03	0.87	0.61	1.65	1.04	0.39	0.10	25.22	99.70	0.64	0.04
1,369.45	Opal-A	56.21	10.07	4.93	0.06	1.20	1.02	1.99	1.32	0.45	0.75	22.00	100.00	0.54	0.05
1,920.82	Opal-A+CT	70.68	6.85	3.04	0.03	0.82	1.10	1.49	0.73	0.32	0.15	14.40	99.60	0.80	0.03
1,922.20	Opal-A+CT	68.12	8.01	3.36	0.03	1.02	0.91	1.67	0.87	0.36	0.13	14.50	98.98	0.73	0.04
2,284.70	Opal-CT	68.32	8.15	3.52	0.03	1.14	0.68	1.80	1.03	0.37	0.11	13.61	98.76	0.75	0.04
3,461.48	Opal-CT	62.46	10.68	4.38	0.03	1.04	0.65	1.75	1.68	0.48	0.22	15.92	99.28	0.64	0.05
3,468.53	Opal-CT	82.85	3.22	1.35	0.01	0.28	0.30	1.19	0.54	0.15	0.11	9.47	99.47	0.88	0.01
3,469.76	Opal-CT	66.95	7.98	3.54	0.02	0.80	0.57	1.61	1.37	0.37	0.18	15.11	98.50	0.64	0.05
6,104.32	Quartz	56.46	13.01	4.49	0.03	1.10	1.56	0.98	1.99	0.60	0.34	19.05	99.60	0.53	0.06
6,111.10	Quartz	55.47	13.07	4.61	0.03	1.01	1.23	0.98	2.08	0.58	0.29	20.13	99.48	0.52	0.04
6,111.23	Quartz	67.19	8.07	2.59	0.02	0.65	1.19	0.79	1.34	0.35	0.52	17.29	99.99	0.63	0.04
12,505.25	Quartz	64.30	12.37	3.85	0.02	0.87	1.66	1.12	1.96	0.45	0.64	12.45	99.70	0.75	0.04
12,509.00	Quartz	61.26	13.38	4.77	0.03	1.10	1.54	1.00	2.30	0.59	0.65	13.67	100.28	0.53	0.07
12,510.34	Quartz	76.37	5.55	2.32	0.02	0.59	1.54	0.54	0.84	0.23	0.15	10.32	98.47	0.79	0.03

Major oxides from ICP-MS analysis, 1-5 gram samples crushed in a steel ball mill, sieved to ASTM E-11 Std no. 200 (75 mircon / 0.029 in), and analyzed by ACT Laboratories. SiO2 and Al2O3 were correlated to Si and Al x-ray fluorescence (XRF) counts which were normalized to total counts measured and corrected for fluorescence yield (Fig. 10). Silica phase verified by x-ray diffraction (XRD). See Appendix A for XRF fluorescence yield correction.

APPENDIX C

LEEB HARDNESS (HLD) DATA

APPENDIX C: Leeb Hardness (HLD) Data

Category	Burial Group	Biogenic and Diagenetic Silica Group (%)								
		10-20	20-30	30-40	40-50	50-60	60-70	70-80	80-90	90-100
Mean HLD	opal-A	344.7	312.9	327.0	330.2	311.0				
	opal-A+CT	422.8	472.1	492.2	508.2	543.3	501.3			
	opal-CT	376.2	475.5	508.9	531.0	574.0	624.8	655.0	656.3	
	6k'-quartz	530.1	548.0	591.5	601.0	637.7	680.0	644.8	663.7	657.8
	12'-quartz	680.4	708.7	742.7	751.8	788.1	816.5	821.6	822.9	
Min HLD	opal-A	305.3	295.5	297.0	311.0	311.0				
	opal-A+CT	409.7	417.3	425.9	441.8	464.0	501.3			
	opal-CT	357.5	406.1	452.2	485.1	490.7	527.8	555.0	583.2	
	6k'-quartz	422.6	470.0	491.3	498.0	570.1	598.6	617.3	635.6	630.3
	12'-quartz	628.0	674.4	646.0	692.6	720.0	750.8	744.7	778.0	
Max HLD	opal-A	383.4	415.9	419.0	404.4	311.0				
	opal-A+CT	436.0	499.8	538.7	553.0	600.2	501.3			
	opal-CT	458.5	515.9	567.0	590.8	624.5	670.8	728.3	714.8	
	6k'-quartz	630.8	635.2	651.0	719.3	736.8	731.6	704.2	712.0	669.6
	12'-quartz	730.7	774.7	788.3	827.2	839.2	864.0	871.9	848.0	
Mean Silica %	opal-A	17.2	26.0	34.3	42.1	50.0				
	opal-A+CT	19.4	25.7	35.2	43.7	53.5	60.8			
	opal-CT	18.7	25.4	34.7	44.5	54.3	65.4	75.5	81.2	
	6k'-quartz	15.2	26.1	36.0	44.2	55.7	62.9	75.9	84.4	91.9
	12'-quartz	16.0	25.3	36.5	45.3	55.2	65.0	74.3	82.7	

Mean, minimum, and maximum values for data in this study by 10% classes of silica used in Figures 13, 18, & 28. Raw data for average of 5-8 measurements at 1,546 locations are available upon request.

APPENDIX D

ILLITE/SMECTITE ANALYSIS

APPENDIX D: ILLITE/SMECTITE ANALYSIS

Hower et al. (1976) and Awwiller (1993) suggest that illitiziation can be identified in the following elemental changes relative to aluminum: 50-80% increase in potassium, 50% increase in iron, a general decrease in calcium, and decrease in silica (if silica is expelled from an open system). The plots below demonstrate those ratios with depth and data from this study that are still poorly understood.

Simple elemental ratios from the siliceous mudstones of the Belridge oil field are not consistent with the signals suggested by Hower et al. (1976) and Awwiller (1993) and provide no clear evidence for an open-system of illitization within the siliceous shales of the Monterey Formation. Small stratigraphic dissimilarities and lateral variation between sediments of 6k'-quartz and 12k'-quartz are not accounted for. However, the classically studied illitte/smectite transformations studied in high permeability Gulf of Mexico sandstones may be significantly different than the transformation within a low permeability and highly siliceous succession of the low matrix permeability Monterey Formation. The differences of open and closed geochemical systems may complicate what signals are preserved. Without much further geochemical, mineralogical, and SEM analysis the illitization of mixed layered I/S is still expected, but unclear.

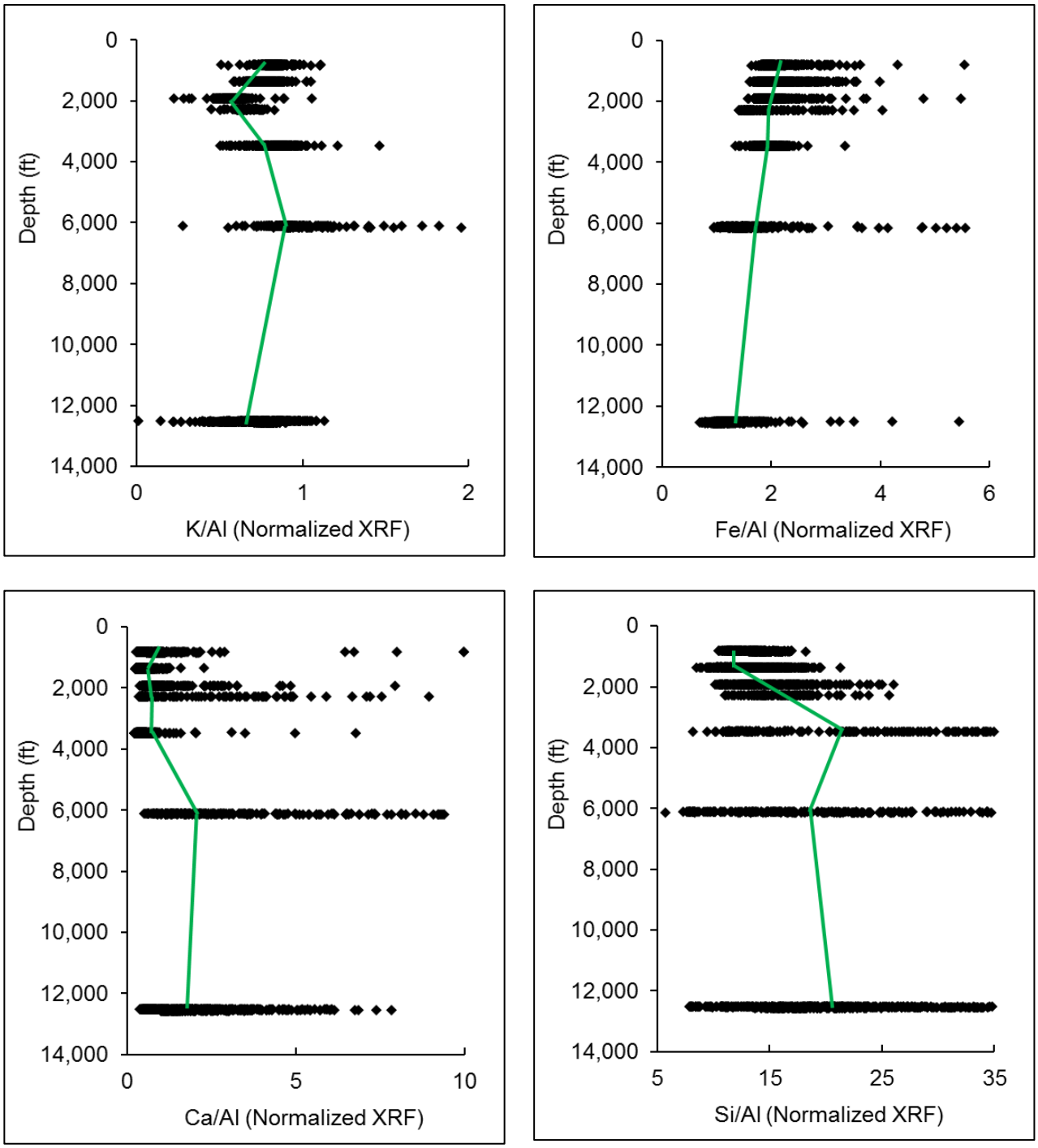

Plots of XRF elemental ratios important to identifying illitization trends with increasing depth, green trend line intersects median values.

REFERENCES

REFERENCES

Alberty, M. W., 1992, Standard interpretation; part 4—wireline methods, *in* Morton-Thompson, D. and Woods, A.M., eds., Development Geology Reference Manual: Tulsa, OK, AAPG Methods in Exploration Series 10, p. 180–185.

Allan, A.M., Clark, A.C., Vanorio, T., Kanitpanyacharoen, W., and Wenk, H.-R., 2016, On the evolution of the elastic properties of organic-rich shale upon pyrolysis-induced thermal maturation: Elasticity of pyrolyzed shale: Geophysics, v. 81, p. D263–D281, doi: 10.1190 /geo2015-0514.1.

Allan, M. E., & Lalicata, J. J., 2011, The Belridge giant oil field-100 years of history and a look to a bright future, *in* Proceedings, AAPG International Conference and Exhibition, Milan, Italy, p. 23-77.

Allan, M.E., Gold, D.K., and Reese, D.W., 2010, Development of the Belridge field's diatomite reservoirs with hydraulically fractured horizontal wells: From first attempts to current ultra-tight spacing, *in* Proceedings, Society of Petroleum Engineers Annual Technical Conference and Exhibition, Florence, Italy, Society of Petroleum Engineers, SPE-133511, doi: 10.2118 /133511-MS

Aoki, H., and Matsukura, Y., 2008, Estimating the unconfined compressive strength of intact rocks from Equotip hardness: Bulletin of Engineering Geology and the Environment, v. 67, p. 23–29, doi: 10.1007/s10064-007-0116-z.

Awwiller, D.N., 1993, Illite/smectite formation and potassium mass transfer during burial diagenesis of mudrocks: A study from the Texas Gulf Coast Paleocene-Eocene: Journal of Sedimentary Research, v. 63, 501-512.

Bai, M., 2016, Why are brittleness and fracability not equivalent in designing hydraulic fracturing in tight shale gas reservoirs: Petroleum, v. 2, p. 1–19, doi:10.1016/j.petlm.2016 .01.001.

Becerra Rondon, D. M., 2017, Integrated geological characterization at the bed scale of the Woodford Shale at the I-35 outcrop, southern Oklahoma [M.S. thesis]: Norman, University of Oklahoma, 202 p.

Behl, R.J., 1999, Since Bramlette (1946): The Miocene Monterey Formation of California Revisited: Classic Cordilleran Concepts: A View from California: Geological Society of America, Special Paper, v. 338, p. 301–313.

Behl, R.J., and Garrison, R.E., 1994, The origin of chert in the Monterey Formation of California (USA): Siliceous, phosphatic and glauconitic sediments of the Tertiary and Mesozoic: Proceedings of the 29th International Geological Congress, Part C, p. 101–132.

Belfield, W.C., Helwig, J., Pointe, P.L., and Dahleen, W.K., 1983, South Ellwood Oil Field, Santa Barbara Channel, CA: A Monterey Formation fractured reservoir, *in* Petroleum Generation and Occurrence in the Miocene Monterey Formation, California: Los Angeles, California, Pacific Section, Society of Economic Paleontologists and Mineralogists, p. 213–222.

Blake, G. H., 1981, Biostratigraphic relationship of Neogene benthic foraminifera from the southern California outer continental borderland to the Monterey Formation, *in* Garrison, R. E., and Douglas, R. G., eds., The Monterey Formation and Related Siliceous Rocks of California: Los Angeles, Pacific Section, Society of Economic Paleontologists and Mineralogists, p. 1–14.

Blood, D.R., Lash, G.G., and Bridges, L.C., 2013, Biogenic silica in the Devonian shale succession of the Appalachian Basin, USA: American Association of Petroleum Geologists Search and Discovery Article 50864.

Boles, J.R., and Franks, S.G., 1979, Clay diagenesis in Wilcox sandstones of Southwest Texas: Implications of smectite diagenesis on sandstone cementation: Journal of Sedimentary Research, v. 49, p. 55–70, doi: 10.1306/212F76BC-2B24-11D7-8648000102C1865D.

Bowersox, J.R., 1990, Geology of the Belridge diatomite, northern South Belridge field, Kern County, California, *in* Kuespert, J. G., and Reid, S. A., eds, Structure, Stratigraphy and Hydrocarbon Occurrences of the San Joaquin Basin, California: Los Angeles, AAPG Pacific Section, p. 215-223.

Boyce, M.L., 2010, Sub-surface stratigraphy and petrophysical analysis of the Middle Devonian Interval of the Central Appalachian Basin; West Virginia and Southwest Pennsylvania [Ph.D thesis]: Morgantown, West Virginia University, 153 p.

Bramlette, M. N., 1946, The Monterey Formation of California and the origin of its siliceous rocks: U.S. Geological Survey Professional Paper 212, 57 p.

Britt, L.K., and Schoeffler, J., 2009, The geomechanics of a shale play: What makes a shale prospective, *in* Proceedings, Society of Petroleum Engineers Eastern Regional Meeting, Charleston, West Virginia, SPE-125525, doi: 10.2118/125525-MS.

Broz, M.E., Cook, R.F., and Whitney, D.L., 2006, Microhardness, toughness, and modulus of Mohs scale minerals: American Mineralogist, v. 91, p. 135–142, doi: 10.2138/am.2006.1844.

Chang, C., Zoback, M.D., and Khaksar, A., 2006, Empirical relations between rock strength and physical properties in sedimentary rocks: Journal of Petroleum Science and Engineering, v. 51, p. 223–237, doi: 10.1016/j.petrol.2006.01.003.

Chase, C.A.J., and Dietrich, J.K., 1989, Compaction within the South Belridge diatomite: SPE Reservoir Engineering, v. 4, p. 422–428, doi: 10.2118/17415-PA.

Compton, J.S., 1991a, Origin and diagenesis of clay minerals in the Monterey Formation, Santa Maria Basin area, California: Clays and Clay Minerals, v. 39, p. 449–466.

Compton, J.S., 1991b, Porosity reduction and burial history of siliceous rocks from the Monterey and Sisquoc Formations, Point Pedernales area, California: GSA Bulletin, v. 103, p. 625–636, doi: 10.1130/0016-7606(1991)103<0625:PRABHO>2.3.CO;2.

Crawford, B.R., Gaillot, P.J., and Alramahi, B., 2010, Petrophysical methodology for predicting compressive strength in siliciclastic "sandstone-to-shale" rocks, *in* Proceedings, 44th US Rock Mechanics Symposium and 5th US-Canada Rock Mechanics Symposium: Salt Lake City, Utah, American Rock Mechanics Association, ARMA-10-196.

Curtis, M.E., Cardott, B.J., Sondergeld, C.H., and Rai, C.S., 2012, Development of organic porosity in the Woodford Shale with increasing thermal maturity: International Journal of Coal Geology, v. 103, p. 26–31, doi: 10.1016/j.coal.2012.08.004.

Dholakia, S.K., Aydin, A., Pollard, D.D., and Zoback, M.D., 1998, Fault-controlled hydrocarbon pathways in the Monterey Formation, California: AAPG Bulletin, v. 82, p. 1551–1574.

Dong, T., Harris, N.B., Ayranci, K., and Yang, S., 2017, The impact of rock composition on geomechanical properties of a shale formation: Middle and Upper Devonian Horn River Group shale, Northeast British Columbia, Canada: AAPG Bulletin, v. 101, p. 177–204, doi: 10.1306/07251615199.

Dræge, A., Jakobsen, M., and Johansen, T.A., 2006, Rock physics modelling of shale diagenesis: Petroleum Geoscience, v. 12, p. 49–57, doi: 10.1144/1354-079305-665.

Dunham, J. B., and Blake, G. H., 1987, Guide to coastal outcrops of the Monterey Formation of western Santa Barbara county, California, *in* Dunham, J. B., ed., Guide to Coastal outcrops of the Monterey Formation of western Santa Barbara County, California: Los Angeles, Pacific Section, Society of Economic Paleontologists and Mineralogists, Special Publication v. 53, p. 1-36.

Farquhar, R.A., Somerville, J.M., and Smart, B.G.D., 1994, Porosity as a geomechanical indicator: An application of core and log data and rock mechanics, *in* Proceedings, European Petroleum Conference: London, United Kingdom, Society of Petroleum Engineers, SPE-28853, doi: 10.2118/28853-MS.

Gale, J.F.W., Reed, R.M., and Holder, J., 2007, Natural fractures in the Barnett Shale and their importance for hydraulic fracture treatments: AAPG Bulletin, v. 91, p. 603–622, doi: 10.1306/11010606061.

Gale, J.F.W., Laubach, S.E., Olson, J.E., Eichhubl, P., and Fall, A., 2014, Natural fractures in shale: A review and new observations, AAPG Bulletin, v. 98, p. 2165–2216, doi: 10.1306/08121413151.

Graham, S.A., and Williams, L.A., 1985, Tectonic, depositional, and diagenetic history of Monterey Formation (Miocene), central San Joaquin basin, California: AAPG Bulletin, v. 69, p. 385–411.

Gross, M.R., 1995, Fracture partitioning: Failure mode as a function of lithology in the Monterey Formation of coastal California: Geological Society of America Bulletin, v. 107, p. 779–792.

Holt, R.M., Fjaer, E., Nes, O.M., and Alassi, H.T., 2011, A shaly look at brittleness, *in* 45th U.S. Rock Mechanics Geomechanics Symposium, San Francisco, California. American Rock Mechanics Association, ARMA-11-366.

Horsrud, P., 2001, Estimating mechanical properties of shale from empirical correlations: SPE Drilling & Completion, v. 16, p. 68–73, doi: 10.2118/56017-PA.

Hosford Scheirer, A., ed., 2007, Petroleum systems and geologic assessment of oil and gas in the San Joaquin Basin province, California: U.S. Geological Survey Professional Paper USGS Numbered Series 1713.

Hovorka, S.D., 1998, Facies and Diagenesis of the Austin Chalk and Controls on Fracture Intensity: A Case Study from North-Central Texas: Austin, Texas, Bureau of Economic Geology, University of Texas at Austin, 47 p.

Hower, J., Eslinger, E.V., Hower, M.E., and Perry, E.A., 1976, Mechanism of burial metamorphism of argillaceous sediment: 1. Mineralogical and chemical evidence: GSA Bulletin, v. 87, p. 725–737, doi: 10.1130/0016-7606(1976)87<725:MOBMOA>2.0.CO;2.

Hucka, V., and Das, B., 1974, Brittleness determination of rocks by different methods: International Journal of Rock Mechanics and Mining Sciences & Geomechanics Abstracts, v. 11, p. 389–392, doi: 10.1016/0148-9062(74)91109-7.

Ingle, J. C., Jr., 1981, Cenozoic depositional history of the northern continental borderland of southern California and the origin of associated Miocene diatomites, *in* Isaacs, C. M., ed., Guide to the Monterey Formation in the California coastal area, Ventura to San Luis Obispo: Los Angeles, Pacific Section, AAPG Special Publication 52, p. 1–8.

Ingram, G.M., and Urai, J.L., 1999, Top-seal leakage through faults and fractures: The role of mudrock properties: Geological Society, London, Special Publications, v. 158, p. 125–135, doi: 10.1144/GSL.SP.1999.158.01.10.

Isaacs, C. M., 1980, Diagenesis in the Monterey Formation examined laterally along the coast near Santa Barbara, California [Ph.D. thesis]: Stanford, Stanford University, 329 p.

Isaacs, C.M., 1981a, Field characterization of rocks in the Monterey Formation along the coast near Santa Barbara, California, *in* Isaacs, C.M., ed., Guide to the Monterey Formation in the California Coastal Area, Ventura to San Luis Obispo: Los Angeles, Pacific Section, Society of Economic Paleontologists and Mineralogists, p. 39–54.

Isaacs, C. M., 1981b, Porosity reduction during diagenesis of the Monterey Formation, Santa Barbara coastal area, California, *in* Garrison, R. E., and Douglas, R. G., eds., The Monterey Formation and Related Siliceous Rocks of California: Los Angeles, Pacific Section, Society of Economic Paleontologists and Mineralogists, p. 257–271.

Isaacs, C.M., 1981c, Outline of diagenesis in the Monterey Formation examined laterally along the Santa Barbara Coast, California, *in* Isaacs, C.M., ed., Guide to the Monterey Formation in the California Coastal Area, Ventura to San Luis Obispo: Los Angeles, Pacific Section, Society of Economic Paleontologists and Mineralogists, p. 25–38.

Isaacs, C.M., and Rullkötter, J., 2001, The Monterey Formation: From Rocks to Molecules: New York, Columbia University Press, 563 p.

Ishii, E., Sanada, H., Iwatsuki, T., Sugita, Y., and Kurikami, H., 2011, Mechanical strength of the transition zone at the boundary between opal-A and opal-CT zones in siliceous rocks: Engineering Geology, v. 122, p. 215–221, doi: 10.1016/j.enggeo.2011.05.007.

Jarvie, D.M., Hill, R.J., Ruble, T.E., and Pollastro, R.M., 2007, Unconventional shale-gas systems: The Mississippian Barnett Shale of north-central Texas as one model for thermogenic shale-gas assessment: AAPG Bulletin, v. 91, p. 475–499, doi: 10.1306 /12190606068.

Josh, M., Esteban, L., Delle Piane, C., Sarout, J., Dewhurst, D.N., and Clennell, M.B., 2012, Laboratory characterisation of shale properties: Journal of Petroleum Science and Engineering, v. 88–89, p. 107–124, doi: 10.1016/j.petrol.2012.01.023.

Kahoul, A., Abassi, A., Bahri, D., and Nekkab, M., 2011, K-shell fluorescence yields for elements with $6 \leq Z \leq 99$: Radiation Physics and Chemistry, v. 80, p. 369–377, doi: 10.1016 /j.radphyschem.2010.11.011.

Kahraman, S., 2001, Evaluation of simple methods for assessing the uniaxial compressive strength of rock: International Journal of Rock Mechanics and Mining Sciences, v. 38, p. 981–994, doi: 10.1016/S1365-1609(01)00039-9.

Kamp, P.C. van de, 2008, Smectite-illite-muscovite transformations, quartz dissolution, and silica release in shales: Clays and Clay Minerals, v. 56, p. 66–81, doi: 10.1346/CCMN. 2008.0560106.

Kassa, T.G., 2016, Pore structure of opal-CT and quartz porcelanites, Monterey Formation, California [M.S. thesis]: Long Beach, California State University, 113 p.

Keller, M.A., and Isaacs, C.M., 1985, An evaluation of temperature scales for silica diagenesis in diatomaceous sequences including a new approach based on the Miocene Monterey Formation, California: Geo-Marine Letters, v. 5, p. 31–35, doi: 10.1007/BF02629794.

Kennedy, M.J., Pevear, D.R., and Hill, R.J., 2002, Mineral surface control of organic carbon in black shale: Science, v. 295, p. 657–660, doi: 10.1126/science.1066611.

Kennett, J.P., 1977, Cenozoic evolution of Antarctic glaciation, the circum-Antarctic Ocean, and their impact on global paleoceanography: Journal of Geophysical Research, v. 82, p. 3843–3860, doi: 10.1029/JC082i027p03843.

Kompatscher, M., 2004, Equotip-rebound hardness testing after D. Leeb, *in* Proceedings, Conference on Hardness Measurements Theory and Application in Laboratories and Industries, p. 11–12.

Kumar, V., Sondergeld, C.H., and Rai, C.S., 2012, Nano to macro mechanical characterization of shale, *in* SPE Annual Technical Conference and Exhibition, San Antonio, Texas, Society of Petroleum Engineers, SPE-159804, doi: 10.2118/159804-MS.

Kuuskraa, V., Stevens, S.H., and Moodhe, K.D., 2013, United States, Energy Information Administration, and Advanced Resources International (Firm): Technically recoverable shale oil and shale gas resources: an assessment of 137 shale formations in 41 countries outside the United States: http://www.eia.gov/analysis/studies/worldshalegas/ (accessed March 2018).

Larue, D.K., Smithard, M., and Mercer, M., 2018, Three deep resource plays in the San Joaquin Valley compared with the Bakken Formation: AAPG Bulletin, v. 102, p. 195–243, doi: 10.1306/04241716143.

Lashkaripour, G.R., 2002, Predicting mechanical properties of mudrock from index parameters: Bulletin of Engineering Geology and the Environment, v. 61, p. 73–77, doi: 10.1007/s100640100116.

Laubach, S.E., Olson, J.E., and Gross, M.R., 2009, Mechanical and fracture stratigraphy: AAPG Bulletin, v. 93, p. 1413–1426, doi: 10.1306/07270909094.

Lee, J.S., 2015, Calibration of rebound hardness numbers to unconfined compressive strength in shale formations: Journal of Petroleum Technology, v. 67, p. 41–45, doi: 10.2118/0115-0041-JPT.

Lee, J.S., Smallwood, L., and Morgan, E., 2014, New application of rebound hardness numbers to generate logging of unconfined compressive strength in laminated shale formations, *in* Proceedings, 48th U.S. Rock Mechanics/Geomechanics Symposium: Minneapolis, Minnesota, American Rock Mechanics Association, ARMA-2014-6972.

Leeb, D., 1979, Dynamic hardness testing of metallic materials: NDT International, v. 12, p. 274–278, doi: 10.1016/0308-9126(79)90087-7.

Lockman, D., 2012, Monterey Formation opal-A to opal-CT transition core display Plains Exploration & Production Company, Reardon 330 L North Midway-Sunset Field, CA: Monterey Formation Seminar and Core Workshop, AAPG Annual Convention and Exhibition: Long Beach, AAPG, p. 103–107.

Lorenz, J.C., Sterling, J.L., Schechter, D.S., Whigham, C.L., and Jensen, J.L., 2002, Natural fractures in the Spraberry Formation, Midland Basin, Texas: The effects of mechanical stratigraphy on fracture variability and reservoir behavior: AAPG Bulletin, v. 86, p. 505–524, doi: 10.1306/61EEDB20-173E-11D7-8645000102C1865D.

Miller, D.D., and McPherson, J.G., 1992, South Belridge Field - U.S.A. San Joaquin Basin, California, *in* Miller, D.D., and McPherson, J.G., eds, Structural Traps VII, v. 21, p. 221–244.

Mizutani, S., 1977, Progressive ordering of cristobalitic silica in the early stage of diagenesis: Contributions to Mineralogy and Petrology, v. 61, p. 129–140, doi: 10.1007/BF00 374363.

Mohs, F., 1825, Treatise on Mineralogy: Or, The Natural History of the Mineral Kingdom, Volume 1: London, Hurst, Robinson, and Company, 498 p.

Mount, V.S., and Suppe, J., 1987, State of stress near the San Andreas fault: Implications for wrench tectonics: Geology, v. 15, p. 1143–1146.

Mosher, A., 2013, Detailed lithostratigraphic characterization of Chico Martinez Creek, California [M.S. thesis]: Long Beach, California State University, 115 p.

Murata, K.J., and Larson, R.R., 1975, Diagenesis of Miocene siliceous shales, Temblor range, California: Journal of Research of the US Geological Survey, v. 3, p. 553–566.

Murray, C.D., 2015, Mechanical stratigraphy and sonic log relationships using the Proceq Bambino in the Niobrara Formation, Denver Basin [M.S. thesis]: Golden, Colorado School of Mines, 88 p.

Narr, W., and Suppe, J., 1991, Joint spacing in sedimentary rocks: Journal of Structural Geology, v. 13, p. 1037–1048, doi: 10.1016/0191-8141(91)90055-N.

Offurum, C.G., 2016, Integrated geochemical, mechanical, and lithological characterization of the Marcellus Shale, Pennsylvania [M.S. thesis] Fort Worth, Texas Christian University, 125 p.

Olson, J.E., Laubach, S.E., and Lander, R.H., 2009, Natural fracture characterization in tight gas sandstones: Integrating mechanics and diagenesis: AAPG Bulletin, v. 93, p. 1535–1549, doi: 10.1306/08110909100.

Palchik, V., 1999, Influence of porosity and elastic modulus on uniaxial compressive strength in soft brittle porous sandstones: Rock Mechanics and Rock Engineering, v. 32, p. 303–309, doi: 10.1007/s006030050050.

Passey, Q.R., Bohacs, K., Esch, W.L., Klimentidis, R., and Sinha, S., 2010, From oil-prone source rock to gas-producing shale reservoir - Geologic and petrophysical characterization of unconventional shale gas reservoirs, *in* Proceedings, International Oil and Gas Conference and Exhibition in China: Beijing, China, Society of Petroleum Engineers, SPE-131350, doi: 10.2118/131350-MS.

Pisciotto, K.A., 1981, Diagenetic trends in the siliceous facies of the Monterey Shale in the Santa Maria region, California: Sedimentology, v. 28, p. 547–571, doi: 10.1111/j.1365-3091.1981.tb01701.x.

Pisciotto, K. A., and Garrison, R. E., 1981, Lithofacies and depositional environments of the Monterey Formation, California, *in* Garrison, R. E., and Douglas, R. G., eds., The Monterey Formation and Related Siliceous Rocks of California: Los Angeles, Pacific Section, Society of Economic Paleontologists and Mineralogists, p. 97–122.

Pitman, J.K., Price, L.C., and LeFever, J.A., 2001, Diagenesis and fracture development in the Bakken Formation, Williston Basin: Implications for reservoir quality in the Middle Member: U.S. Department of the Interior, U.S. Geological Survey, USGS Professional Paper 1653, 28 p.

Reis, J.C., 1990, Variations in thermal properties with lithology in the San Joaquin Valley, California, *in* Proceedings, SPE California Regional Meeting: Ventura, California, Society of Petroleum Engineers, SPE-20085, doi: 10.2118/20085-MS.

Rickman, R., Mullen, M.J., Petre, J.E., Grieser, W.V., and Kundert, D., 2008, A practical use of shale petrophysics for stimulation design optimization: All shale plays are not clones of the Barnett Shale, *in* Proceedings, SPE Annual Technical Conference and Exhibition: Denver, Colorado, Society of Petroleum Engineers, SPE-115258, doi: 10.2118/115258-MS.

Ritz, E., Honarpour, M.M., Dvorkin, J., and Dula, W.F., 2014, Core hardness testing and data integration for unconventionals, *in* Proceedings, Unconventional Resources Technology Conference: Denver, Colorado, USA, URTEC-1916004, doi: 10.15530/URTEC-2014-1916004.

Rolfs, S.A., 2015, Integrated geomechanical, geophysical, and geochemical analysis of the Bakken Formation, Elm Coulee field, Williston Basin, Montana [M.S. thesis]: Golden, Colorado School of Mines, 122 p.

Ross, D.J.K., and Bustin, R.M., 2008, Characterizing the shale gas resource potential of Devonian–Mississippian strata in the Western Canada sedimentary basin: Application of an integrated formation evaluation: AAPG Bulletin, v. 92, p. 87–125, doi: 10.1306/09040707048.

Rothwell, R.G., and Croudace, I.W., 2015, Twenty years of XRF core scanning marine sediments: What do geochemical proxies tell us?, *in* Micro-XRF Studies of Sediment Cores: Dordrecht, Springer, Developments in Paleoenvironmental Research, p. 25–102, doi: 10.1007/978-94-017-9849-5_2.

Schwalbach, J.R., Gordon, S.A., O'Brien, C.P., Lockman, D.F., Benmore, W.C., Huggins, C.A., Knauer, L.C., and Britton, A., 2009, Reservoir characterization of Monterey Formation siliceous shales: Tools and applications, *in* Knauer, L.C., ed., Contributions to the Geology of the San Joaquin Basin: Los Angeles, AAPG Pacific Section, MP48, p. 119-146.

Schwartz, D.E., 1988, Characterizing the lithology, petrophysical properties, and depositional setting of the Belridge Diatomite, South Belridge Field, Kern County, California, *in* Graham, S.A., ed., Studies of the Geology of the San Joaquin Basin: Los Angeles, Pacific Section Society of Economic Mineralogists and Paleontologists, v. 60, p. 281-301.

Snyder, W. S., Brueckner, H. K., and Schweickert, R. A., 1983, Deformational styles in the Monterey Formation and other siliceous sedimentary rocks, *in* Isaacs, C. M., and Garrison, R. E., eds., Petroleum Generation and Occurrence in the Miocene Monterey Formation, California: Los Angeles, Pacific Section Society of Economic Paleontologists and Mineralogists, p. 151–170.

Sonnenfeld, M., Ohlson, C., Zahm, C., and Odegard, M., 2015, The impact of multiple, thin bentonites on proppant placement and effective fracture continuity within the Niobrara Formation, Weld County, Colorado, *in* Proceedings, Unconventional Resources Technology Conference: San Antonio, Texas, URTEC-2171548, doi: 10.15530/URTEC-2015-2171548.

Strickland, H.M., 2013, Fracture networks and mechanical stratigraphy in the Monterey-equivalent Pismo Formation and its relationship to primary sedimentology and stratigraphy at Montana de Oro State Park, California [M.S. thesis]: Long Beach, California State University, 154 p.

Strubhar, M.K., Medlin, W.L., Nabi, S.M., and Andreani, F.S., 1984, Fracturing results in diatomaceous earth formations, South Belridge Field, California: Journal of Petroleum Technology, v. 36, p. 495–502, doi: 10.2118/10966-PA.

Thyberg, B., and Jahren, J., 2011, Quartz cementation in mudstones: Sheet-like quartz cement from clay mineral reactions during burial: Petroleum Geoscience, v. 17, p. 53–63, doi: 10.1144/1354-079310-028.

Vernik, L., Bruno, M., and Bovberg, C., 1993, Empirical relations between compressive strength and porosity of siliciclastic rocks: International Journal of Rock Mechanics and Mining Sciences & Geomechanics Abstracts, v. 30, p. 677–680, doi: 10.1016/0148-9062(93) 90004-W.

Verwaal, W., and Mulder, A., 1993, Estimating rock strength with the Equotip hardness tester: International Journal of Rock Mechanics and Mining Sciences & Geomechanics Abstracts, v. 30, p. 659–662, doi: 10.1016/0148-9062(93)91226-9.

Wang, F.P., and Gale, J.F.W., 2009, Screening criteria for shale-gas systems: Gulf Coast Association of Geological Societies Transactions, v. 59, p. 779-793

Wirtz, Y., 2017, Strain variation between the Monterey and Sisquoc Formations, Southern Santa Maria Basin, California, USA: Implications for structural assessment of fold and thrust belts [M.S. thesis]: Long Beach, California State University, 85 p.

Yang, S., Harris, N., Dong, T., Wu, W., and Chen, Z., 2015, Mechanical properties and natural fractures in a Horn River Shale core from well logs and hardness measurements, *in* EUROPEC: Madrid, Spain, Society of Petroleum Engineers, SPE-174287, doi: 10.2118/174287-MS.

Yang, Y., Sone, H., Hows, A., and Zoback, M.D., 2013, Comparison of brittleness indices in organic-rich shale formations, *in* Proceedings, 47th U.S. Rock Mechanics/Geomechanics Symposium: San Francisco, California American Rock Mechanics Association, ARMA-2013-403, doi: 10.2118/174287-MS.

Zahm, C.K., and Enderlin, M., 2010, Characterization of rock strength in Cretaceous strata along the Stuart City Trend, Texas: Gulf Coast Association of Geological Societies Transactions, v. 60, p. 693–702.

Zargari, S., Prasad, M., Mba, K.C., and Mattson, E., 2011, Organic Maturity, hydrous pyrolysis, and elastic property in shales, *in* Proceedings, Canadian Unconventional Resources Conference: Calgary, Alberta, Canada Society of Petroleum Engineers, SPE-149403, doi: 10.2118/ 149403-MS.

Zhao, L., Qin, X., Han, D.-H., Geng, J., Yang, Z., and Cao, H., 2016, Rock-physics modeling for the elastic properties of organic shale at different maturity stages, Geophysics, v. 81, p. D527–D541, doi: 10.1190/geo2015-0713.1.

Zoback, M.D., 2010, Reservoir Geomechanics: New York, Cambridge University Press, 505 p.